Author/s:
Fernando, Liyanadurage Priyaga Supun Kumari

Title:
Investigation of hyporheic flow through meandering rivers: Implications for nitrogen processing

Date:
2019

Investigation of hyporheic flow through meandering rivers: Implications for nitrogen processing

Liyanadurage Priyaga Supun Kumari Fernando

0000-0001-7467-2342

Doctor of Philosophy

October 2019

Department of Infrastructure Engineering

School of Engineering

The University of Melbourne

Australia

Submitted in total fulfillment for the degree of Doctor of Environmental Engineering

[This page left intentionally blank]

Abstract

Increased nitrogen loads have significant negative consequences in streams. The hyporheic zone of streams, where surface-subsurface water exchange happens, provides significant attenuation for nitrogen compounds from the fluvial system. From many geomorphic features that contribute to hyporheic flow, meanders are particularly important for these biogeochemical reactions. Meanders provide longer residence times to allow complete denitrification of various nitrate to nitrogen gas, which can support more significant improvements in water quality compared to other channel features that only allow for partial denitrification due to short residence time. From the published literature, it is evident that there is not enough understanding about the extent of temporal variation of meander driven hyporheic flow except for few theoretical studies that have been performed to investigate the physical behavior of water and solute movement. Therefore, this research aims to investigate how meandering morphology impacts on transport characteristics of water and dissolved solutes in the hyporheic zone and to identify primary mechanisms controlling the flow. This was achieved through a set of laboratory experiments and a three-dimensional numerical model developed for meandering stream.

Laboratory experiments were conducted in a recirculating flume with a set of river discharges and meandering morphologies. Residence time distribution and downwelling water flux were determined by continuously monitoring the exchange of a conservative tracer (Rhodamine WT) introduced into the surface flow. The experimental results show that both; stream discharge and meander wavelength affect the residence time and water flux into the sediment bed, hence affecting the rates of biogeochemical reactions. Most importantly, change in stream discharge affects residence times in the hyporheic zone, but the importance of considering river flow conditions in modeling hyporheic flow through meanders has been neglected in previous studies.

The three-dimensional model developed in this study is based on the combination of surface flow modeled with Reynold average Navier-Stokes equation and subsurface flow modeled with Continuity equation for groundwater flow and Darcy’s law equation. This mathematical model was solved using COMSOL Multiphysics® Modelling Software (will be referred to as COMSOL henceforth), and water transport characteristics in the hyporheic zone were estimated using a numerical particle tracing technique in COMSOL. The model predicted the observed residence time distributions of laboratory tracer experiments with an R^2 of 0.95. Results show that there are two primary mechanisms driving hyporheic flow through meanders; 1) Lateral flow caused by channel slope at the scale of meander wavelength (Floodplain HE) and 2) vertical flow caused by surface water acceleration due to the curvature of the channel at the scale of channel width (Fluvial HE).

This three-dimensional model was then used to study the effect of meander morphology on the hyporheic residence time distribution and water flux complemented by Taguchi orthogonal array design. Channel sizes considered in the simulations range from 1m to1000m in widths. We propose three empirical relationships to predict downwelling water flux and characteristics of residence time distribution (mean and standard deviation). Also, we found that the hyporheic residence time distribution induced by three-dimensional meanders follows a log-normal distribution. Meander wavelength has a significant effect on the hyporheic residence time as well as the downwelling water flux, demonstrating the importance of channel size on the hyporheic flow processes. However, the sinuosity of the river does not affect much on the time that water spends in the hyporheic zone but alters the volume of water entering the hyporheic zone. Most importantly, meanders produce significant vertical hyporheic flow in addition to lateral flow. Increasing the channel curvature (increased sinuosity or decreased wavelength) increases the vertical flow, hence higher downwelling water flux but the reduction in the residence time.

Finally, we looked at how meander induced hyporheic flow influences on nitrogen processing. We consider a dimensionless number (Da, Damköhler number), defined as the ratio between the median residence time and the critical concentration of dissolved oxygen below which nitrogen removal reactions occur (reaching anaerobic conditions). Meanders, being large morphologic features, observed to provide high Da values (>20) suggest the availability of hyporheic regions with prevailing anaerobic conditions for nitrogen removal reactions.

In recent decades, fate and transport of nitrogen in hyporheic zones have been significantly influenced by flow modifications, increased water pollution, and channel straightening. Increased straight channels and impervious surfaces confine the hydrological flow paths and residence times in the hyporheic zone, which may limit sufficient treatment. In order to support this important ecological service, implementing restoration solutions is vital. Understanding the underlying mechanisms and effect of urbanization on nitrogen transformation is a prerequisite for minimizing stream degradation and achieving restoration goals. Therefore, our findings can potentially be incorporated in river restoration practices and to design rivers as natural nitrogen filters. This study represents a step forward for the analysis of large-scale channel features and their residence times, which are less understood in previous literature but are very important for biogeochemical cycling in rivers.

Declaration

I declare that,

1. The thesis comprises only my original work towards the Doctor of Philosophy except where indicated in the preface
2. Due acknowledgment has been made in the text to all other material used
3. The thesis is less than the maximum 100,000 words in length, exclusive of tables, bibliographies, and appendices

Liyanadurage Fernando

October 2019

Preface

This dissertation presents the sole and original work of me (Liyanadurage Fernando) as part of my Ph.D. candidature at the Department of Infrastructure Engineering, The University of Melbourne, Australia. However, my supervisors (Prof Michael Stewardson and Dr. Meenakshi Arora) always support me by providing technical guidance, critical feedback, and continuous monitoring throughout my Ph.D. candidature. Any additional contributions of this dissertation have been suitably acknowledged and cited. Financial support provided by The University of Melbourne, including Melbourne International Research Scholarship (MIRS) and Melbourne International Fee Remission Scholarship (MIFRS), is acknowledged with gratitude. I would like to acknowledge laboratory and software facilities provided by the School of Engineering, The University of Melbourne.

Four journal papers presented in the dissertation were first drafted by me and revised multiple times according to the critical feedback received from my supervisors; Prof Michael Stewardson and Dr. Meenakshi Arora.

- Paper 1 has been submitted as *Fernando, L.P.S.K., Stewardson, M.J., & Arora, M. Effect of multiple scales on nitrogen transformation in the hyporheic zone: A review*. Submitted to *Hydrological Processes*, and currently in revision.
- Paper 2 will be submitted as *Fernando, L.P.S.K., Stewardson, M.J., & Arora, M. Stream meander wavelength affects hyporheic residence time: Implications for nitrogen processing*. To be submitted to *Water Resources Research, and currently under internal revision*.
- Paper 3 will be submitted as *Fernando, L.P.S.K., Stewardson, M.J., & Arora, M. Modeling hyporheic flow in meandering rivers*. To be submitted to *Water Resources Research*, and currently under internal revision.
- Paper 4 will be submitted as *Fernando, L.P.S.K., Stewardson, M.J., & Arora, M. Residence time of meander-driven hyporheic exchange*. To be submitted to *Water Resources Research*, and currently under internal revision.

Acknowledgments

I am very much grateful to my supervisors, Prof Michael Stewardson and Dr. Meenakshi Arora, for their support, valuable directions, and excellent coaching during my Ph.D. candidature. Your friendly admiring made my Ph.D. research more interesting. I especially thank my principal supervisor, Prof Michael Stewardson for offering me the opportunity to work with him and for the critical feedback throughout this Ph.D. candidature.

Special thanks to Prof Andrew Western for chairing my advisory committee and for the fruitful comments during my review meetings.

I would like to acknowledge The University of Melbourne for offering me the postgraduate opportunity and Scholarship office for awarding MIFRS, MIRS scholarships, and travel grants for conference travel.

I'm grateful to Mr. Rodger Ian Young, for supporting me to design and build laboratory set up for tracer experiments, as well as for his expert pieces of advice to conduct my laboratory experiments successfully. Special thanks to Mr. Clifford Ogleby for helping me to select a better scanning method. I would like to express my gratitude to Dr. Kourosh Khoshelham and his Ph.D. student Ha Tran for teaching me laser scanning procedures and software. Thank you, Mr. George Fox, for providing me equipment and tools that were required for lab experiments.

I would like to gratefully remember late Dr. Alexander McCluskey for his kind support during my first year of Ph.D. and his expert advice during my laboratory experiments.

I sincerely thank A/Prof Angus Webb for all the support during my candidature and his wife Annette Webb for welcoming me to their house when my laboratory experiments were away from my home.

I'm grateful to Shivansh Srivastava and Garima Lakhanpa for continuous support and encouragement.

Thank you to the academic and non-academic staff in Water Group, for sharing their experiences and knowledge with me. Special thanks to all the members of the Ecohydraulics lab group for arranging practice talks and giving useful comments to improve my Ph.D. review presentations and conference presentations. Thank you, writing club for encouraging me to write papers and giving critical feedback.

I would like to acknowledge Nikolas Makasis for supporting me with COMSOL software and Shuci Liu for helping me with the statistical analysis of my simulation data. I Acknowledge Keirnan Fowler, Margarita Saft, Roser Casas-Mulet, and Elise King for sharing their knowledge during this period.

Thank you, Infrastructure RHDs, specially Chinchu Mohan, Adrian Servin, Lubna Meempatta, Muktha Sapkota, Erandathi Ekanayake, and Sewwandi Wijesuriya.

I am very much grateful to the academic and non-academic staff of the Department of Chemical and Process Engineering, University of Peradeniya, Sri Lanka, for encouraging me for higher education. Special thanks to Prof. Rajaratnam Shanthini, Dr. C.S. Kalpage and Dr. Aruna Manipura for their kind support and encouragements since my undergraduate studies.

Thanks to all my friends in Melbourne and back in Sri Lanka for the caring and accompany during this period, particularly Marian Opanayake and Lakmal Punchibandage, for being my family in Australia. Special Thank you to Shihara Perera, Aruna Ukwatta and Tharindu Pathirana for guiding me throughout of my PhD and for all support during this period.

I would like to thank my mother, father, brother, and sister, for their never-ending support and understanding. I really appreciate my mother and father for all the sacrifices you’ve made for me.

Lastly, but not least, thank you to my husband Sudesh for being with me and for the endless encouragement and faith in me. He was my biggest inspiration, and I am appreciative of his support for my laboratory experiments without any hesitation. I am sincerely thankful for his love and patience throughout this period.

Table of Contents

Abbreviations

AIC	Akaike Information Criteria
AM	Ammonification or mineralization
ANA	Anaerobic ammonium oxidation (ANAMMOX)
BM	Biomass
DN	Denitrification
DNRA	Dissimilatory reduction of nitrate to ammonium nitrogen
DO	Dissolved Oxygen
DOC	Dissolved Organic Carbon
HE	Hyporheic Exchange
MSM	Multi-Scale Model (Stonedahl et al., 2013, Stonedahl et al., 2010)
NA	Nitrogen (inorganic nitrogen) Assimilation into the plant and/ or microbial biomass
NEXSS	Networks with EXchange and Subsurface Storage model (Gomez-Velez and Harvey, 2014)
NI	Nitrification
PASS	Pumping And Streamline Segregation model (Azizian et al., 2015)
RT	Residence Time
RTD	Residence Time Distribution
WSI	Water sediment interface

Notations

$C_{NH_4^+}$	Concentration of ammonium
$C_{NO_3^-}$	Concentration of nitrate
C_{O_2}	Concentration of dissolved oxygen
C_{DOC}	Concentration of dissolved organic carbon
$R_{NH_4^+}$	Biological reaction rates of ammonium
$R_{NO_3^-}$	Biological reaction rates of nitrates
R_{O_2}	Biological reaction rates of oxygen
R_{DOC}	Biological reaction rates of dissolved organic carbon
T_1, T_2	Reaction time of 1) nitrification and 2) denitrification
μ_{AR}	Maximum substrate utilization rate for aerobic respiration
μ_{DN}	Maximum substrate utilisation rate for denitrification
μ_{NI}	Maximum substrate utilization rate for nitrification
A	Meander amplitude
COMSOL	Multiphysics® Modelling Software
Da	Damköhler number
J	Meander Sinuosity
$k1_{DN}$	First order rate constant for denitrification.
$k1_{DOC}$	First order rate constant for aerobic respiration
$k1_{NI}$	First order rate constant for nitrification
k_d	Linear distribution coefficient
KI	Inhibition constant for the denitrification reaction
k_{NI}	Bimolecular nitrification rate constant
N_2	Nitrogen gas
N_2O	Nitrous Oxide
NH_4^+	Ammonium nitrogen
NO_2^-	Nitrite nitrogen
NO_3^-	Nitrate nitrogen
Q	River discharge
R	Radius of curvature

R_{min}	Maximum respiration rate of sediment organic matter
S	Slope
W/D	Width to depth ratio
W_b	Meander channel belt width
X_{AR}	Biomass of respiration functional group
X_{DN}	Biomass of denitrifiers functional group
X_{NI}	Biomass of nitrification functional group
y_{NH4+}	Partition coefficient for aerobic respiration, and for nitrification
y_O (–)	Partition coefficient for aerobic respiration
θ	Porosity of the sediment bed
Υ_{AR}	Use coefficient for aerobic respiration
Υ_{DN}	Use coefficient for denitrification
W	Channel width
λ	Meander wavelength

Table of Figures

List of tables

Chapter 1: Introduction

1.1 Background

Water scarcity and water pollution are universal challenges of the modern world in the face of the growing population and variable climate. All living beings, including animals and plants, rely upon the availability of sufficient water of a required quality that is fit for purpose. One significant global water quality concern is blue-green algal blooms and eutrophication (Conley et al., 2009); due to increased nutrient (mainly nitrogen and phosphorus) levels in lakes, rivers, and streams. Over the last century, excessive application of nitrogen-based fertilizer on pastures and agriculture fields, improper management of landfill leachate, exhaust from cars and other internal combustion engines, and other pollution sources have approximately doubled nitrogen loads entering the environment including groundwater and surface water bodies (Hoven et al., 2008, Smil, 1999, Mazza et al., 2014, Zarnetske et al., 2012). There is an urgent need to reduce the input of anthropogenic nitrogen sources into receiving waters and develop suitable management practices in catchments as well as in streams to reduce nitrogen concentrations to mitigate eutrophication.

This research aims to extend the current knowledge of natural nitrogen attenuation strategies to tackle this globally significant challenge.

In addition to eutrophication, excessive nitrogen levels have other detrimental impacts on the environment, humans, and aquatic ecosystems. Rivett et al. (2008) documented elevated ammonium levels can increase chlorine demand and be toxic for fish. Nitrate can also cause increased risks of methaemoglobinaemia (blue baby syndrome) in infants and cancer. In addition, rivers can contribute to greenhouse gas (N_2O) emissions due to incomplete denitrification reactions (Marzadri et al., 2014). Further, total nitrogen levels in some

Australian water sources are not compliant with water quality regulations. A recent incident on massive fish deaths in Marry river is one of the sad consequences we saw in this regard. Therefore, there is an urgent need to understand nitrogen cycling and the factors affecting this cyclic transformation in aquatic systems.

Several studies identify the hyporheic zone of streams as a particularly important location to control nitrogen levels in fluvial systems (Azizian et al., 2015, Boano et al., 2014, Marzadri et al., 2011, Zarnetske et al., 2011). The hyporheic zone is the porous sediment layer beneath the water column and in riparian areas of the river, which can facilitate the exchange of surface and subsurface water. The hyporheic zone is composed of many aquatic organisms, such as microorganisms, micro and macroinvertebrates, and fish (Buss et al., 2009). As a biologically active zone, the hyporheic zone provides suitable conditions for nitrogen transformation processes (Lawrence et al., 2013). River water enters the hyporheic zone at high-pressure zones, travels slowly in the pore sediment space, mixes with groundwater, and re-enter the river at low-pressure zones. Longer contact time with the sediment bed and its living microbial community enhances biological reactions supporting pollutant reduction and biogeochemical cycling (Boano et al., 2014, Sheibley et al., 2003).

Hyporheic flow occurs due to pressure variation along the river bed, which are affected by river hydraulics (hydrodynamic pressure) and hydrostatic pressure acting on the river bed from bed elevation and depth of the water flow. The pressure head gradient at the river bed depends on the morphology and slope of the river. Three-dimensional morphology affects river water hydraulics resulting in acceleration and deceleration of water and advective pumping of water into the hyporheic zone. River morphology largely affects the free water surface depths on the river bed, influencing static head changes. The literature identifies three primary morphology features/ scales (river bedforms, bars, and meanders) as hyporheic flow drivers in natural rivers.

Literature suggests (Chapter 2) that meandering streams provide more extended residence time distributions for water and dissolved compounds in the hyporheic zone, which is very important for nitrogen removal from streams, compared to other morphology features that contribute to hyporheic exchange. However, there is a lack of understanding of how meandering morphology impacts on hyporheic residence times. Therefore, this study focused on developing a greater understanding of the impact of meanders on hyporheic flow and residence times and its implications for river nitrogen cycling. This objective was achieved through a combination of experimental and three-dimensional modeling study.

1.2 Thesis structure

The dissertation is composed of six chapters, including four chapters that are written in the format of journal papers that address the above issues. A brief overview of the thesis is presented below:

Chapter 1- Introduction: presents an overview of my research and the thesis structure.

Chapter 2- Literature Review and research questions: presents a comprehensive literature review that details the research questions of my research and the overview of flow and nitrogen processes occurring in the hyporheic zone. This summarizes dominant nitrogen reactions, their kinetics, and reaction time required to achieve effective nitrogen removal from the stream bed. This section also presents residence time distributions associated with different river morphology features from literature. I identify that meanders are significant morphology features with longer residence times and could be essential locations for river nitrogen processing.

Chapter 3- presents the laboratory experiments conducted at the University of Melbourne, Burnley Campus, to examine solute transport in meandering rivers. This chapter discusses the effects of channel discharge, meander wavelength, and channel slope on the residence time distribution and interfacial flux through a set of laboratory tracer experiments. I present three-dimensional meandering morphology to analyze solute transport in the hyporheic zone of meandering channels. Comparing the experiment results for varied flow and topographic conditions, I found that the hyporheic exchange (solute residing time and interfacial water flux into the surface) around meanders are primarily influenced by channel flow rates and meander wavelength (or sinuosity). These experimental results were used to compare with the projected results from a numerical model developed to predict hyporheic flow fields.

Chapter 4 describes the three-dimensional numerical model modified from existing models (Boano et al., 2006, Cardenas, 2009a, Gomez et al., 2012, Stonedahl et al., 2013, Stonedahl et al., 2010). I have included hydrodynamic pressure variation in the model by considering Reynold averaged Navier-Stokes with turbulence effect for the surface flow. Gravitational pressure head variation due to the slope of the river and the water depths on the sediment bed were considered by creating the channel and sediment geometry in a global coordinate system to capture elevation difference along downstream. The model performed well in reproducing residence time distributions for a set of laboratory tracer experiments with a meandering morphology. Results show that there are two major mechanisms driving hyporheic flow through meanders; 1) Lateral flow caused by channel slope at the scale of meander wavelength and 2) vertical flow caused by surface water acceleration due to the curvature of the channel at the scale of channel width.

Chapter 5 investigates the effect of meander morphology (sinuosity and meander wavelength) on residence time and water flux into the hyporheic zone using a series of numerical simulations. I have considered six wavelengths according to corresponding river widths, $\lambda = 7.5\,W^{1.12}$ (Williams, 1986) and six sinuosities. Channel widths considered in the simulations ranged from 1m to1000m. I found that the hyporheic residence time distribution induced by three-dimensional meanders follows a log-normal distribution. My study showed that the meander wavelength has a significant effect on the hyporheic residence time as well as the downwelling water flux, demonstrating the importance of channel size on the hyporheic flow processes. However, the sinuosity of the river does not affect much on the time that water spends in the hyporheic zone but will alter the volume of water entering the hyporheic zone.

Chapter 6 is a small chapter that provides background information about nitrogen issues in a stream ecosystem. In this chapter, I have analyzed residence times with respect to nitrogen reaction times. I used a dimensionless number (Damköhler number, Da) to identify anaerobic and aerobic conditions within the hyporheic zone.

Chapter 7 presents a discussion on all the components of my research and the effect of meander induced hyporheic residence times and interfacial fluxes on nitrogen fate and transport in rivers.

Chapter 8 provides the conclusions of my research and future research directions

Chapter 2: Literature review and research questions of the study

The research presented in this thesis is based on a well-organized and focused critical review of literature on the current state of the hyporheic researches. There are three parts of the literature review. The first part (section 2.1) presents an overview of the hyporheic zone and underlying processes. The second part is prepared as a journal manuscript (Paper 1) and presented in section 2.2. This manuscript discusses the importance of coupled physical and biogeochemical transport to achieve better nitrogen processing in streams. This covers nitrogen processes occurring in the hyporheic zone by identifying critical biogeochemical reactions and their reaction times. The manuscript also examines the hyporheic zone features at different scales used in previous literature and their corresponding residence times to determine which scales/features are essential for hyporheic nitrogen processing. I found that meanders could be a potential place for complete nitrogen removal reactions given the longer residence times associated with meandering streams.

Section 2.3 presents the second part of my literature review. This section includes a comprehensive literature review that details the background, state of research, and open research questions around meander induced hyporheic flow. There is little progress in understanding the relative effect of meandering morphology on nitrogen processing in the hyporheic zone.

2.1 Hyporheic zone and transport processes

2.1.1 Hyporheic zone

The hyporheic zone is one of the important components in the stream ecosystem, composed of permeable sediments and lay beneath and sideways of streams (Boano et al., 2014, Buss et al., 2009). This is home for many aquatic organisms, such as microorganisms, micro and macroinvertebrates, and fish (Buss et al., 2009). The hyporheic zone continuously transports surface water through flow paths that return to surface water (Azizian et al., 2015).

The exchange of stream water across the sediment bed (hyporheic flow) is controlled by dynamic hydraulic head developed over the water-sediment interface (Elliott and Brooks, 1997a, Azizian et al., 2015, Grant et al., 2014, Boano et al., 2014). The magnitude of these hydraulic heads is determined by the kinetic and potential energy gradients generated over the water-sediment interface (Boano et al., 2014). Hydraulic head can be devoted by two components; static and dynamic. The static part is the summation of the hydrostatic pressure head and elevation head, whereas the dynamic pressure head represents the summation of the total velocity head (Boano et al., 2014). Even though both hydrostatic forces and hydrodynamic forces tend to have significant impacts on the hyporheic exchange, their influences seem to be more scale-dependent.

Hydrostatically driven hyporheic exchange occurs mainly due to the pressure head induced on the water-sediment interface by the overlying surface water. Hence this exchange heavily depends on the height and slope of the stream water surface. Even though hydrostatically driven hyporheic fluxes can occur at any spatial scale, static pressure contribution monopolizes at larger topographic features (Boano et al., 2014, Cardenas, 2008b).

Hydrodynamically driven hyporheic exchange takes place due to the velocity head created by acceleration and deceleration of stream water flow over sediment bed. These forces push water and dissolved solutes into the sediment bed in high-velocity zones and out of the sediment bed in low-velocity zones (Azizian et al., 2015). `Hyporheic fluxes induced due to hydrodynamic forces seems to deteriorate instantly over distances of the order of the stream's depth. Hydrodynamic forces dominate over small scale topographic features (Boano et al., 2014). The magnitude of hydrodynamically driven hyporheic flow positively proportion with sediment permeability, height of the topographic feature and the shear stress of the bed (Boano et al., 2014) and depth depends as a portion of the wavelength of the topographic feature (Cardenas and Wilson, 2007a, Elliott and Brooks, 1997a).

Hyporheic zone connects rivers with surrounding floodplains and underlying aquifers vertically and laterally and continuously exchange water with surrounding saturated sediments (Findlay, 1995, Boano et al., 2010c). Hyporheic exchange has found to have control over patterns of sediment bed permeability and riverbed hydraulic conductivity at smaller scales. Riverbed hydraulic conductivity and porosity can be spatially very heterogeneous, and an increasing number of studies have been developed to predict spatial patterns of them (Buss et al., 2009).

2.1.2 Different scales at which hyporheic exchange occurs

Hyporheic flow occurs across at a wide range of river morphology features, including vertical exchange from river bedforms such as pool-riffle, ripples-dunes, and emerged bars and lateral exchange from river side forms such as alternate bars and meanders. Since the first scale framework proposed by Frissell (1986) (* in Table 2.1), there have been several attempts to identifying features of rivers at different scales and arranging these hierarchically. However, there is no explicit agreement in the literature regarding the scale hierarchies for hyporheic exchange with variation in the terms and defining features used to classify exchange at different scales. Each investigation has its own hierarchical decomposition of the hyporheic zone according to their study perspectives. Ecological studies centered on hyporheic exchange have defined spatial scales emphasizing the functional significance of the hyporheic zone at different scales. Scale approach has been used as a conceptual structure for the ecological investigations of a single-unit scale to the entire ecosystem (Boulton, 1998) to characterize the effects of surface-subsurface exchange at various scales and to examine interactions among them. There are limited attempts to establish a straightforward scale explanation for hyporheic research consistent with previously published scale approaches of stream systems. Table 2.1 represents scale hierarchical descriptions proposed for the hyporheic zone based on previously published literature. Boulton (1998) proposed three spatial scales to understand the interaction between fate and transport of processes occurring in the hyporheic zone; catchment, reach, and sediment scale. As noted in Dent et al. (2001), the general goal of defining scales is to study the hyporheic behavior in relation to stream morphology or morphology features at each scale (Table 2.1).

Table 2.1 Hierarchical descriptions proposed for the hyporheic zone.

Spatial dimension /m	1000-10000	100-1000	10-100	1-10	0.1-1
* Frissell et al. (1986)	Stream	Segment	Reach	Pool/riffle	Microhabitat
Dent et al. (2001)	Segment	Reach (constrained or unconstrained)	Channel unit (run, riffle or pool)	Channel sub-unit (boulders, logs, gravel bars, and plant hummocks)	Particle (bed form)
Ebersole et al. (2003)	Catchment	Segment	Reach	Habitat patch	Habitat unit

Stream water that infiltrates into the hyporheic zone generates shorter flow paths at ripples and dunes, moderate flow paths at pool-riffle and bars, and longer flow paths at the meander scale (Ebersole et al., 2003). Residence time distributions rely upon the length of hyporheic flow paths, which varies with scales. Hence, nitrogen attenuation and transformation processes can create spatially diverse patterns of nitrogen concentrations over distances of many kilometers to few centimeters (Bhaskar et al., 2012). As illustrated by Stonedahl et al. (2010), the average residence time of water in the hyporheic zone is proportional to the length of topographic feature and inversely proportional to the permeability of the sediment bed.

Azizian et al. (2015) have conceptualized hyporheic flow paths as a bundle of individual tubes that carry stream water into the sediment bed and back again to the stream channel performing as a biochemical reactor. When a water molecule is moving in a flow path, a set of parallel and series biogeochemical reactions take place. Stream water is initially with high oxygen and nitrogen concentrations. First, dissolved oxygen is consumed by nitrification and aerobic respiration processes and increase nitrate concentration along the hyporheic flow path. As dissolved oxygen is depleted and there is sufficient flow path length further, denitrification starts to remove nitrate produced by nitrification. Consequently, short hyporheic flow paths may be a source of nitrate to the stream, whereas longer paths would be a sink of nitrate caused by the increased residence time of water in the subsurface. Therefore, the residence times have to be long enough to perform the hyporheic zone as a natural nitrogen attenuation unit. (Lansdown et al., 2015) has highlighted the importance of using both biogeochemical reaction rates and residence time to valuation of nitrate removal, because ignoring residence time has miscalculated the nitrate removal.

2.2 Paper 1: Effect of multiple scales on nitrogen transformation in the hyporheic zone- A review

2.2.1 Abstract

The hyporheic zone is identified as a hot spot for nitrogen attenuation in fluvial systems. Therefore, understanding and modeling of dominant nitrogen transformation processes in this zone, their behavior, and critical controlling factors are vital in optimally designing streams (river restoration) as natural bio-filters to reduce excess nitrogen. However, hyporheic researchers are still looking for more understanding to make realistic predictions of nitrogen cycling in response to catchment management practices. Coupled reaction kinetics and physical transport are the two most significant factors that control nitrogen behavior in streams. Nitrification, denitrification, and aerobic respiration are the primary reactions considered in previous studies. Our findings suggest that ammonification (mineralization), anaerobic ammonium oxidation (anammox), dissimilatory reduction of NO_3^- to NH_4^+ (DNRA), and inorganic nitrogen assimilation into the plant or microbial biomass are also important reactions in the hyporheic sediments. Whilst hyporheic flow is known to occur at multiple spatial and temporal scales; including exchange through bedforms, bars, and meander bends, current nitrogen modeling approaches only represent reactions and processes in individual geomorphic features. In this research, we reviewed published residence times for different geomorphic features and compared them with nitrogen reaction times. Our findings suggest that bedforms always act as nitrate sources to the stream due to small residence time and bars and meanders can be nitrogen sinks due to longer path lengths and thus longer residence times, which allows complete transformations of nitrogen. However, interacting nitrogen transformations occur at multiple temporal scales and hence, at various residence times within the hyporheic zone. Therefore, we suggest that multi-scale representation and catchment scale predictions are required to model nitrogen cycling in the hyporheic zone.

Keywords. Hyporheic, nitrogen fate and transport, residence time, reaction time, multi-scale

2.2.2 Introduction

Over the last century, excessive application of nitrogen-based fertilizer on agricultural and pasture lands, improper management of landfill leachate and exhaust from cars and other internal combustion engines have approximately doubled nitrogen loads entering the environment including groundwater and surface water bodies and nitrogen loads continue to grow (Hoven et al., 2008, Kessler et al., 2012, Smil, 1999, Mazza et al., 2014, Zarnetske et al., 2012). Nitrogen is an essential element for stream ecology, especially for the growth of plants; however, serious environmental problems such as eutrophication and blue-green algal blooms occur when water bodies receive excessive nitrogen loads beyond their carrying capacity (Fields, 2004, Follett and Hatfield, 2001). Of the three forms of nitrogen generally occurring in stream ecosystems: ammonium (NH_4^+), nitrate (NO_3^-), and nitrite (NO_2^-) (Zhou et al., 2014); elevated concentrations of ammonium and nitrate are most common (Marzadri et al., 2011). Elevated ammonium levels can: increase chlorine demand; be toxic for fish; and result in eutrophication with excessive phytoplankton growth leading to depletion of oxygen (Lee et al., 2006, Omnes et al., 1996). Elevated levels of nitrate cause increased risks of methaemoglobinaemia (blue baby syndrome) in infants and cancer (Rivett et al., 2008) and environmental problems such as fast algal and aquatic growth of plants (Rivett et al., 2008, Saunders and Kalff, 2001, VanZomeren et al., 2013).

Recent research suggests that stream microbial processes are a leading means for attenuating nitrogen loads from stream water (Marzadri et al., 2012). The hyporheic zone, the subsurface region at sediment-water interface, where there is exchange of water between surface and subsurface (Buss et al., 2009), has a rich microbial community (Marzadri et al., 2012) and can be a particularly significant location for nitrogen processing (Mulholland et al., 2008, Sheibley et al., 2003). Dissolved pollutants enter into the hyporheic zone, interact with the sediment bed and its living microbial community with the possibility of longer contact time, are assimilated or transformed due to enhanced biogeochemical reactions and then transported slowly back to the stream channel (Boano et al., 2014, Sheibley et al., 2003). The consequent nitrogen transformations are controlled by both physical transport and biogeochemical reaction kinetics (Haggerty et al., 2002, Zarnetske et al., 2012), and there is an opportunity to enhance nitrogen removal capacity of streams by manipulating these controlling processes (Azizian et al., 2015).

The multi-scale nature of hyporheic flow in river channels has only recently been recognized in river modeling investigations (Cardenas and Wilson, 2007a, Boano et al., 2010c, Stonedahl et al., 2010, Gomez-Velez and Harvey, 2014) These scales are typically associated with different channel features, with longer flow paths and residence times generally associated with larger channel features (Boano et al., 2014, Stonedahl et al., 2010, Buss et al., 2009). Existing models representing the role of hyporheic flow in nitrogen transformation generally deal with exchange produced by a single channel feature type and scale (Boulton, 1998, Stonedahl et al., 2010, Painter, 2018) such as bedforms (Elliott and Brooks, 1997a, Elliott and Brooks, 1997b, Azizian et al., 2015, Cardenas and Wilson, 2007a, Wörman et al., 2007), bars (Zarnetske et al., 2015, Zarnetske et al., 2011) or meander bend (Cardenas, 2009b, Boano et al., 2006). Interacting effects of the exchange produced by different channel features (and hence scales) for nitrogen transformations have received little attention but are likely significant and should be addressed in models of nitrogen transformation through river networks (Gomez-Velez and Harvey, 2014, Painter, 2018, Stonedahl et al., 2010).

This study aims to provide an in-depth critical review of the available literature on nitrogen transformation processes in the hyporheic zone, their reaction times and how hyporheic exchange at different spatial and temporal scales impact on nitrogen cycling. Previous studies do not systematically report or synthesize the literature on hydraulic residence times and nitrogen reaction times. Multiple scales lead to complex patterns in hyporheic residence times, altering the rates of nitrogen biogeochemical reactions. This determines the hyporheic zone behavior as a source or sink of nitrogen across the entire river network. We analyzed residence times for different channel features and reaction times of biogeochemical processes to understand how residence time and reaction time interact with each other. We consider the proposition that a multi-scale representation is required for modeling the coupled hyporheic transport and nitrogen reactions in streams.

2.2.3 Nitrogen transformations in the hyporheic zone

2.2.3.1 Key nitrogen reactions occurring in the hyporheic zone

Modeling nitrogen transformations in the hyporheic zone generally requires some simplification to tackle the multiple interacting reactions and processes involved. In hyporheic zone nitrogen transformations include: ammonification (mineralization); nitrification (oxidation of ammonium to nitrate); denitrification (reduction of nitrate to nitrogen gas that harmlessly escapes to environment); nitrogen fixation; anaerobic ammonium oxidation (anammox); dissimilatory reduction of NO_3^- to NH_4^+; inorganic nitrogen assimilation into plant or microbial biomass; NH_3 volatilization; and NH_4^+ adsorption and desorption (Zhou et al., 2014). A variety of simplifications have been applied for modeling studies in literature (Azizian et al., 2015, Bardini et al., 2012, Hester et al., 2014, Hu et al., 2014, Kessler et al., 2013, Marzadri et al., 2011, Marzadri et al., 2012, Zarnetske et al., 2012). However, it is unclear which processes are dominant and hence, which simplification is justified. Conversion of ammonia and nitrate into gaseous nitrogen by nitrification and denitrification is the primary process considered in many models. In addition to these two main processes, nitrogen assimilation into microbial biomass (Marzadri et al., 2012) and ammonification (Azizian et al., 2015, Kessler et al., 2013, Zarnetske et al., 2012, Azizian et al., 2017) have been considered. However, recent experimental studies (Table 2.2) indicate that the hyporheic zone can be hotspots for other processes (ammonification, nitrogen assimilation into microbial biomass, anammox and Dissimilatory reduction of NO_3^- to NH_4^+) that have been neglected (Pinay et al., 2009, Wang et al., 2012, VanZomeren et al., 2013, Zhou et al., 2014, Bonin et al., 1998, Takeuchi, 2006, van den Berg et al., 2015). According to Zhou et al. (2014), biogeochemical reactions are strongly interconnected, neglecting one can affect the rates and overall predictions. Therefore, it is necessary to identify all critical processes and develop novel biogeochemical models incorporating their controlling factors and reaction rates.

Table 2.2 Nitrate reduction rates reported in field studies by other nitrogen processes except for nitrification and denitrification.

Process	Study	Site details		Reported rates
		Location	River bed sediment	
AM	(VanZomeren et al., 2013)	Coastal Louisiana	bayou sediment (low flow conditions)	14.8 ± 0.9 NH_4-N m^{-2} d^{-1}
			marsh soil (high flow conditions)	23.0 ± 4.1 NH_4-N m^{-2} d^{-1}
	(Garban et al., 1995)	River Seine, downstream from Paris	River sediment beneath WSI	13.4t d^{-1} (467 kg km^{-1} d^{-1})
	(Fernex et al., 1992)	Marica lagoon (Rio de Janeiro, Brazil)	Sand (Surficial sediments)	0.072 µmol cm^{-3} d^{-1}
NA	(Pinay et al., 2009)	Lynx Creek in Alaska, U.S.A.	Finer and coarse riparian soil	NA - 14mgNO_3^- -N L^{-1} DN - 4mgNO_3^- -N L^{-1}
DNRA	(Bonin et al., 1998)	Carteau Cove (French Mediterranean Coast)	Coastal marine sediment	DNRA - 2.3 - 83.2 µmol L^{-1} d^{-1} (40-100% of the total nitrate reduction) DN – 0 - 19.8 µmol L^{-1} d^{-1} (0-43% of the total nitrate reduction)
	(Lansdown et al., 2012)	River Leith, Cumbria, United Kingdom	a mixture of sand, gravel, and cobbles	below detection (< 1.9 nmol N g^{-1} to 20 nmol of N g^{-1}
ANA	(Zhu et al., 2013)	Baiyangdian Lake, North China	Superficial interface sediments	7–20 nmol N g^{-1} h^{-1} (11-35% of total nitrogen removal)
	(Meyer et al., 2005)	Logan/ Albert river system in Australia	Sediment cores	0.5-8 nmol N cm^{-3} h^{-1} (0-9% of total N_2 production in sediment)

DN - Denitrification, AM –Ammonification or mineralization, NA - inorganic nitrogen assimilation into plant or microbial biomass, DNRA - Dissimilatory reduction of NO_3^- to NH_4^+ and ANA – Anaerobic ammonium oxidation (ANAMMOX)

Ammonification is one of the important processes delivering nitrogen (NH_4^+) into the system and should be included in biogeochemical models (Garban et al., 1995, Azizian et al., 2015). Organic nitrogen ammonification often occurs in parallel with nitrification in aerobic regions of the hyporheic zone (i.e., downwelling zones) (Jones et al., 1995). Ammonification produces NH_4^+, and hence accelerates nitrification reaction rates (Holmes et al., 1994). Coupled nitrification and ammonification can decrease potential nitrogen reduction capacity by denitrification due to increased nitrate concentrations in downwelling zones of the hyporheic zone (VanZomeren et al., 2013).

NH_4^+, NO_3^- and NO_2^- assimilation by benthic biofilms and macrophytes plays a significant role in the hyporheic nitrogen cycle (Trauth et al., 2014, Marzadri et al., 2011, Marzadri et al., 2012, SWQMS, 2000, VanZomeren et al., 2013, Zhou et al., 2014). Nitrogen assimilation can either occur in aerobic or anaerobic regions of the hyporheic zone (Zhou et al., 2014). However, high nitrogen assimilation rates are observed near the exists of upwelling hyporheic flow areas (Fisher et al., 1998). Nitrogen assimilation is higher in meandering streams compared to straight channels (Fisher et al., 1998). In some studies, nitrogen assimilation accounts for a more substantial fraction of total nitrogen removal from the hyporheic zone compare to denitrification (Pinay et al., 2009).

DNRA is another source of NH_4^+ in the hyporheic zone upwelling regions, converting NO_3^- into NH_4^+. DNRA bacteria are commonly observed in anoxic conditions and low nitrate concentrations (Keslo et al., 1997). Several studies have observed the occurrence of DNRA in sediments and its competition with denitrification for NO_3^- (Bonin et al., 1998, Takeuchi, 2006, Storey et al., 2004, van den Berg et al., 2015).

ANAMMOX is one of the dominant nitrogen transformation processes in marine sediments (Aubeneau et al., 2015, Dalsgaard et al., 2003, Dalsgaard et al., 2005, Zhou et al., 2014, Zhu et al., 2013). Recent studies indicated that hyporheic sediments are also hotspots for the ANAMMOX process in removing nitrogen from stream ecosystems (Zhu et al., 2013, Wang et al., 2012, Meyer et al., 2005). ANAMMOX occurs under anaerobic conditions. Wang et al. (2012) provide experimental evidence for the coexistence of anammox bacteria in the hyporheic zone, which is important for hyporheic nitrogen removal.

Water is generally high in oxygen and nitrogen when it first enters into a hyporheic streamline. In downwelling zones, dissolved oxygen is consumed by nitrification which is expected to increase NO_3^- (nitrate) concentration along the hyporheic flow path while consuming NH_4^+ nitrogen. Organic nitrogen mineralization (Ammonification) also occurs in parallel with nitrification in aerobic regions of the hyporheic zone (Jones et al., 1995) providing NH_4^+ nitrogen into the system by consuming organic nitrogen compounds. Reduction of dissolved oxygen is also caused by the aerobic respiration of microorganisms in downwelling zones when they produce energy from organic carbon compounds. Therefore, in downwelling zones, rapid depletion of dissolved oxygen occurs along the hyporheic streamlines and given sufficient flow path length (i.e., residence time), conditions become anaerobic. Most of the nitrogen removal reactions occur in the resulting anaerobic zones such as denitrification and anaerobic ammonium oxidation, which convert nitrate and ammonia into nitrogen gas and inorganic nitrogen assimilation into the plant and microbial biomass (More details on these processes are given in section 3). Consequently, hyporheic flow paths with short residence times become a source of nitrate to the stream, whereas longer paths provide a sink for nitrate caused by the larger residence time for water/nitrate in the subsurface than the reaction times required for complete denitrification. Moreover, when anaerobic flow paths are not sufficiently long for complete denitrification, nitrous oxide (N_2O), a greenhouse gas emission occurs as an intermediate product of the denitrification reaction (Silvennoinen et al., 2008, Quick et al., 2016, Marzadri et al., 2014).

With the evidence from previous field studies, we propose a simplified conceptual model for the expected interactions of nitrogen reactions in the hyporheic zone (Figure 2.2). AM, NI, and NA occur in aerobic zones of the hyporheic zone while DN, DNRA, NA, and ANAMMOX occur in anaerobic zones of the hyporheic zone. DNRA, DN, NA, and ANAMMOX compete for substrate NO_3^- in the system under anaerobic conditions (van den Berg et al., 2015, Bonin et al., 1998, Takeuchi, 2006). Upwelling zones are likely locations for anaerobic reactions and downwelling zones for aerobic reactions in the hyporheic zone.

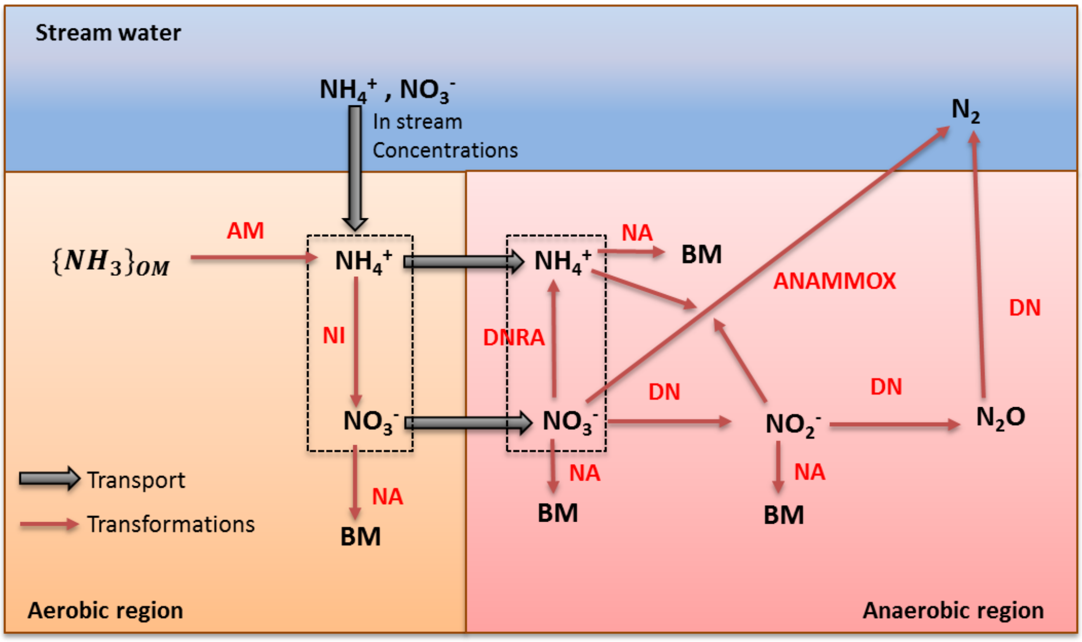

Figure 2.1 Expected interactions of nitrogen reactions in the hyporheic zone (BM- Living biomass).

NH_4^+, NO_3^- and oxygen are the two primary nitrogen substrates required for most biogeochemical reactions given that the carbon (DOC and POC) abandonly available. Therefore, the availability of NH_4^+, NO_3^- and oxygen would determine the occurrence of these processes (van den Berg et al., 2015), and limiting substrate concentration is a significant factor in kinetic rate models.

Table 2.3 Stoichiometric equations of nitrogen reactions occurring in the hyporheic zone and limiting substrate concentrations.

Nitrogen process	Reaction	Limiting substrate concentration	Aerobic/ Anaerobic
NI	$NH_4^+ + 2O_2 \rightarrow NO_3^- + 2H^+ + H_2O$	C_{O_2}> 2 mg L-1	Aerobic
DN	$0.8NO_3^- + 0.8H^+ + CH_2O \rightarrow 0.4N_2 + CO_2 + 6H_2O$	C_{O_2}< 2 mg L-1 $C_{NO_3^-}$ > 1 mg L-1	Anaerobic
AM	$\{NH_3\}_{OM} + H^+ \rightarrow NH_4^+$	C_{O_2}> 2 mg L-1	Aerobic
NA	$5CH_2O + HCO_3^- + NH_4^+ \rightarrow C_5H_7NO_2 + 4H_2O + CO_2$	-	Aerobic and Anaerobic
DNRA	$2H^+ + NO_3^- + 2CH_2O \rightarrow NH_4^+ + 2CO_2 + H_2O$	-	Anaerobic
ANAMMOX	$NH_4^+ + 1.31NO_3^- + 0.066HCO_3^- + 0.13H^+ \rightarrow 1.02N_2 + 0.26NO_3^- + 0.066CH_2O_{0.5}N_{0.15} + 2.03H_2O$	$C_{O_2} \leq$ 0.2 mg L-1	Anaerobic

(Carrera et al., 2003, Khin and Annachhatre, 2004, Kulikowska and Klimiuk, 2004, Metcalf and Eddy, 1991, Schmidt et al., 2003, Zhu et al., 2008, Azizian et al., 2015, Zarnetske et al., 2012, Boano et al., 2010b)

2.2.3.2 biogeochemical reaction times

Biogeochemical reaction time, the time required to achieve equilibrium concentrations varies for each of the nitrogen transformations listed in table 2.3. The travel time for water passing through the hyporheic zone (i.e., the hyporheic residence time) can limit the extent of reactions where it is less than reaction times. This is the critical interaction between physical transport processes and biogeochemical processes. If residence times fall well-short of reaction times, then transformations will be incomplete and hence sensitive to changes in hyporheic flow conditions. If residence times are in excess of the reaction times, then full transformation can be expected, and there will be limited sensitivity to altered hyporheic flow conditions. In this section, we estimate reaction times based on available model formulations for the restricted set of nitrogen processes that have received attention by modelers. However, there are other approaches used in the literature to calculate nutrient processing in the hyporheic zones such as use of biogeochemical reactions of organic carbon degradation (Boano et al., 2010b).

We analyzed reaction times for two processes; nitrification and denitrification for seven studies that have examined nitrogen dynamics in the hyporheic zone. These studies have used a variety of approaches to model the total biological reaction rates of oxygen (R_{O_2}), ammonium ($R_{NH_4^+}$,), nitrate ($R_{NO_3^-}$) and dissolved organic carbon (R_{DOC}) including variation in the choice model formulation and parameter values (Table 2.4 and 2.5). These models include linear kinetic equations, Monod kinetics, and empirical equations based on experimental data. Therefore, we have calculated nitrification and denitrification reaction times for each study using their kinetic model but for the same set of biogeochemical parameters (Table 2.5). Reaction times also vary with initial in-stream concentrations of nitrogen, dissolved oxygen, and organic carbon. Therefore, we used a generic set of initial concentration values for our simulations (Table 2.5) to align with the range of previous literature. Reaction times were simulated in two stages;

Stage 1 – Calculation of nitrification reaction time (T_1)

We have defined nitrification reaction time as the time required to reduce DO concentration in the hyporheic zone to nitrification, limiting DO concentration. Nitrification occurs under aerobic conditions and ceases when DO concentration depletes below a threshold defining anaerobic conditions. The threshold DO concentration in our analysis was assumed to be 2 mgL^{-1} – O_2 (Marzadri et al., 2011, Bardini et al., 2012, Rivett et al., 2008) when estimating nitrification time (T_1). We have also considered substrate (ammonia) availability as a limiting factor. When ammonia is no longer available, nitrification will stop before the system become anaerobic and T_1 becomes shorter.

Stage 2 – Calculation of denitrification reaction time (T_2)

Denitrification occurs under anaerobic conditions. For a given anaerobic environment, nitrate concentrations are the main limiting factor for denitrification reactions; therefore, the denitrification reaction time is defined as the time required to lower nitrate concentrations to an acceptable threshold. We use the threshold of 0.25 mgL^{-1}, which is the threshold above which the risk of adverse effects due to nitrogen concentrations will occur in freshwater systems (ANZECC and ARMCANZ, 2000).

Aerobic respiration and nitrification start concurrently at the beginning of hyporheic flow. Denitrification commences with the onset of anaerobic conditions. Therefore T_1 and T_2 were determined by the combined rate equations of nitrification, aerobic respiration and denitrification considering above mentioned limiting concentrations of oxygen and nitrate. The behavior of the flow path was idealized with Azizian et al. (2015)'s segregated streamline hypothesis with continuous flowing conditions. Chemical concentrations and kinetic model parameters for rate equations for hyporheic sediments are given in Table 2.5. Kinetic parameters tend to vary with temperature. However, in this study, we did not consider temperature effect (or seasonal effect) on reaction times and used mostly observed rate constants from previous models.

Table 2.4 Kinetic representation of nitrogen reaction rates occurring in the hyporheic zone according to previous literature.

Study	Formula			
	$R_{NH_4^+}$	$R_{NO_3^-}$	R_{O_2}	R_{DOC}
(Azizian et al., 2015)	2nd order kinetics $-k_{NI}C_{O_2}C_{NH_4^+}$	Monod kinetics $k_{NI}C_{O_2}C_{NH_4^+} - 0.05\left(\frac{K_{O_2}^{inh}}{C_{O_2}+K_{O_2}^{inh}}\right)\left(\frac{R_{min}C_{NO_3^-}}{C_{NO_3^-}+K_{NO_3^-}^{sat}}\right)$	Monod kinetics $-\frac{R_{min}C_{O_2}}{C_{O_2}+K_{O_2}^{sat}} - 2\,k_{NI}C_{O_2}C_{NH_4^+}$	-
(Bardini et al., 2013)	2nd order kinetics $-k_{NI}C_{O_2}C_{NH_4^+}$	Monod kinetics $-0.8k1_{DOC}C_{DOC}f_{DN} + k_{NI}C_{O_2}C_{NH_4^+}$ $f_{DN} = (1-f_{AR}).\begin{cases}\frac{C_{NO_3^-}}{C_{NO_{3,lim}^-}} if\ C_{NO_3^-} < C_{NO_{3,lim}^-} \\ 1\ if\ C_{NO_3^-} \geq C_{NO_{3,lim}^-}\end{cases}$	Monod kinetics $-k1_{DOC}C_{DOC}f_{AR,O_2} - 2k_{NI}C_{O_2}C_{NH_4^+}$ $f_{AR,O_2} = \begin{cases}\frac{C_{O_2}}{C_{O_{2,lim}}} if\ C_{O_2} < C_{O_{2,lim}} \\ 1\ if\ C_{O_2} \geq C_{O_{2,lim}}\end{cases}$	1st order kinetics $k1_{DOC}C_{DOC}$
(Hu et al., 2014)	Monod kinetics $-\mu_{NI}\left(\frac{C_{O_2}}{C_{O_2}+K_{O_2}^{sat}}\right)\left(\frac{C_{NH_4^+}}{C_{NH_4^+}+K_{NH_4^+}}\right)X_N$	Monod kinetics $-\mu_{DN}\left(\frac{C_{NO_3^-}}{C_{NO_3^-}+K_{NO_3^-}}\right)\left(\frac{C_{DOC}}{C_{DOC}+K_{DOC}}\right)\left(\frac{K_{O_2}^{inh}}{C_{O_2}+K_{O_2}^{inh}}\right)X_{DN}$ $+\mu_{NI}\left(\frac{C_{O_2}}{C_{O_2}+K_{O_2}^{sat}}\right)\left(\frac{C_{NH_4^+}}{C_{NH_4^+}+K_{NH_4^+}}\right)X_{NI}$	Monod kinetics $-y_0\mu_{AR}\left(\frac{C_{DOC}}{C_{DOC}+K_{DOC}}\right)\left(\frac{C_{O_2}}{C_{O_2}+K_{O_2}^{sat}}\right)X_{AR}$ $-(1$ $-y_0)\mu_{NI}\left(\frac{C_{O_2}}{C_{O_2}+K_{O_2}^{sat}}\right)\left(\frac{C_{NH_4^+}}{C_{NH_4^+}+K_{NH_4^+}}\right)X_{NI}$	Monod kinetics $-y_0\mu_{AR}\left(\frac{C_{DOC}}{C_{DOC}+K_{DOC}}\right)\left(\frac{C_{O_2}}{C_{O_2}+K_{O_2}^{sat}}\right)X_{AR}$ $-\mu_{DN}\left(\frac{C_{NO_3^-}}{C_{NO_3^-}+K_{NO_3^-}}\right)\left(\frac{C_{DOC}}{C_{DOC}+K_{DOC}}\right)\left(\frac{K_{O_2}^{inh}}{C_{O_2}+K_{O_2}^{inh}}\right)X_{DN}$
(Zarnetske et al., 2012)	Monod kinetics $-\mu_{NI}y_{NH_4^+}X_{NI}\left(\frac{C_{NH_4^+}}{C_{NH_4^+}+K_{NH_4^+}}\right)$ $\left(\frac{C_{O_2}}{C_{O_2}+K_{O_2}}\right)$	Monod kinetics + Michaelis-Menten kinetics $-\mu_{DN}X_{DN}\left(\frac{K_I}{K_I+C_{O_2}}\right)\left(\frac{C_{NO_3^-}}{C_{NO_3^-}+K_{NO_3^-}}\right)\left(\frac{C_{COD}}{C_{COD}+K_{COD}}\right)$	Monod kinetics $-\mu_{AR}X_{AR}y_0\left(\frac{C_{DOC}}{C_{DOC}+K_{DOC}}\right)\left(\frac{C_{O_2}}{C_{O_2}+K_{O_2}}\right)$ $-\mu_{AR}(1$ $-y_0)X_{NI}\left(\frac{C_{NH_4^+}}{C_{NH_4^+}+K_{NH_4^+}}\right)\left(\frac{C_{O_2}}{C_{O_2}+K_{O_2}}\right)$	1st order kinetics $k1_{DOC}k_dC_{DOC}$
(Kessler et al., 2012, Kessler et al., 2013)	2nd order kinetics $k_{NI}C_{O_2}C_{NH_4^+}$	Based on experimental data $R_{NO_3^-} = \begin{cases}0.05\theta^{inh}(0.392C_{NO_3^-} + 29.8\times10^{-6})\ if\ C_{NO_3^-} \geq C_{crit} \\ 0.05\theta^{inh}1.88C_{NO_3^-}\ if\ C_{NO_3^-} < C_{crit}\end{cases}$ $\theta^{inh} = \begin{cases}1\ if\ C_{O_2} \geq 2\,K_{O_2}^{inh} \\ \left(1-\frac{C_{O_2}}{2\,K_{O_2}^{inh}}\right) if\ C_{O_2} < 2\,K_{O_2}^{inh}\end{cases}$	Based on experimental data $-2k_{NI}C_{O_2}C_{NH_4^+}$ $-\begin{cases}0.392C_{O_2} + 29.8\times10^{-6}C_{O_2}\ if\ C_{O_2} \geq C_{crit} \\ 1.88C_{O_2}\ if\ C_{O_2} < C_{crit}\end{cases}$	Based on experimental data $R_{DOC} = \begin{cases}0.392C_{O_2} + 29.8\times10^{-6}C_{O_2}\ if\ C_{O_2} \geq C_{crit} \\ 1.88C_{O_2}\ if\ C_{O_2} < C_{crit}\end{cases}$
(Hester et al., 2014)	-	Monod kinetics $-\left(\frac{X_{DN}}{\theta}\right)(\gamma_{DN})(\mu_{DN})\left(\frac{C_{DOC}}{C_{DOC}+K_{DOC}}\right)\left(\frac{C_{NO_3^-}}{C_{NO_3^-}+K_{NO_3^-}}\right)\left(\frac{K_I}{C_{O_2}+K}\right.$	Monod kinetics $-\left(\frac{X_{AR}}{\theta}\right)(\gamma_{AR})(\mu_{AR})\left(\frac{C_{DOC}}{C_{DOC}+K_{DOC}}\right)\left(\frac{C_{O_2}}{C_{O_2}+K_{O_2}}\right.$	$-\left(\frac{X_{AR}}{\theta}\right)(\mu_{AR})\left(\frac{C_{DOC}}{C_{DOC}+K_{DOC}}\right)\left(\frac{C_{O_2}}{C_{O_2}+K_{O_2}}\right)$ $-\left(\frac{X_{DN}}{\theta}\right)(\mu_{DN})\left(\frac{C_{DOC}}{C_{DOC}+K_{DOC}}\right)\left(\frac{C_{NO_3^-}}{C_{NO_3^-}+K_{NO_3^-}}\right)\left(\frac{K_I}{C_{O_2}+K_I}\right.$
(Marzadri et al., 2011, Marzadri et al., 2012)	Monod kinetics $-k1_{NI}K_{NH_4^+}\left(\frac{C_{NH_4^+}}{C_{NH_4^+}+K_{NH_4^+}}\right)$	Monod kinetics $-k1_{DN}K_{NO_3^-}\left(\frac{C_{NH_4^+}}{C_{NH_4^+}+K_{NH_4^+}}\right) + k1_{NI}K_{NO_3^-}\left(\frac{C_{NH_4^+}}{C_{NH_4^+}+K_{NH_4^+}}\right)$	Monod kinetics $-(k1_{AR}+k1_{NI})C_{O_2}$	-

Where, C_{O_2}, $C_{NH_4^+}$, $C_{NO_3^-}$ and C_{DOC} are the steady-state concentration of dissolved oxygen, ammonium, nitrate, and dissolved organic carbon. R_{min} is the maximum respiration rate of sediment organic matter. k_{NI} is the bimolecular nitrification rate constant. $k1_{DOC}$, $k1_{NI}$, and $k1_{DN}$ are first-order rate constant for aerobic respiration, nitrification, and denitrification. k_d is the linear distribution coefficient. K_{O2}, K_{O2}^{inh}, K_{NO2}^{sat} and $K_{NH_4^+}$ are half-saturation constants for aerobic respiration, oxygen inhibition, denitrification, and nitrification. *KI* is the inhibition constant for the denitrification reaction. μ_{NI}, μ_{DN}, and μ_{AR} are maximum substrate utilization rate for nitrification, denitrification, and aerobic respiration. Υ_{DN} *and* Υ_{AR} are the use coefficient for denitrification and aerobic respiration. X_{NI}, X_{DN}, and X_{AR} are the biomass of nitrification functional group, denitrifiers, and aerobic respiration functional group. y_O *(–)* and y_{NH4+} are partition coefficient for aerobic respiration, and for nitrification. θ is the porosity of the sediment bed.

Table 2.5 Kinetic model parameters and in-stream concentrations of dissolved oxygen, ammonia, nitrate, and dissolved organic carbon used in the simulations.

Parameter	Values from literature	Source	Value used in the simulation
$k_{NI}[m^3mol^{-1}s^{-1}]$	3.96E-04, 2.78E-05, 3.96E-04	Azizian et al. (2015), Bardini et al. (2012), Kessler et al. (2012)	3.96 E-04
$k1_{DOC}[h^{-1}]$	0.018, 0.0002, 0.001	Bardini et al. (2012), Zarnetske et al. (2012), Marzadri et al. (2012)	0.018
$k1_{NI}[h^{-1}]$	0.144	Marzadri et al. (2012)	0.144
$k1_{DN}[h^{-1}]$	0.088, 0.094	Marzadri et al. (2012), Zarnetske et al. (2015)	0.094
$k_d[L^3kg^{-1}]$	50	Zarnetske et al. (2012)	50
$K_{O_2}^{inh}[mgL^{-1}]$	0.16, 0.1, 0.24, 0.16, 0.24, 1	Azizian et al. (2015), Hu et al. (2014), Zarnetske et al. (2012), Kessler et al. (2012), Hester et al. (2014), Gu et al. (2012)	0.16
$K_{NO_3^-}^{sat}[mgL^{-1}]$	2.48, 2.5, 1.64, 1.64, 1	Azizian et al. (2015), Hu et al. (2014), Zarnetske et al. (2012), Hester et al. (2014), Gu et al. (2012)	2.48
$K_{O_2}^{sat}[mgL^{-1}]$	1.28, 5.2, 5.28, 5.28	Azizian et al. (2015), Hu et al. (2014), Zarnetske et al. (2012), Hester et al. (2014)	1.28
$K_{NH_4^+}[mgL^{-1}]$	0.5, 0.43	Hu et al. (2014), Zarnetske et al. (2012)	0.5

$K_{DOC}[mgL^{-1}]$	10, 8.68, 8.68, 2	Hu et al. (2014), Zarnetske et al. (2012), Hester et al. (2014), Gu et al. (2012)	8.68
$K_I[mgL^{-1}]$	0.24, 0.24, 0.1, 1	Zarnetske et al. (2012), Hester et al. (2014), Hu et al. (2014), Gu et al. (2012)	0.24
$\mu_{NI}[h^{-1}]$	1.08, 1.08	Hu et al. (2014), Zarnetske et al. (2012)	1.08
$\mu_{DN}[h^{-1}]$	1.8, 3.98, 3.98	Hu et al. (2014), Zarnetske et al. (2012), Hester et al. (2014)	3.98
$\mu_{AR}[h^{-1}]$	1.8, 1.97, 1.97	Hu et al. (2014), Zarnetske et al. (2012), Hester et al. (2014)	1.97
$X_{NI}[gm^{-3}]$	5.0	Hester et al. (2014)	5.0
$X_{DN}[gm^{-3}]$	4.9, 0.32	Hester et al. (2014), Zarnetske et al. (2012)	4.9
$X_{AR}[gm^{-3}]$	5.0, 8.3	Hester et al. (2014), Zarnetske et al. (2012)	5.0
$y_0(-)$	0.64, 0.64	Hu et al. (2014), Zarnetske et al. (2012)	0.64
$y_{NH_4^+}$	0.4	Zarnetske et al. (2012)	0.4
γ_{DN}	1.65	Hester et al. (2014)	1.65
γ_{AR}	1.07	Hester et al. (2014)	1.07
θ	0.35, 0.3, 0.32	Hester et al. (2014), Bardini et al. (2013), Jones et al. (1995)	0.35
$C_{NO_{3,lim}^-}[mgL^{-1}]$	1.24, 0.5, 1.24	Azizian et al. (2015) ,Bardini et al. (2012), Kessler et al. (2013)	1.24
$C_{O_{2,lim}}[mgL^{-1}]$	1, 2, 4	Bardini et al. (2012), Rivett et al. (2008), Marzadri et al. (2012)	2
$R_{min}[mol\ m^{-3}s^{-1}]$	2.27E-05	Azizian et al. (2015)	2.27E-05
$C_{O_2}(0)\ [mgL^{-1}]$	8, 8, 10, 7.62, 7.04, 10, 7.7	Azizian et al. (2015), Gu et al. (2012), Hu et al. (2014), Jones et al. (1995), Kessler et al. (2013), Marzadri et al. (2012), Jones et al. (1995)	8
$C_{NO_3^-}(0)\ [mgL^{-1}]$	3.7, 10, 3.7, 8.8, 0.17, 3.1, 1.325, 0.17	Azizian et al. (2015), Gu et al. (2012), Hoven et al. (2008), Hu et al. (2014), Jones et al. (1995), Kessler et al. (2013), Jones et al. (1995)	3.7
$C_{NH_4^+}(0)\ [mgL^{-1}]$	0.09, 0.06, 0.05, 0.026, 0.374, 0.03	Azizian et al. (2015), Hoven et al. (2008), Hu et al. (2014), Jones et al. (1995), Marzadri et al. (2012), Jones et al. (1995)	0.09
$C_{DOC}(0)\ [mgL^{-1}]$	15, 4, 3.4	Gu et al. (2012), Hu et al. (2014), Jones et al. (1995)	15

$C_{O_2}(0)$, $C_{NO_3^-}(0)$, $C_{NH_4^+}(0)$ and $C_{DOC}(0)$ are the initial in-stream concentrations of dissolved oxygen, nitrate, ammonium, and dissolved organic carbon, respectively.

Several assumptions were made when simulating reaction times. We assumed that nitrates derived from nitrification and in-stream concentrations are both available for denitrification under anaerobic conditions. Nitrification and respiration rates are zero (i.e., the concentration of DO does not change along the streamline) after hyporheic streamlines became anaerobic. Reaction times were simulated, assuming steady-state hyporheic flow conditions. Table 2.6 provides simulation results for nitrification and denitrification times.

Table 2.6 Reaction times of nitrification and denitrification

Study	Reaction time (h)	
	T_1	T_2
Azizian et al. (2015)	2.79	28.71
Bardini et al. (2013)	8.33	17.78
Hu et al. (2014)	4.4	22.65
Zarnetske et al. (2012)	1.75	13.5
Kessler et al. (2012) and Kessler et al. (2013)	3.5	24.38
Hester et al. (2014)	0.45	3.5
Marzadri et al. (2011) and Marzadri et al. (2012)	8.5	44.1

We found that nitrification reaction times (0.45 -8.5 h) tend to be much smaller when compared to denitrification reaction times (3.5 – 44.1 h). Therefore, less time is required for the system to become anaerobic, while nitrogen removal reactions take a longer time.

However, reaction times vary considerably across different models, even though we have used the same set of kinetic parameters. Hence, we performed a sensitivity analysis using Monte Carlo simulation to explore variation in residence time with different biogeochemical models. We assumed that the T_1 and T_2 are normally distributed. We found that T_1 and T_2 could be described by 4.2 ± 3 hrs and 21.6 ± 12.4 hrs respectively.

2.2.4 Residence time distribution at different scales

Nitrogen transformation processes rely upon both physical and biogeochemical characteristics in the hyporheic zone. The total flux of dissolved nitrogen entering the hyporheic zone sets an upper bound on the rate of transformation along a stream reach, and residence time distributions within the hyporheic zone control the contact time and hence the extent of nitrogen transformation. The flux and residence times are regulated by hydraulic head gradients developed at the water-sediment interface (WSI), flow path length within the hyporheic zone, and bed sediment properties within the hyporheic zone (Zarnetske et al., 2012). At smaller scales, river water flow conditions, size and shape of bedforms features have been used as proxies to calculate hydraulic head gradient, while, riverbed slope, sinuosity, width to depth ratio (W/D), valley width and surface water storage capacity have been considered to impact pressure head gradients at larger scales (Buss et al., 2009). Characteristic residence times for water in the hyporheic zone is proportional to the length of the topographic feature and inversely proportional to the head gradient across these features (Stonedahl et al., 2013). Biochemical conditions affecting reaction kinetics include concentrations of dissolved oxygen (DO), organic carbon (DOC) and nitrogen species (NO_3^- ,NH_4^+, NO_2^- and N_2), pH, and temperature (Storey et al., 2004, Buss et al., 2009, Cirmo and McDonnell, 1997), which regulate microbial evolution and dominant interactions in the hyporheic zone. These interactions determine whether hyporheic zone could be a source or sink of nitrogen to the stream. A conceptual diagram (Figure 2.3) has been developed, linking critical elements discussed above.

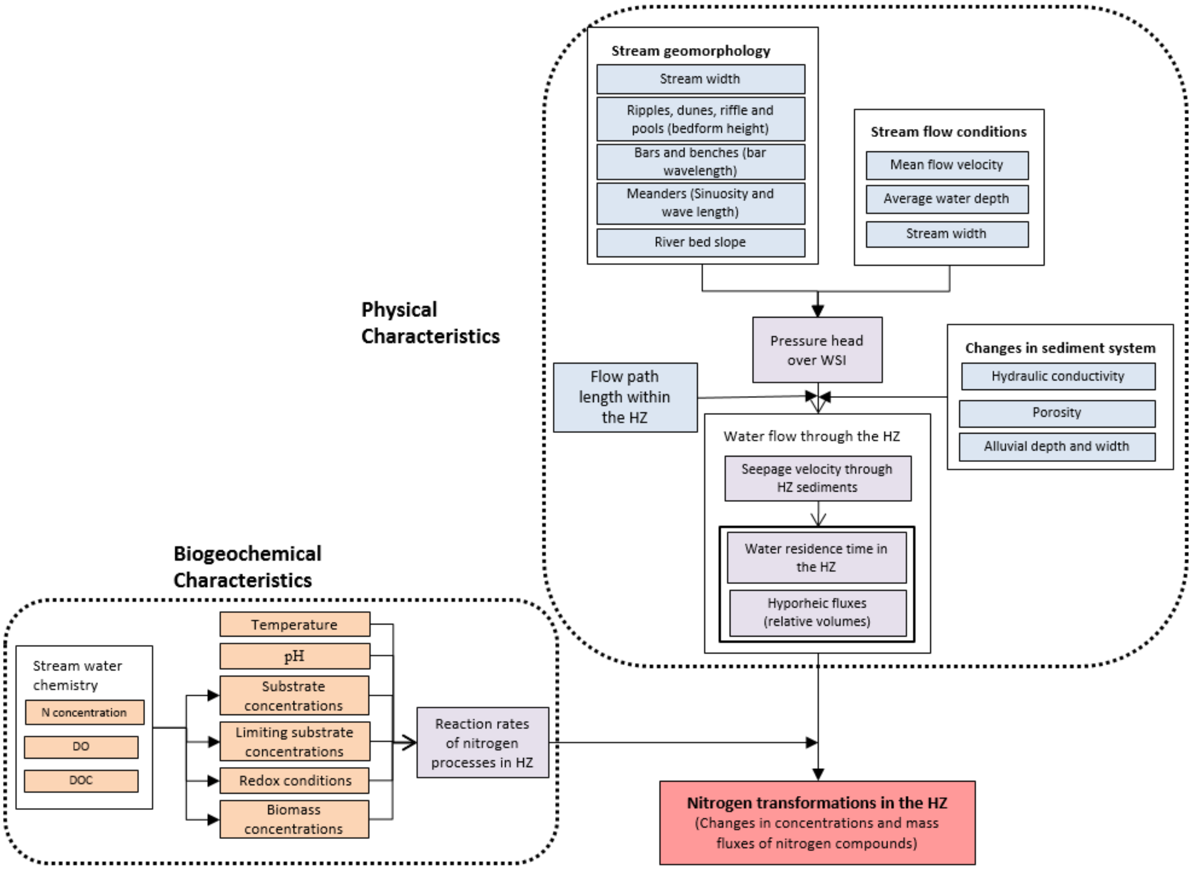

Figure 2.2 Conceptual diagram of key variables controlling water flow and nitrogen evolution in the hyporheic zone.

Furthermore, there are other factors such as chemical and physical heterogeneity that control the microbial community and hence the influence on biological nitrogen processing in the hyporheic zone. The composition and growth of microbial biomass is influenced by several physical metrics such as particle size, depth and distribution of benthic sediments (Parker et al., 2018, Boulton et al., 2010). Distribution of sediments can alter velocity and residence time of water and hence biogeochemical properties (supply of substrate and oxygen) within the sediment bed. This create variations in oxidation-reduction reaction potentials and diversity of microsites in hyporheic water (Briggs et al., 2015b, Parker et al., 2018) and hence affecting nitrogen reactions in the hyporheic zone. Furthermore, Sediment invertebrates and microorganisms affect porosity of the sediment bed affecting rates of metabolism and nitrogen cycle in the hyporheic zone (Zimmer and Lautz, 2015).

The residence time of water in the hyporheic zone relies upon the length of hyporheic flow paths. Hydraulic head gradients developed at the water-sediment interface (WSI) determines relative hyporheic water flux across the hyporheic zone. A wide range of river morphology features has been identified to influence hydraulic head gradients over WSI including vertical hyporheic exchange from river bedforms such as pool-riffle, ripples-dunes and emerged bars and lateral hyporheic exchange from river plan form features such as alternate bars and river meanders (Painter, 2018, Stonedahl et al., 2010, Buffington and Tonina, 2009, Tonina and Buffington, 2009). These individual geomorphic features could connect between upstream and downstream longitudinally through the channel, floodplain, and riparian zone, and vertically through subsurface sediments (Dent et al., 2001). Therefore, stream water that infiltrates into the hyporheic zone generates shorter flow paths (0-1m) at ripples and dunes, moderate flow paths (10-100m) at pool-riffle and bars, and longer flow paths (100-1000m) at the meander scale (Ebersole et al., 2003). Hence, nitrogen attenuation and transformation processes can create spatially diverse patterns over distances of many kilometers to few centimeters (Bhaskar et al., 2012).

This section examines how these spatial scales have been characterized and classified in the literature and current understanding of residence times associated with exchange at different spatial scales. We have analyzed published literature on individual scales and their associated residence times (Table 2.7 and Figure 2.4). Residence times in the published literature were extracted from conservative tracer experiments done in field and laboratory studies or numerical particle tracing using modeling studies. In the literature, it is common to study HE at individual geomorphic features, such as dunes and ripples, riffle-pool, alternate bars, and river meanders. However, there are several experimental studies examining hyporheic flow behavior at reach scales with several bedform structures such as riffle-pool sequences and emergent bars or reaches containing boulders, logs, and other colluvium deposits. Here we have extracted a sample of possible data from studies that reports residence time within the hyporheic zone. Table 2.7 summarises residence time for all these studied scales.

In order to put scales of hyporheic exchange into context, we define a characteristic length scale (hyporheic dimension) for each morphology feature (Table 2.7). For small scale studies, bedform wavelength was considered as the hyporheic dimension while bar wavelength was taken for alternate bar and meander morphology. The hyporheic dimension for river reaches were defined with straight distance along the river. All the river reaches considered in this study were associated with sequences of river bedforms.

Previous literature characterizes the residence time either as a range or as a single value (mean or median). Since our objective is to identify the temporal variation of hyporheic flow compared to the spatial dimensions, we have considered all these characteristic residence time values and then defined an approximate temporal region for each channel feature, as presented in Figure 2.4.

Table 2.7 Hyporheic residence times of various channel features.

Study	Dimension (m)	Residence time (h)	Bed material	Study	Channel feature	Average linear pore water velocity (m/h)
Azizian et al. (2015)	0.1	0.6	sediment from Port Phillip Bay, Melbourne	experimental (flume) and modeling study	Dunes	0.17
Hester et al. (2014)	0.914	0.24 - 2.4	coarse sand	modelling study	Dunes	3.81 – 0.38
Käser et al. (2013)	0.6	9	Represent gravels, cobbles or boulders	modeling study	Microforms	0.07
(Trauth et al., 2013)	10	0.7-19	Coarse gravel with sandy sediment fillings	modeling study	pool-riffle system	14.29 – 0.53
Burkholder et al. (2008)	120	11.76	Gravel	field study	mid-channel bar	10.2
	80	288	gravel	field study	point bar	0.28
	480	24960	Gravel	field study	lateral meander bar	0.0016
Zarnetske et al. (2011)	10	3.8 – 28.5	Gravel	field study	alternate bars	2.63 – 0.35
Zarnetske et al. (2012)	10	24.2	Gravel	modelling study	alternate bars	0.41
Zarnetske et al. (2015)	10	14.05	sand, gravel, cobbles & boulders	field study	alternate bars	0.71

(Trauth et al., 2015)	20	8.3	Gravel	Field and modeling study	mid-channel bar	2.41
Hu et al. (2014)	75	171.6	Gravel	modeling study	reach with macro forms	0.44
	75	34.32	Gravel	modeling study	reach with macro forms and microforms	2.19
Naranjo et al. (2015)	165	240-1080	sandy gravel	field and modeling study	reach with riffle-pool sequences	0.69 – 0.15
Hester and Doyle (2008)	30	480 – 960	gravel and cobble	field and modeling study	reach with in-stream geomorphic structures	0.063 – 0.031
Gooseff et al. (2003)	306.4	114.72	mixture of sand, gravel, cobbles, and boulders	field study	Reach with large boulders and logs	2.67
	212.2	86.39			Reach with step-pool/step-riffle morphology	2.46
	379.2	82.22-1116.67			Braided alluvial reach	4.61 – 0.34
Acuña and Tockner (2009)	5	5.52-21.36	limestone and flysch	field study	reaches with different flow path lengths	0.91 – 0.23
	15	34.8				0.43
	30	27.84-50.4				1.08 – 0.6
	50	14.4-27.6				3.47 – 1.81
	120	42-48.72				2.86 – 2.46
	130	21.6-52.32				6.02 – 2.48
	80	24.96-70.8				3.21 – 1.13
	120	23.04-90.99				5.21 – 1.32
	125	30.48-68.64				4.1 – 1.82
Osenbrück et al. (2013)	120	72 - 199.2	sandy gravel	field study	Meander	1.67 – 0.6
Pinay et al. (2009)	2 - 15	0.17 – 7.5	Gravel	field study	Meander	11.76 – 2
Hoven et al. (2008)	70	1440	clayey, sandy silt deposit	field and modeling study	Meander	0.049

Observed residence times vary over orders of magnitude with a positive correlation between temporal and spatial dimensions, which also vary over several orders of magnitudes (Figure 2.4). This creates a nested system of hyporheic flow paths with lengths from several millimeters to kilometers and residence from minutes to years. Similar synthesis analysis have been reported by Boano et al. (2014), and my compilation verifies their work by using previously reported residence time distributions. Small bedforms such as dunes provide shorter residence times (ranging from several minutes to few hours). Alternate bars yield a higher range of residence times (ranging from several hours to months) and meander yield the longest residence time (from days to years). Residence times at meanders sometimes overlap with bar morphologies as the higher sinuosity meanders shorten the hyporheic flow paths.

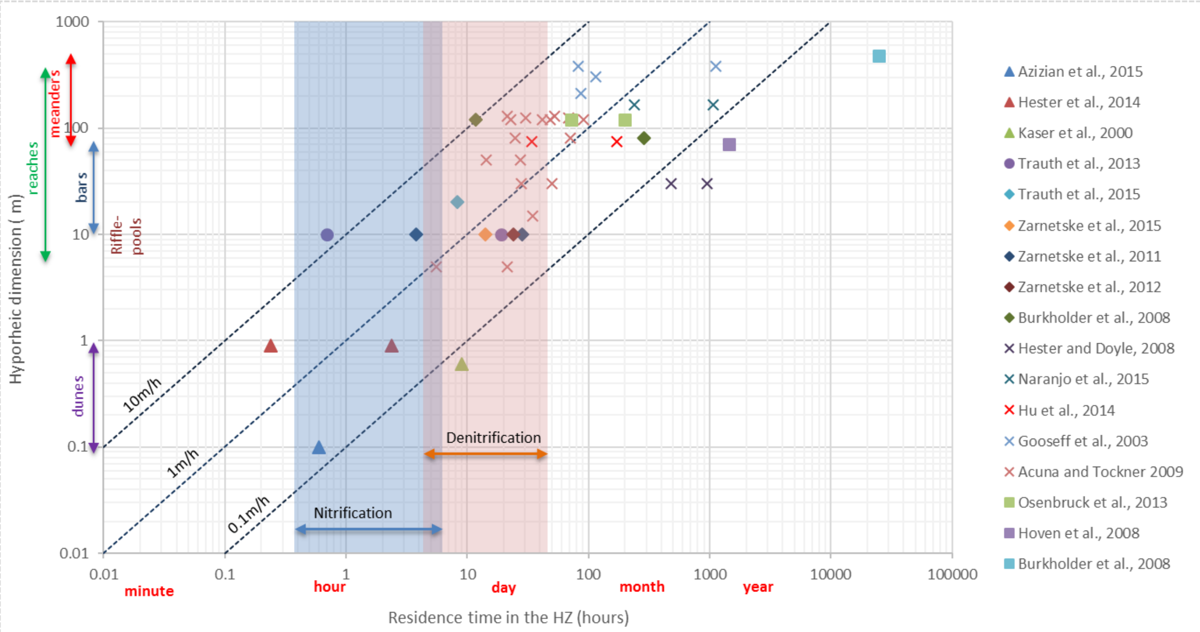

Figure 2.3 Hyporheic residence times discretized by different scales based on previous literature. Blue area and orange area respectively represent the reaction times of nitrification and denitrification calculated in section 3.1. Dashed lines show the velocity of 0.1 m/h, 1 m/h and 10 m/h. Residence time data for dune morphology were extracted from laboratory flume systems only. Other river scale/ features represent data from either lab or field systems.

Comparing residence times (Table 2.6) for different channel features and reaction times for nitrogen transformation processes, we observed that the bedform features (dunes and bars) are potential nitrate sources to the stream as the residence time is insufficient for complete denitrification to occur (Figure 2.4). Meanders facilitate more significant residence times, which can support the complete denitrification. Therefore, meanders are potential nitrogen attenuation spots. Some bars may provide sufficient residence time for complete nitrogen removal, while some may result in incomplete denitrification, which could lead to N_2O released to the environment. However, the hyporheic exchange is characterised by a distribution of residence time that can favor several reactions at the same time and hence nitrogen potential of a morphology. This study has used a single value of residence time and not the best descriptor for biogeochemical estimations.

Though hyporheic flux is also an essential factor for the extent of nitrogen reactions, there is not enough published data available for flux (or pore water velocities) associated with these scales. Therefore, we have defined pore water velocities (Table 2.7 and black dashed line in Figure 2.4) as the hyporheic dimension of the channel feature divided by the characterized residence time, which are not very accurate but provide a sufficient basis for comparison. Bedforms and bars bring maximum pore water velocities (10 m/h – 0.1 m/h) into the hyporheic zone while meanders yield smaller velocities (<1 m/h) into the hyporheic zone. This result is in agreement with Gomez-Velez and Harvey (2014), showing that bedforms yield more significant fluxes per unit length of channel (equivalent to velocity and has the unit of velocity) compared to bars and meanders. Therefore, the relative contribution of scales on nitrogen transformations may vary due to the supply limitation of the substrate for nitrogen reactions.

Whilst the size of channel features has substantial control over residence times; other factors can also be important. In particular, observed variations in residence time for channel features of similar length may be due to changes in pore water velocity due to differences in riverbed hydraulic conductivity, or pressure gradients. Riverbed hydraulic conductivity can be spatially very heterogeneous (Stewardson et al., 2016), affecting pore-water flow in the hyporheic zone. Therefore, the residence times should be further modified by the hydraulic conductivity of the sediment bed and head gradient.

2.2.5 Interactions across scales

The hyporheic literature suggests that the range of spatial scales at which exchange occurs varies from individual grains to entire river valleys. We argue that the various nitrogen reactions can be associated with a particular spatial scale, with larger-scale processes generally producing longer flow paths and hence, longer residence times. In this section, we discuss how residence times interact with nitrogen reaction times to understand the importance of different spatial scales.

We conceptualize the effect of different channel features and their associated residence time and reaction time of nitrogen transformation processes in the hyporheic zone (Figure 2.5). All potential nitrogen transformation processes discussed in section 2.1 have been considered. It is assumed that both nitrate and ammonia will be available in the stream water when water first enters hyporheic streamlines.

Ammonia concentration (dashed line in Figure 2.5(b)) is expected to decrease along aerobic regions due to nitrification and further in anaerobic regions due to ANAMMOX and plant and microbial uptake. Ammonia produced by ammonification reaction will be consumed by nitrifying microorganisms in aerobic areas, and ammonia produced by DNRA in anaerobic areas will be consumed by ANAMMOX reaction. Nitrate concentration (dotted line in Figure 2.5 (b)) is expected to increase in the aerobic zone due to nitrification. All nitrate attenuation reactions (i.e., denitrification, anaerobic ammonium oxidation, and inorganic nitrogen assimilation into the plant and microbial biomass) occur in anaerobic regions of the hyporheic zone; therefore, nitrate concentration will decrease in anaerobic regions (Figure 2.5). Production of dinitrogen gas (solid line in Figure 2.5 (b)) starts when the hyporheic zone becomes anaerobic and will reach an equilibrium when residence time exceeds reaction times.

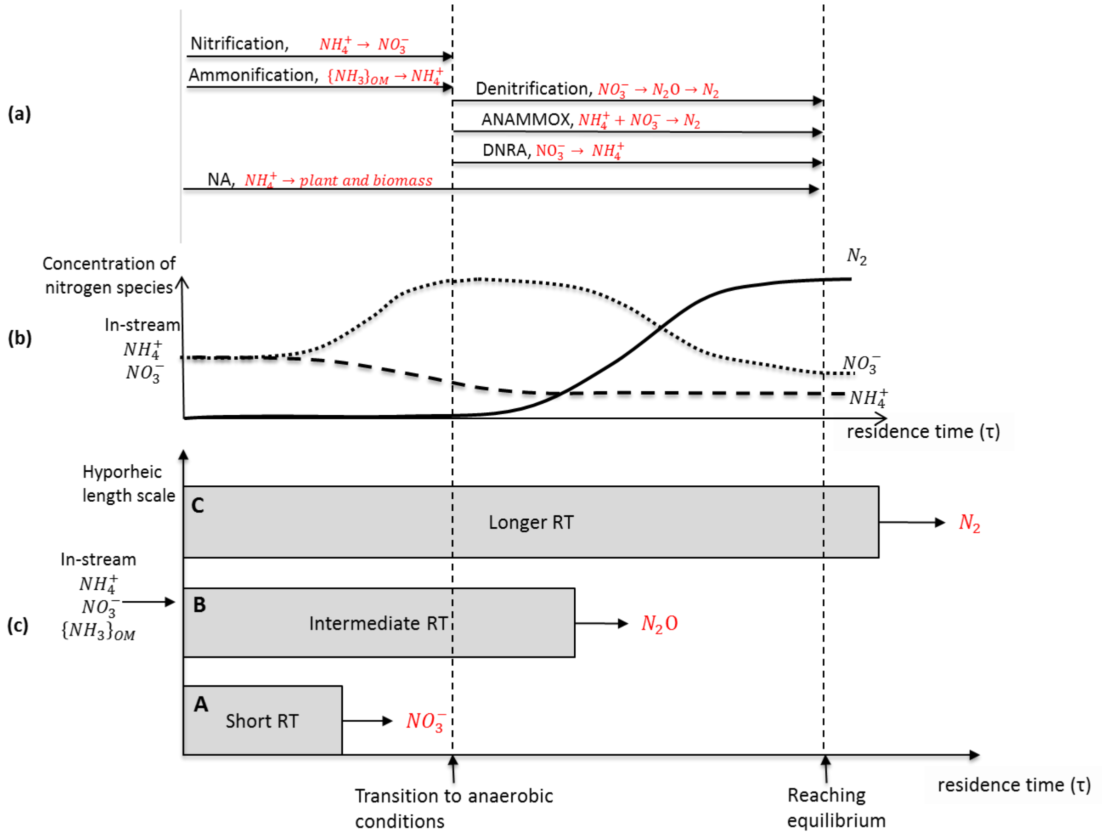

Figure 2.4 Effect of different scales and reactions on nitrogen evolution in the hyporheic zone. Residence time on the horizontal axis denotes the travel time of water entering the hyporheic zone, and the first vertical dashed line shows the transition of the aerobic region into the anaerobic region. (a) corresponding nitrogen reactions (basic conversions are given in red). (b) Predicted variation of nitrogen species along streamline with respect to the residence time (modified after (Zarnetske et al., 2011)). (c) Hyporheic length scales and their corresponding residence times.

Following this conceptualization, we hypothesize that the existence of a channel feature with optimum conditions (Residence time > Reaction time) is required for nitrogen removal reactions to occur (C in figure 2.5). Larger channel features (and hence longer residence times) provide sufficient time for nitrogen attenuation reactions. For smaller channel features where residence time is small relative to reaction times of complete aerobic and anaerobic reactions, the nitrogen removal capacity will be limited by reaction rates (A in Figure 2.5). Under these conditions, shorter residence times keep hyporheic streamlines always under aerobic conditions promoting nitrification and thus more nitrate into the stream. When flow paths are long enough for complete aerobic reactions but not sufficient for full anaerobic reactions, it will result in nitrous oxide (N_2O) emissions into the environment due to incomplete denitrification reaction (Quick et al., 2016). From the residence time distribution for each scale/ stream features, we can conceptualize dunes being A in Figure 2.5(c) with shorter residence times, alternate bar being B in Figure 2.5(c) with intermediate residence times and meanders being C in Figure 2.5(c) with longer residence times. However, permeability of the hyporheic zone will also affects the residence time and hence nitrogen transformation potential. At lower permeability, residence time will be higher and also less nitrogen will be supplied to the streambed, and a supply limitation will be encountered within the streambed, reducing the streambed's denitrification capacity. At higher permeability conditions, longer travel distances will be required to achieve anaerobic conditions; the anaerobic zone will therefore contract towards the upwelling region, and the transformation capacity of the streambed will be reduced.

2.2.6 Discussion

Hyporheic exchange models have generally been limited to specific scales or individual geomorphic features. For example, several modeling frameworks have only been developed for hyporheic exchange across rectangular dunes, ripple pool sequences, emergent bars, and meanders. Even though this understanding has provided a great insight into nitrogen cycling in the hyporheic zone, little has been done to understand nitrogen transformation behavior produced by superposition of exchange at multiple scales and at basin scales. There are a few physically-based models; NEXSS (Gomez-Velez and Harvey, 2014), MSM (Stonedahl et al., 2013, Stonedahl et al., 2010) and Lateral HE throughout the Mississippi River Network (Kiel and Bayani Cardenas, 2014) developed to study HE occurring at multiple scales. Integrating nitrogen transformation processes with such models remains a significant challenge. However, a recent study by Painter (2018) provides excellent insight for modeling multicomponent reactive transport in rivers with respect to multiple scales.

The hyporheic zone can be a source or a sink of nitrate depending on the time the water parcel spends in the sediment bed (residence time), demand for biological nitrogen, availability of required substrates, and abiotic factors such as pH and temperature. Zarnetske et al. (2012) and

Mazza et al. (2014) showed that the net nitrate source and sink function of the hyporheic zone is primarily a function of water residence times and oxygen uptake rates. Application of PASS model (Azizian et al., 2015) in a variety of freshwater and marine systems demonstrated that river bedforms are almost always net sources of nitrate to the system due to short residence times. Even though lateral HE (via alternate bars and meander bends) does not contribute much for the net fluid flux, it has a favorable residence time distribution for denitrification (Kiel and Bayani Cardenas, 2014). In-stream water chemistry also has a considerable influence on nitrogen cycling in the hyporheic zone. The hyporheic zone could perform as a strong nitrate sink in a nitrogen-rich agricultural stream (Hill et al. (1998); Storey et al. (2004)).

As discussed in section 4, the residence time and thus, the hyporheic flow lengths of channel features have a significant effect on the nitrogen transformation. However, along a river, there would be interactions across these channel features. These may connect with stream and with other channel features laterally and vertically and can exert variation in nitrogen evolution along the stream. It is to be expected that the flux-weighted distribution of residence times over all channel features are essential in determining how these reactions interact to produce trends in forms of nitrogen through the channel and hence supply of different nitrogen forms to the sediments (Figure 2.5).

We propose a hypothesis that, if flux through short residence time units (typically bedforms) is high relative to prolonged residence time units (typically river meanders), then nitrate concentrations can be expected to climb. If flux through long RT units is large relative to short RT units, then the nitrate concentrations can be expected to decline. Either way, it is the flux through long residence time units that will regulate the extent of denitrification as a mechanism of nitrogen removal. If this is low relative to Q/W (river discharge divided by channel width), then not enough water passes through the streambed to have much influence on the stream nitrogen concentrations.

This review shows that previous field, experimental, and modeling studies have targetted single channel features, either a small scale bed form or larger scale stream meander. We observed that though the physical understanding of hyporheic flow has stepped forward to include multiple scales, the coupled understanding of nitrogen transformations in the hyporheic zone is still constrained to a single geomorphic feature. One of the central problems is to identify the most appropriate scale to model nitrogen dynamics in the hyporheic zone.

The residence time of water in the hyporheic zone determines whether the hyporheic zone acts as a sink or a source of nitrogen. In this study, we synthesized residence time distribution with reaction times. The temporal and spatial regions of geomorphic features were studied in order to see how they impact on nitrogen transformations. Our study finding suggested that bedforms are potential sources of nitrate into streams and associated with more significant hyporheic fluxes, which could provide more frequent nitrate into the stream. Even though meanders are likely hot spots for nitrogen removal, relative contribution for total nitrogen reduction could be low as meanders are associated with smaller pore water velocities. Water fluxes into the hyporheic zone would determine the amount of substrate available for nitrogen reactions in the hyporheic zone. Therefore relative flux across different geomorphic features is potentially the critical factor that determines nitrogen transformation potential over a river reach containing several geomorphic features. The difference in fluxes and hence the supply of nitrogen into the hyporheic zone may impact on overall nitrogen transformation processes. Further studies are required to quantify the relative contribution of various scales in river catchment scales.

2.2.7 Conclusions

This literature review argues that nitrogen cycling in the hyporheic zone must be understood as a multi-scale system. The hyporheic exchange occurs over a wide range of geomorphic features with widely varying residence time distributions and pore water flux, and reaction times for the different nitrogen transformation also vary significantly. The topographic structure of a stream can be complex, and interactions between various scale features could result in complex hyporheic flow conditions, hence nitrogen attenuation potential.

Understanding significant microbial transformations of nitrogen in hyporheic sediments is critical to the removal of excess nitrogen from streams. There is no well-defined agreement on a biogeochemical model that is applicable in stream hyporheic zone. In previous studies, many of the nitrogen transformation processes have been neglected without any apparent justification, even though they are observed to have a significant impact on the field in river sediments. Nitrification and denitrification have been the main processes studied in the last two decades of hyporheic research history. However, there are other processes (ammonification (mineralization), anaerobic ammonium oxidation (anammox), dissimilatory reduction of NO^{3-} to NH^{4+} (DNRA), and inorganic nitrogen assimilation into the plant or microbial biomass) that play important roles in the hyporheic sediments.

Coupled physical transport and reaction kinetics control the nitrogen cycling in the hyporheic zone. A greater understanding of these processes and their interaction will be important for the design of river restoration measures to enhance streams function as natural biological filters for pollutants such as excess nitrogen. However, the interaction between physical aspects and stream nitrogen dynamics are poorly understood, and there is no clear mechanistic representation at larger scales such as a watershed or a catchment. This literature review reveals gradual advancements in physical flow models while there are still significant gaps in coupled understanding.

2.3 Hyporheic exchange in meandering channels and knowledge gaps

Over the last few decades, studies have focused on understanding the hyporheic flow occurring at various channel scales/ features; including bedforms, alternate bars, and meanders, as discussed in section 2.1. However, we observed that meandering morphology as an important scale for nitrogen biogeochemical reactions to ensure the complete transformation of ammonia and nitrate to harmless nitrogen gas. Several studies have examined hyporheic flow in meandering rivers with field experiments (Fossing et al., 2004, Burkholder et al., 2008, Hoven et al., 2008, Osenbrück et al., 2013) and provide evidence of longer residence times at meander bends through field tracers and temperature profiles.

Several mathematical models have also been developed to explain the hyporheic flow in meanders based on physical principles. Most of these are two-dimensional numerical models that neglect any vertical flow (Boano et al., 2006, Cardenas, 2009a, Gomez et al., 2012, Goldman et al., 2017). Cardenas (2008a) model captures two-dimensional behavior of hyporheic flow in meandering streams due to lateral HE. This model considers the hydrostatic head when calculating the pressure distribution along the WSI. Recently, several three-dimensional numerical models have also been developed to describe hyporheic flow in meandering rivers to examine water flow fields (Fossing et al., 2004, Balbarini et al., 2017, Pescimoro et al., 2019, Stonedahl et al., 2013, Stonedahl et al., 2010). However, all these studies use the river head gradient (based on the river valley slope) as the primary driver of the hyporheic flow. Even though its well known that hyporheic flow at small scale topographic features is typically characterized by river hydraulics (Boano et al., 2013, Cardenas and Wilson, 2007a, Chen et al., 2015, Tonina and Buffington, 2007, Tonina and Buffington, 2011), meandering rivers have not been studied considering river flow conditions. Additionally, natural meandering rivers are comprised of point bars at the inner bank of meanders spanning from one side to the other (creating riffles and pools) and associated secondary currents within the channel due to meandering curvature. These features are likely to produce significant vertical hyporheic flow in addition to lateral flow, contrary to the assumptions used for two-dimensional modeling.

Boano et al. (2010a) has been the first to study hyporheic flow induced by the meandering channels considering surface flow and meandering morphology. This study highlights the existence of vertical flux due to the point bar morphology. However, this theoretical understanding requires field or laboratory validation in order to confirm the nature and extent of exchange processes happening in the hyporheic zone of meandering channels. There is no published research based on laboratory investigation of hyporheic flow characteristics driven by river meanders.

Furthermore, in section 2.1, we argue that hyporheic flow behavior needs to be understood at the catchment scale. This requires a well-defined characterization of residence times and flux at each scale of interest. Even though residence and flow characteristics are well defined for dune-like bedforms (Cardenas and Wilson, 2007b, Cardenas et al., 2008, Elliott and Brooks, 1997a, Elliott and Brooks, 1997b), fully submerged pool-riffle morphology (Marzadri et al., 2010) and for partially submerged pool-riffle morphology (Tonina and Buffington, 2007, Tonina and Buffington, 2011), there is a need for further analysis and characterization of these properties for meanders.

2.4 Overall aim and research questions

Based on the above-mentioned research gaps in available literature, my PhD research is aimed **to identify the primary mechanisms that drive hyporheic flow in meandering rivers and model hyporheic flow field within meanders and apply this model to establish the impacts of meandering morphology and river flow conditions on water flux and residence time distribution in the hyporheic zone**. This overall aim will be achieved through a series of specific research questions listed below:

1. How meandering wavelength, stream discharge, and slope affect the residence time distribution (RTD) in the hyporheic zone?
2. What are the processes driving hyporheic flow in meandering streams?
3. How meandering morphology impacts flux and RTD in meandering streams?
4. How does meandering morphology impact hyporheic nitrogen cycling?

Chapter 3: Stream meander wavelength affects hyporheic residence time: Implications for nitrogen processing

Chapter three presents the research methodology, results, and discussion to answer research question one (How meandering wavelength, stream discharge, and slope effect on the residence time distribution (RTD) in the hyporheic zone?) of my Ph.D. research and is presented as a journal article (Paper 2). I have used a comprehensive experimental approach based on a range of conservative tracer experiments conducted in a recirculating flume. There are no previous laboratory simulations performed to estimate residence time distributions in river meandering morphology, as most laboratory analyses are restricted to small scale topographic features such as dunes and riffle-pools. Laboratory experiments were conducted at the University of Melbourne, Burnley campus by varying channel discharge, meander wavelength and channel slope. Experimental channels present three-dimensional morphology. Additional details on experimental apparatus including physical dimensions, sediment properties, and experimental design, are demonstrated in the method section of the paper. Experimental results demonstrated that the hyporheic exchange (solute residing time and interfacial water flux into the surface) through meanders are primarily influenced by channel flow rates and meander wavelength. To better understand the interactions of channel flow and characteristics of the meandering morphology, we require a more detailed understanding of processes occurring in the hyporheic zone. The sound findings of these laboratory experiments motivated me to develop a model for meandering streams, which is my second research question.

Paper 2: Stream meander wavelength affects hyporheic residence time: Implications for nitrogen processing

3.1 Abstract

The hyporheic zone has been identified as an important region for removing excess nitrogen loads from rivers and wetlands. Of the many geomorphic features that contribute to hyporheic flow, meanders are particularly crucial for these biogeochemical reactions. Meanders provide longer residence times, which can support more significant improvements in water quality than any other channel feature. However, residence times of meander-driven hyporheic flow is poorly understood. We conducted a set of flume experiments to investigate the impact of meander wavelength and discharge on solute transport. Experimental meanders were created as low gradient sand bed rivers with three-dimensional meander morphologies extending over a range of wavelengths and discharges. Residence time distributions and water fluxes into the bed were estimated from an advective pumping model, and breakthrough curves of a conservative tracer (Rhodamine WT) added into the surface flow. A comparison of the observed residence time distributions demonstrated that both discharge and meander wavelength affect the residence time distribution. However, hyporheic flow is most affected by advection. The average residence time is proportional to the wavelength and inversely proportional to the stream discharge. This study presents the first laboratory analysis of solute transport through meandering streams. Meander induced hyporheic flow exhibits similar behavior as bedforms and alternate bars in the field where flow and channel morphology controls water transport into river sediments. Changing stream velocity and meander wavelength affect residence times and water flux into the sediment bed, hence affecting rates of biogeochemical reactions. These findings can potentially be incorporated into river restoration practices to design rivers as natural nitrogen filters. This study represents a step forward for the analysis of large-scale channel features and their residence times, which are less understood in hyporheic literature but are very important for biogeochemical cycling in rivers. Our results show that the meander wavelength has a major effect on hyporheic residence time, demonstrating the importance of this little-studied aspect of channel structure. Most importantly, the channel flow rate affects residence time highlighting the importance of considering river hydraulics in modeling hyporheic flow through meanders.

Keywords: meandering rivers, hyporheic flow, residence time, downwelling flux, flow rate, wavelength, sinuosity

3.2 Introduction

Human activities are increasing the rate at which nitrogen compounds enter water bodies (Evrard et al., 2012, Hoven et al., 2008, Zarnetske et al., 2012, Galloway et al., 2008). Even though nitrogen is an essential element for ecological life, many adverse effects arise when water bodies receive excessive amounts, including blue-green algal blooms, eutrophication, emission of greenhouse gas (N_2O), and toxic on fish other aquatic life (Fields, 2004, Follett and Hatfield, 2001). Catchment-scale interventions to reduce nitrogen delivery rates, such as the construction of riparian buffer, can be costly. Therefore, major research and management practices are essential to promote the processing and removal of nitrogen in streams.

Hyporheic zones of rivers, saturated sediment layer where exchange of surface and subsurface water happens, provide significant benefits to the river ecosystem, especially for the natural nitrogen removal processes of streams (Azizian et al., 2017, Bardini et al., 2012, Dahm et al., 1998, Gomez-Velez and Harvey, 2014, Marzadri et al., 2014, Pinay et al., 2009, Zarnetske et al., 2012). Portion of the river water continuously circulates through the hyporheic zone and gets longer contact times with sediment biota and microorganisms. This flow occurs due to the hydraulic head gradients at the water-sediment interface (Boano et al., 2014). Different geomorphic features are associated with varying pressure gradients and flow path lengths, hence the time that water flux spends in the hyporheic zone. From many different geomorphic features that contribute to HE, such as ripples, dunes, riffle-pools, meanders, and alternate bars, our previous study suggested that meanders provide sufficiently long residence times, which is essential for nitrogen biogeochemical cycling (Chapter 2).

Residence time and flux are the key variables controlling the biogeochemical capacity of the hyporheic zone (Boano et al., 2010a, Boano et al., 2010b, Cardenas, 2008b, Gomez-Velez et al., 2017, Marzadri et al., 2011, Tonina and Buffington, 2007, Zarnetske et al., 2011). However, there is a lack of understanding about how meanders influence the residence time and water flux into the hyporheic zone. Even though several previous experimental and modeling studies (Azizian et al., 2017, Cardenas et al., 2008, Cardenas and Wilson, 2007a, Cardenas and Wilson, 2007b, Elliott and Brooks, 1997a, Elliott and Brooks, 1997b) focus on HE occurring at small scale features like bedforms; there is lack of studies investigating residence time through meanders. A few mathematical models and laboratory experiments have dealt with meandering morphology, but they do not provide a reasonable explanation for meander induced hyporheic flow behavior (residence time distributions and flux). Stonedahl et al. (2010) conducted a flume experiment with meandering morphology, but this experiments only measures variations in the hydraulic pressure at the water-sediment interface.

Hyporheic flow through meanders are known to be driven by river sinuosity and valley slope of the river considering meanders as large channel features (Cardenas, 2009a, Stonedahl et al., 2010, Tonina and Buffington, 2011). Flow is controlled by the gravitational variations induced by water depths. Given the importance of the channel curvature (sinuosity), river velocity could also exert a significant effect on the hyporheic flow. The literature reports generation of secondary currents in rivers due to the channel curvature, which could change subsurface hydraulics as well. Apart from that, the meander wavelength is also an important parameter that determines the size of the river. Therefore, it is crucial to improve our understanding of how these factors influence water flow through the hyporheic zone of meandering streams. The objective of this study was to examine the hyporheic exchange and associated residence time distributions of solute in the hyporheic zone of meandering streams (low gradient sand bed streams) for a range of wavelengths and discharge.

To achieve this objective, we performed a series of dye tracer experiments in a recirculating flume with meandering morphology. We introduced a known amount of Rhodamine WT as a conservative tracer to the flume channel to capture surface subsurface solute exchange by measuring tracer decay rates. Twelve experiments were carried out spanning over a range of meander wavelengths, discharge, and river slopes.

3.3 Hyporheic flow experiments through meandering rivers: laboratory tracer experiments

We conducted 12 conservative tracer experiments in a recirculating flume with uniform flow conditions to examine the effect of meander morphology (wavelength and sinuosity) and river discharge on residence time distribution in the hyporheic zone of meandering rivers. The experiments included three different planform geometries, two meandering channels of varying wavelengths, and a straight channel. Channel slope and flow rate were varied across each of the four experiments for each of the three channel planforms (Table 3.1).

Table 3.1 Channel morphology and hydraulic characteristics of experiments. The average velocity at the outlet was calculated from the flow rate and the cross-sectional area at the outlet. Meandering planform characteristics are defined in Figure 3.2. Sinuosity is the ratio between channel length and the flume length.

	Wavelength λ, (m)	Amplitude A, (m)	Sinuosity λ/L	Flow rate (L/s)	Slope	Average velocity at the outlet (m/s)
Exp1	2.4	0.4	1.23	0.95	0.0033	0.06
Exp2	2.4	0.4	1.23	1.12	0.0033	0.07
Exp3	2.4	0.4	1.23	1.5	0.0033	0.10
Exp4	1.7	0.2	1.1	0.44	0.0033	0.03
Exp5	1.7	0.2	1.1	0.74	0.0033	0.05
Exp6	1.7	0.2	1.1	1.5	0.0033	0.10
Exp7	Straight	-	1	0.44	0.0033	0.03
Exp8	Straight	-	1	0.74	0.0033	0.05
Exp9	Straight	-	1	0.44	0.0058	0.10
Exp10	Straight		1	0.74	0.0058	0.05
Exp11	2.4	0.4	1.23	1.5	0.0058	0.10
Exp12	1.7	0.2	1.23	1.5	0.0058	0.10

3.3.1 Experimental setup

3.3.1.1 Flume setup and morphology generation

The experiments were conducted in a recirculating flume, 13.6m long, 1.6m wide, and 0.6m deep (Figure 3.1) at the University of Melbourne, Burnley campus. The experimental sediment bed was 12m long, which was five times the maximum experimental meander wavelength, and the average sediment depth was 0.5m. The flume also had an upstream tank (0.6m long, 1.6m wide and 0.6m deep) to deliver water into the channel smoothly by reducing turbulence at the upstream end and a downstream tank (1m long, 1.6 wide and 0.6m deep) to receive water from the channel and act as a sediment trap to protect the pump. The width of these tanks was reduced in order to reduce the mixing time of the Rhodamine tracer (see below) outside of the sediment bed. Effective widths of upstream and downstream tanks are 0.7m and 0.8m respectively. A water level control unit (TUNZE 5017) in the downstream tank of the flume compensated for water losses through evaporation to maintain a constant water volume through the experiment. A V-notch flow meter attached at the end of the flume was used to measure the discharge rate of the flume.

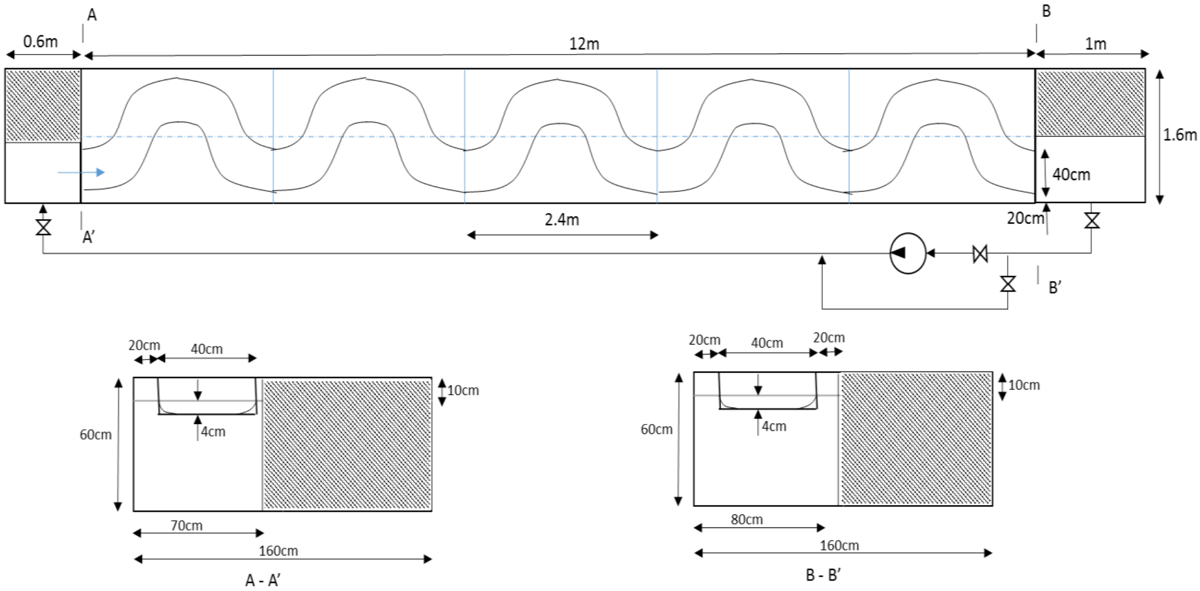

Figure 3.1 Schematic diagram of the flume, including flow rate controlling arrangement.

The sediment bed was constructed using filter sand with a median grain size of 1.37mm (Table 3.2). The sand's hydraulic conductivity was measured using a constant head permeameter in the Geotechnical laboratory at The University of Melbourne and determined to be 0.11cm/s. The sand's porosity was 0.39.

Table 3.2 Grain size distribution (% retained).

Sieve (mm)	Portion of sand by mass (%)
>3.35	0.0
3.35 – 2.8	1.4
2.8 – 2.35	5.8
2.35 – 2.0	9.5
2.0 – 1.7	14.2
1.7 – 1.4	30.3
1.4 – 1.18	23.7
1.18 – 1.0	6.2
< 1.0	8.6

The experimental set-up in this study are designed to represent natural low gradient meandering channels with a regular sequence of meander bends. The channel was created in two steps, firstly a meandering channel was excavated in the sediment bed, and water was recirculated through the flume with a higher velocity than the selected experimental flow conditions that might mobilize sediments on the bed. The objective of this step was to create more natural planforms.

Published relationships between riverbed slope, discharge, channel cross-section, meander wavelength, and amplitude were considered when designing the experimental conditions. The two riverbed slopes and the corresponding discharges used in our experiments (Table 3.1) were selected based on Lane, 1957's threshold values for meandering streams to sustain the meandering morphology; $0.004Q^{-0.25} > S > 7 \times 10^{-4}Q^{-0.25}$. We used these relationships combined with Manning's equation to determine the channel width, depth, discharge, and slope for each experiment. The average channel width was 40cm, and the average channel depth was 4cm, creating a depth to width ratio of 10.

The primary characteristics of meanders (i.e., Wavelength, sinuosity, and amplitude) were designed based on meandering river planforms studies by Stonedahl et al. (2010) and Leopold and Langbein (1966). We used 2.4m and 1.7m meander wavelengths with 0.4m and 0.2m amplitudes respectively (Table 3.3)

Table 3.3 Planform dimensions.

Width, W /m	0.4		
Meandering morphology	1	2	3
Wavelength, λ /m	2.4	1.7	Straight
Amplitude, A /m	0.4	0.2	0
Belt width, W_b /m	1.2	0.4	0.4
Sinuosity, J	1.23	1.1	1

The shape of the meanders were developed using a sine-generated curve method (Mecklenburg and Jayakaran, 2012, Mohamad et al., 2015). Equations for the radius of curvature (R) and arc angle (θ) are as follows:

$$R = \frac{\lambda\, J^{1.27}}{16.34\sqrt{\sqrt{J}-1}} \quad \text{(eq 1)}$$

$$\frac{\theta}{2} = \cos^{-1}\left(\frac{16R^2-8AR+\lambda\sqrt{4A^2-16RA+\lambda^2}}{4A^2-16RA+\lambda^2+16R^2}\right) \quad \text{(eq 2)}$$

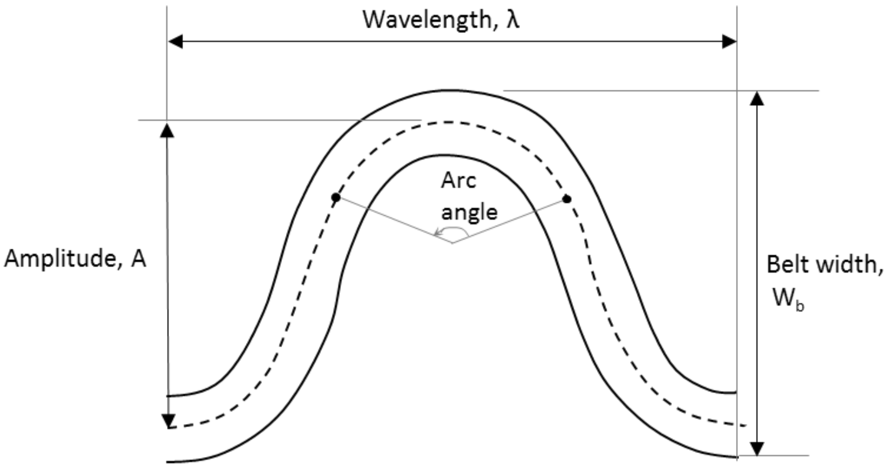

Figure 3.2 Meandering planform (Williams, 1986) (Mecklenburg and Jayakaran, 2012, Mohamad et al., 2015).

The sand bed was molded into pre-designed meandering channel shapes for each experiment using wooden templates (Figures 3.3). The slope of the sediment bed was created by grading the sand with a wooden block on top of two sidebars that had already been fixed to the flume walls with the required slopes (Figure 3.3).

Meandering shapes of the channel were crafted by hand using plywood templates for the desired cross-sections and planform shapes. The channels were initially constructed using a uniform trapezoidal cross-section with a bankfull width of 40cm and a depth of 4cm.

Figure 3.3 Construction of meandering morphology using wooden structures.

A FARO Scanner was used to measure the bed morphology of the flume to enable us to use real bed geometry in the model as well as to compare results with other studies such as Stonedahl et al. (2010). The flume was emptied before taking scans. Four high-resolution scans were taken for each experiment from four directions in order to capture hidden edges from each side. The scans were merged together in FARO software to get a final scan of the sediment bed. Unnecessary parts were removed, and the final scan was meshed in CloudeCompare.

A manual point gauge was used to measure water depth elevation for each discharge and channel shape. These measurements were taken along 15 longitudinal transects across stream widths placed with 50cm spacing.

3.3.1.2 Dye tracer experiments

Rhodamine WT, a conservative tracer, was used to estimate volumetric flux across the sediment-water interface and residence time distribution for solutes within the sediment bed. Dye concertation was recorded every minute in the downstream tank using Stainless Steel Cyclops-7 Rhodamine WT Optics to measure Rhodamine WT concentration change in each experiment. Rhodamine WT was introduced into the channel in two places in order to create the same concentration of Rhodamine in tanks and channel water as quickly as possible. We introduced Rhodamine at the downstream end of the flume and at the upstream tank; at the second location, we used manual mixing to ensure complete mixing. The concentration of Rhodamine was continuously monitored until it approached equilibrium concentrations, typically 3-4 days.

(a) (b)

Figure 3.4 (a) example of a tracer experiment (b) scanned bathymetry of the channel bed (2.4m meander wavelength, 0.8m amplitude, and 0.74 l/s discharge).

3.3.2 Analytical development and calculation of hydraulic residence time distribution and flux from tracer experiments

3.3.2.1 Calculation of residence time distribution and mass transfer

The residence time distribution (RTD) is very important for biogeochemical reactions occurring in the sediment bed. Water parcels exhibit nested flow pathways in the sediment bed and will exit the bed at different time intervals. Therefore, there is a distribution of residence times in the sediment bed. This can be expressed as a probability density function $E(\tau_f)$. τ_f is the final age of a water parcel when it exists in the sediment bed. The quantity $E(\tau_f)d\tau$ is the fraction of water exiting the sediment bed that has spent between t and $t + d\tau$ time in the bed. In hyporheic literature, a cumulative distribution function $\bar{R}(\tau)$ of the RTD is mostly used and defines the fraction of water that remains in the bed after an elapsed time τ.

The net mass transfer into the hyporheic zone is calculated using the residence time function, $R(\tau)$, used by Elliott and Brooks (1997b), defined as the fraction of solutes entering into the stream bed at time t = 0 that remain in the bed after an elapsed time τ. The net mass transfer into the streambed, $m(t)$, is a function of residence time, $\bar{R}(\tau)$ which is the averaged $R(\tau)$ over the whole sediment bed. Relationship among $m(t)$ and $\bar{R}(\tau)$ can be given as Elliott and Brooks (1997b);

$$m(t)C_0 = \bar{q} \int_0^t \bar{R}(\tau)\, C(t-\tau)\, d\tau \qquad \text{(eq 3)}$$

Where $m(t)$ is defined as the mass accumulation per unit plan area of the stream bed divided by the initial concentration, C_0 and has the dimensions of length. Also, $\bar{q}$ is the average water flux into the sediment bed and C_0 is the initial in-stream solute concentration. $C(t-\tau)$ is the concentration of in-stream solute at time $(t-\tau)$.

The net mass transfer to the sediment bed is also related to the average solute penetration depth into the stream bed through a simple mass balance (Salehin et al., 2004) as;

$$C^*(t) = \frac{d\prime}{d' + m(t)\,\theta} \qquad \text{(eq 4)}$$

d' is the total volume of recirculating water in the flume per unit bed surface area (effective depth). θ is the porosity of the sediment bed. $C^*(t) = C(t)/C_0$ is the normalized in-stream solute concentration at time t.

Rearranging the above equations, we arrive at the bellow expression for average cumulative residence time distribution,

$$\bar{R}\ (t) = L^{-1}\left\{\frac{L\left\{\frac{d'}{\bar{q}}\left[\frac{1}{C^*(t)}-1\right]\right\}}{L\{\ C^*(t)\}}\right\} \qquad \text{(eq 5)}$$

The breakthrough curves of tracer concentration measured in flume experiments were used to determine the average cumulative residence time distribution ($\bar{R}(t)$) function and the net mass transfer into the bed using the above relationships. This was solved using Wolfram Mathematica.

We observed that solute breakthrough curves $C^*(t) = C(t)/C_{start}$, (where C_{start} is the initial Rhodamine concentration in stream water) of our flume experiments follow an exponential decay distribution. Therefore, when calculating experimental RTDs, we have first fitted solute breakthrough curves with an exponential decay function. The fitted curve was with two decay rates as shown in the expression below,

$$C^*(t) = (1 - C^*_\infty)[ae^{-k_1 t} + (1-a)e^{-k_2 t}] + C^*_\infty \qquad \text{(eq 6)}$$

Where, C^*_∞ is equilibrium concentration, a is the mixing factor and k_1 and k_1 are first and second exponential decay rates, respectively.

The fitted breakthrough curves of tracer concentration measured in flume experiments were then used to determine the average cumulative residence time distribution ($\bar{R}(t)$) function using the relationship in equation 5.

3.3.2.2 Calculation of hyporheic flux into the sediment bed

The flux of solute entering the sediment (q) is required to calculate residence time distribution from flume tracer experiments. q is the volume flux into the sediment bed. In an ideal scenario, the interfacial flux can be determined by the slope of the concentration decay curve at t=0 (Salehin et al., 2004). At this point, the concentration of tracer in the surface water is maximized, and the concentration of tracer in the subsurface is zero.

Thus, the quantity of tracer concentration transferred into the sediment bed (downwelling) in the first instance represents the actual flux of water to the hyporheic zone. However, at this movement, water trapped in the bed comes back to the channel (upwelling), affecting solute breakthrough curves. Therefore, the slope of the concentration decay curve at t=0 does not exclusively represent the concentration loss due to hyporheic flux and requires further calibration. The interfacial flux calculated based on the concentration decay data represents the maximum possible flux where no other exchange processes are occurring, and the actual flux value is likely to be lower. Therefore, we applied a trial and error approach to calculate the actual flux to the sediment bed. First, we started with the flux as the value of the slope of the breakthrough curve at t=0. Then the cumulative residence time distribution was calculated using this value. We already know that at t=0, the cumulative distribution function should equal to 1 as none of the solutes has entered the sediment bed. Therefore, the flux value was iterated until the cumulative residence time distribution curve started at 1 using Wolfram Mathematica and used that flux value for further research.

3.4 Results

3.4.1 Residence time distributions

The exchange of solutes at the water-sediment interface happens in two stages (Figure 3.5). Solutes are passed through the bed to the channel rapidly at the beginning of each experiment, but the exchange rate decreases comparatively over time (Figure 3.5). More than 50% of the solute exchange happens within this initial rapid exchange phase. The remainder of the exchange happens slowly until the surface and subsurface water reach equilibrium.

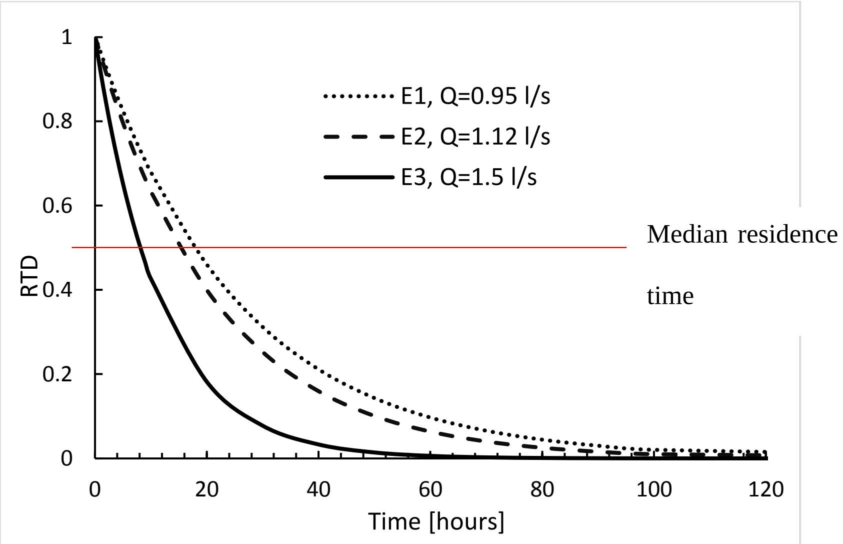

Figure 3.5 Average residence time distribution of Rhodamine in the sediment bed for different channel flow rates for the meander wavelength of 2.4m and the slope of 0.0033. Red continuous line shows the median residence time.

We observe that increasing the river discharge reduces the length of time solutes remain in the subsurface for all the meander topographies used (Figure 3.6(a-c)). Higher discharges produce comparatively rapid initial exchange, and hence large fraction of solutes are associated with shorter residence times. This is similar to previous results found for flume studies with dune-riffle morphologies; (Elliott and Brooks, 1997a, Salehin et al., 2004) due to the advection pumping induced by dynamic pressure gradient. However, in meandering channels higher velocity induces larger warping of the water surface (superelevation) at the bed and hence increase in piezometric head. Therefore, there are larger fraction of solutes that are associated with shorter residence times.

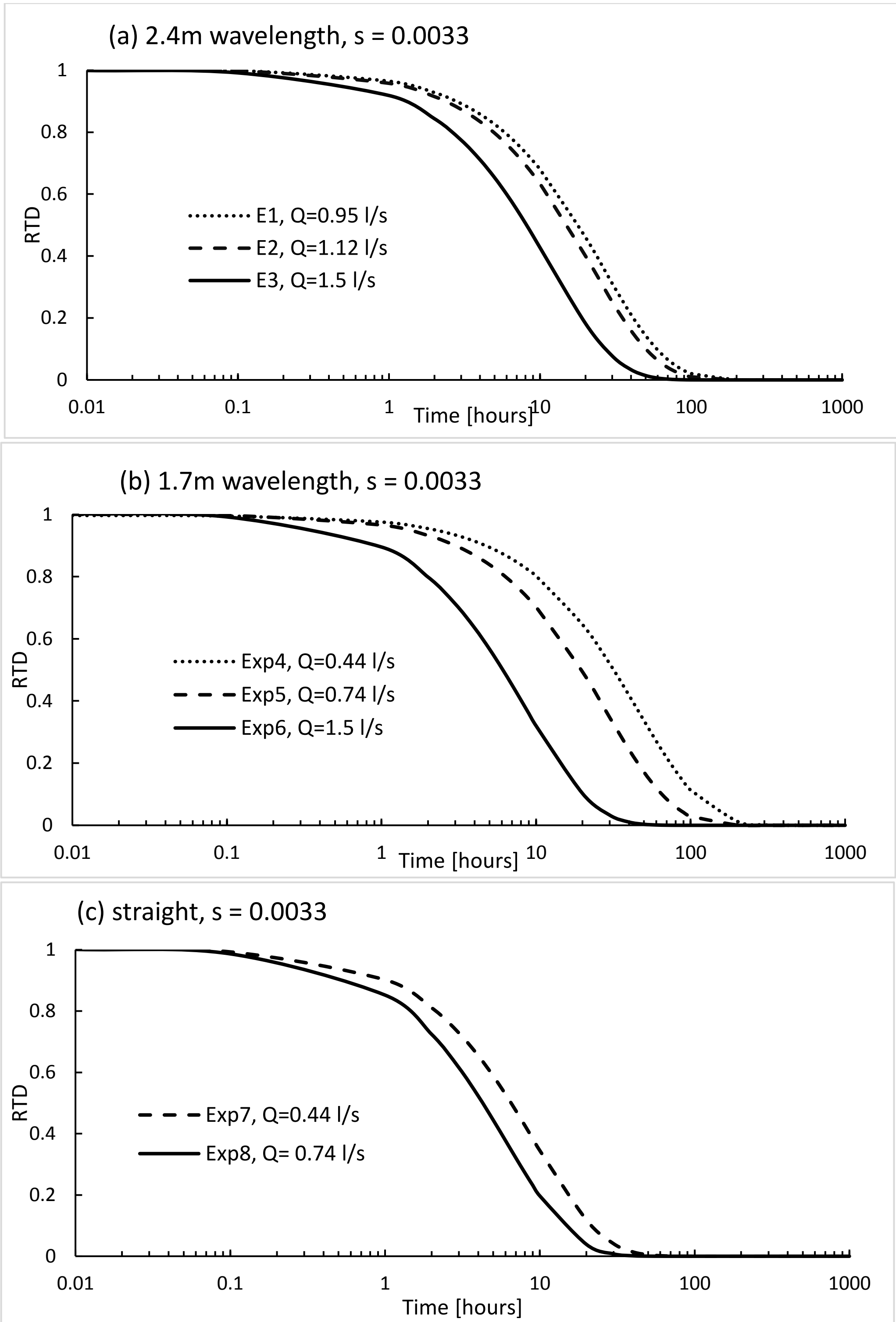

Figure 3.6 Average residence time distribution of Rhodamine in the sediment bed for different channel flow rates grouped according to the meander wavelength (a) 2.4m wavelength (b) 1.7m wavelength and (c) straight channel.

Increasing the river slope decreases the residence time of solutes remaining in the subsurface (Figure 3.7). This is due to the increased hydrostatic pressure acting on the stream bed. The relative size of the meanders is large, and hence water surface would exert variation in water depths and static pressure acting on the stream bed.

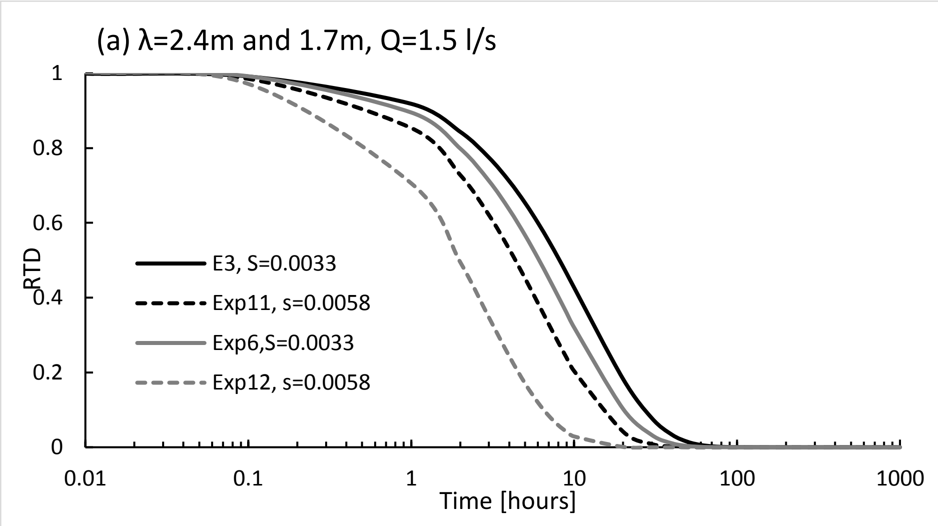

Figure 3.7 Comparison of average RTDs with different slopes, but with same channel shapes and flow conditions.

The effect of meander wavelength on RTD can be found by comparing experiments 3 to 6, 4 to 7 and 5 to 8, all of which were performed at the same flow rates and channel slopes but with different meander wavelengths (Figure 3.8). Meander wavelength has a substantial impact on hyporheic residence time. Water spends longer times in the sediment bed when meander wavelengths are large. For a given discharge, an increase in wavelength increases the length of water flow paths between meanders and hence, the residence times. In contrast, for a given wavelength, an increase in sinuosity decreases the distance between meander peaks and flow path lengths, decreasing solute residence times. Even though the meandering planform with 2.4m wavelength has a high sinuosity of 1.23 compared to 1.1 for the wavelength 1.7m case, the distance between meanders is large for wavelength 2.4m. Experiments 7 and 8 were straight channels with frequent dunes on the bed and shorter residence times compared to experiments 4 and 5 with a wavelength of 1.7m (Figures 3.8(b) and 3.8(c)). This is due to the high number of short flow paths that would accelerate the surface water mixing with the sediment bed.

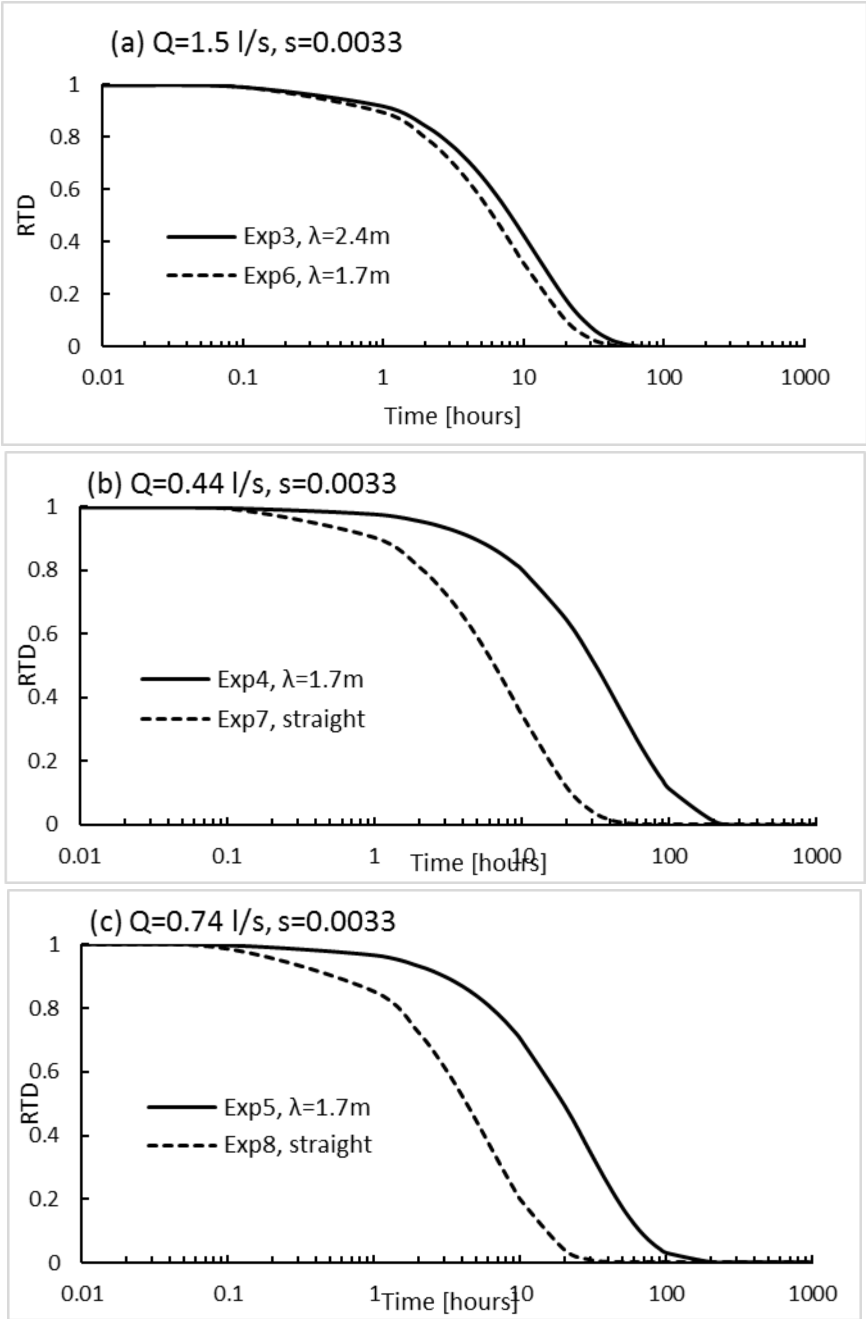

Figure 3.8 Average residence time distribution of Rhodamine in the sediment bed for different channel planform morphologies grouped according to the channel flow rates (a) 1.5 l/s flow rate (b) 0.44 l/s flow rate and (c) 0.74 l/s flow rate.

3.4.2 Interfacial downwelling water fluxes into the sediment bed

Interfacial water flux represents total water volume that comes into the sediment bed per unit time per unit volume. Interfacial water flux values for all twelve tracer experiments are summarised in Figure 3.9. This represents how channel discharge, meander wavelength, and channel slope effect on downwelling water flux.

Downwelling flux increases with an increase in river flow rate and slope (Figure 3.9). The experimental results do not show a very clear relationship between meandering morphologies and average downwelling flux (Figure 3.9). However, in general, I have observed higher downwelling fluxes for wavelength 2.4m compared to that of wavelength 1.7m. However, more experiments with varying meandering wavelengths are required to better conclude the influence.

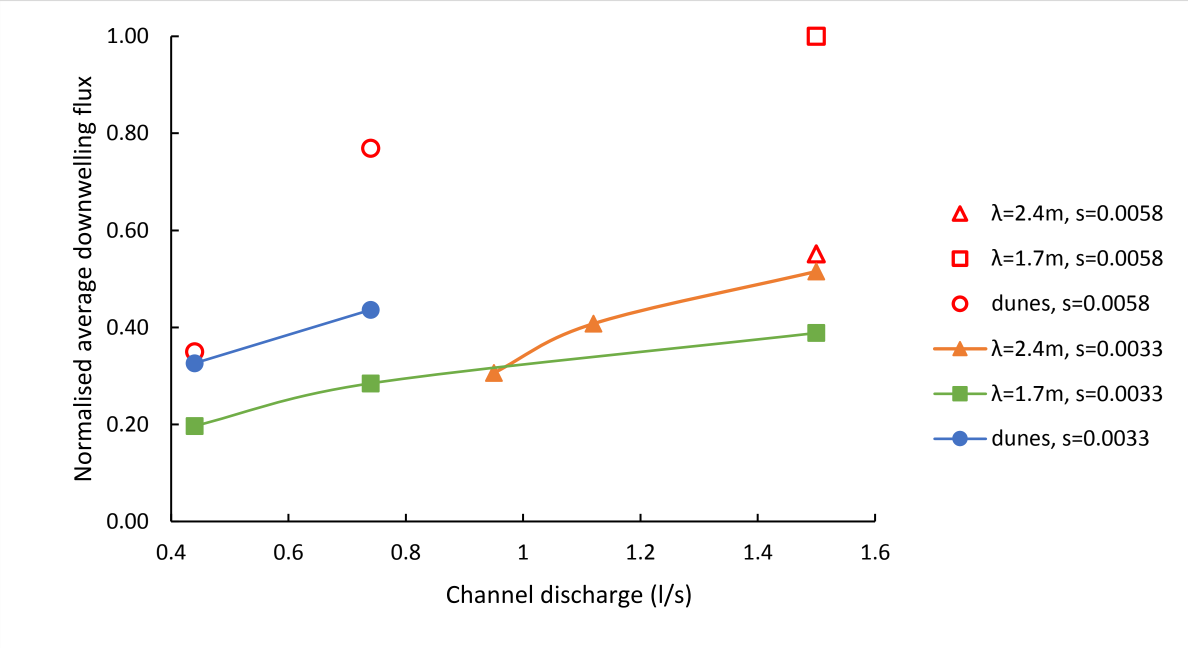

Figure 3.9 average interfacial flux into the bed calculated from solute breakthrough curves, q^x=q/q_max, where q_max is the most significant mean interfacial flux (Exp 12: 1.7m wavelength had the maximum interfacial flux value) verses channel discharge.

Higher river velocities generate more acceleration of river water (increased kinetic gradient) near meander beds forcing more water fluxes into the sediment bed. Generally, downwelling water flux increases with river slopes because of the increased hydrostatic head gradients. Cardenas (2009a) also found that increasing the valley slope increased the downwelling flux.

3.5 Discussion

3.5.1 What processes might drive hyporheic flow through meanders?

Breakthrough curves of the tracer experiments show that the exchange of solutes at the water-sediment interface happens in two stages; 1) a rapid initial exchange of solutes that characterizes either short flow paths or fast pore water velocities in the hyporheic zone and 2) a second stage of slow mixing associated with either long flow paths or slow pore water velocities. Solutes are passed through the bed to the channel rapidly at the beginning of each experiment, but the exchange rates are reduced comparatively over time. Most of the exchange happens in this first stage (more than 50% reduction in solute concentrations) of mixing. The presence of two exchange rates has also been observed by Tonina and Buffington (2007) and Salehin et al. (2004) for riffle-pool channels, characterized as shallow and deep sediment layer mixing by the influence of surface water flow. However, for meandering streams, literature ignore some of the processes when demonstrating the conceptual basis of these observed hyporheic exchange rates.

Hyporheic flow occurs due to the hydraulic head gradient developed at the stream bed. This accounts for both hydrostatic and dynamic pressure components. Hyporheic flow through small topographic features such as (fully submerged bedforms) is known to be influenced by dynamic pressure gradients, which is a function of channel flow rate (Cardenas and Wilson, 2007a, Cardenas and Wilson, 2007b, Elliott and Brooks, 1997a, Elliott and Brooks, 1997b, Tonina and Buffington, 2007). Hydrostatic pressure has minimal impact as the differences due to bedform morphology are small compared to river water heights. Therefore, hyporheic flow through small bedforms are induced by variation in the dynamic head distribution over the bedform. Previous literature has assumed that hyporheic flow through meandering beds is driven by the hydrostatic head and is minimally affected by river hydraulics (Boano et al., 2006, Cardenas, 2009a, Gomez et al., 2012). This is caused by comparatively large size (and hence substantial impacts of gravitational head) of water flow depths. However, residence time and downwelling flux are influenced by both dynamic and gravitational pressure gradients.

We observed that increased channel flow rate reduces the residence time of solutes in the sediment bed and increases interfacial water flux. On the other hand, large wavelengths provide an increase in residence times, but sinuosity would decrease water residence times. At a meander bend, high-velocity areas are generated near the outer bank of the bend due to the point bar cross-section and bend curvature (Kasvi et al., 2017) and produce acceleration of river water. Therefore, the dynamic pressure component increases and exerts advective water pumping into the sediment bed. For higher velocities and large meanders, water flow exerts a dynamic pressure component due to water velocities and a static pressure component due to water depths. Water can enter the sediment bed from the outer bank of the meander bed where pressure is high (influenced by the high velocity and water depth) and may return to the channel at the inner bank of the meander bend where pressure is low (due to the separation of the flow from inner bank to the outer bank).

3.5.2 Effect of river discharge, meander morphology and channel slope on downwelling water flux

The experimental results do not show a direct relationship between meandering wavelength and average downwelling flux. For the lower river slope used, increasing meander wavelength cause an increased in downwelling flux, but for the higher slope used in the experiments, we observed a sharp reduction in flux with increasing the wavelength. Previous literature also reports that increasing sinuosity causes increased downwelling flux due to the increased hydraulic head on the bed(Boano et al., 2006, Cardenas, 2009a, Gomez et al., 2012, Stonedahl et al., 2013). Generally, increasing meander wavelength causes a decrease in interfacial flux (Figure 3.9). We cannot conclusively determine whether the change is directly caused by wavelength or sinuosity, as we have only two cases. For a given discharge, an increase in wavelength (or sinuosity) increases the surface area available for the exchange, hence increasing the interfacial flux. Our results for the straight channels with dune-riffle morphologies show high flux values compare to meandering channels for the same discharges. Dunes have added more flux to the sediment bed compare to meander induced flux.

The fact that hyporheic residence times and downwelling flux are influenced by discharge and river morphology suggest that there is a complex interaction between channel flow conditions and channel morphologies on the solute transport characteristics. We believe that consideration of river hydraulics in modeling of hyporheic flow through meanders are important as the channel curvature would exert advective pumping of river water into the sediment bed. In our experiments, we did not vary sediment properties and alluvium volume, which are also influencing factors as identified in previous literature (Tonina and Buffington, 2007).

3.5.3 Implications for management

The results of our experiments suggest that there is complex hydraulics in the subsurface layer of meandering channels, which exerts complex spatial and temporal variations. Most of the nitrogen biogeochemical reactions occurring in the hyporheic zone are primarily influenced by the flux and residence time. Nitrogen oxidation reactions (i.e., nitrification and ammonification) occur in aerobic conditions while most nitrogen reduction reactions (i.e., Denitrification and anammox) occur in anoxic environments. When river water first enters the hyporheic zone, it is high in dissolved oxygen and create aerobic regions near downwelling areas. As the water passes through the hyporheic flow paths, oxidation reactions use oxygen as a terminal acceptor creating anaerobic conditions in the rest of the flow path. Reduction reactions convert nitrate into dinitrogen gas, so it can escape from the river system. Therefore, long residence times are essential to support anaerobic reactions. Our study shows that favorable hyporheic residence times are achievable by controlling river flow rates, meander wavelengths and river slope.

However, overall reaction rates are affected by the rate at which reactants are supplied, which is dependent on the downwelling fluid flux and in-stream concentration. This leads to competition between reactant supply and demand resulting in nonlinear and nonmonotonic dependence of reaction rates on hyporheic flux (Chen et al., 2015). The results of our study indicate that this nonlinear competition is potentially more complex for meanders because of how hyporheic flux and volume depend on surface flow characteristics and meandering morphology.

Therefore, the right balance between downwelling fluid flux and residence time is critical. Rivers can be natural treatment units if these conditions are met. Dunes have large flux values but short residence times, which would result in incomplete nitrogen removal. However, meanders can induce considerably large interfacial flux and longer residence time, which could effectively remove nitrogen from stream ecosystems.

Beside its ability in processing river nutrients, hyporheic zone contributes for stream ecological services such as providing accommodation for macroinvertebrates and hyporheic organisms (i.e., hyporheos), pollutant buffering and regulation of river water temperature (Hester and Gooseff, 2010). For all these important ecological services, hyporheic residence time and flux are important parameters. Hence hyporheic restoration by controlling these two factors are a critical step toward restoration of stream ecosystem (Hester and Gooseff, 2010, Hester and Gooseff, 2011).

3.6 Conclusions

In this work, we performed laboratory tracer experiments to study flux and residence times of solutes in the hyporheic zone of meandering rivers. This study would be the first flume experiments to study solute transport in meandering rivers. Our experimental results suggest that changing meander morphology and stream velocity will affect residence times and water flux into the sediment bed. Solutes breakthrough curves of our experiments show that there are two stages of mixing occurring in the hyporheic zone of meandering rivers, conveying possible complex spatial and temporal variations of hyporheic flow. This will create different surroundings (aerobic and anaerobic zones) for the microbial community, and hence affecting rates of biogeochemical reactions. These findings can be incorporated in river restoration, channelization, and environmental flow practices into design rivers as natural treatment units for water-borne pollutants. We believe that future research must aim to get a deep understanding of fate and transport processes of pollutants occurring in the hyporheic zone of meandering rivers through numerical modeling and field experiments to support improved river management solutions.

Chapter 4: Modeling hyporheic flow in meandering rivers

Chapter 4 describes the three-dimensional numerical model developed to answer research question 2 (What are the processes driving hyporheic flow in meandering streams?) of my Ph.D. research and presented as a journal paper (Paper 3). This model has been developed by combining several existing models (Boano et al., 2006, Cardenas, 2009a, Gomez et al., 2012, Stonedahl et al., 2013, Stonedahl et al., 2010, Boano et al., 2010a) and tested for six experimental runs discussed in chapter 3. The methodology section of the paper presents mathematical modeling of surface-subsurface flow, morphology modeling, and numerical simulations conducted to determine hyporheic flow paths and solute transport characteristics in the hyporheic zone. Numerical simulations and particle tracing were carried out in COMSOL Multiphysics software. The model performed well (R^2 of 0.95) in reproducing residence time distributions of laboratory tracer experiments. Graphical visualization of particle movement showed that particle movements are not only in the direction (longitudinal flow) of streamflow but also parallel (lateral pumping) to the stream flow direction at meander bends. This longitudinal movement of particles is due to the channel slope at the scale of meander wavelength, and lateral movements of particles are due to surface water acceleration at the curvature of meander bends (at the scale of channel width). Given the two major processes controlling flow in meandering rivers, I extend my research to identify the relative effect of meandering morphology on residence time distributions and flux in the hyporheic zone as research question 4 in chapter 5.

Paper 3: Modelling hyporheic flow in meandering rivers

4.1 Abstract

Meandering channels are particularly important for solute transport in the hyporheic zone and thus fate and transport of water-borne environmental contaminants, as meanders are large topographic features and produce longer residence times in the hyporheic zone. However, our understanding of water residence time distributions in the hyporheic zone of meandering channels is limited, and a number of complex interactions that happen in the hyporheic zone of meandering streams are yet to be discovered. In this paper, we present a three-dimensional model using COMSOL Multiphysics and previous theories of hyporheic exchange to examine primary mechanisms controlling meander induced hyporheic flow. The model is based on a surface flow model with the Reynolds-averaged Navier-Stokes equation and subsurface flow model with Darcy’s flow equation. The model performed well in reproducing residence time distributions for a set of laboratory tracer experiments with a meandering morphology. Results show that there are two major mechanisms driving hyporheic flow through meanders; 1. Lateral flow caused by channel slope at the scale of meander wavelength and 2. vertical flow caused by surface water acceleration due to the curvature of the channel at the scale of channel width. Parametric analysis, which was carried out with a Taguchi design, showed that the residence time of solute in the hyporheic zone (mean and standard deviation) is influenced by meander wavelength, channel discharge, hydraulic conductivity, sinuosity, channel slope, Width to depth ratio and alluvium volume. However, average water interfacial flux to the hyporheic zone will depend mainly on river discharge, hydraulic conductivity, meander wavelength and sinuosity. Previous studies do not deal with river discharge when estimating hyporheic flow through river meanders. Our study highlights the importance of river discharge on hyporheic flux and residence time distribution.

Keywords: Hyporheic flow, meanders, lateral flow, vertical flow

4.2 Introduction

The hyporheic zone is the transition zone between surface and subsurface water. Hyporheic flow is influenced by river morphology features such as bedforms (Azizian et al., 2017, Azizian et al., 2015, Boano et al., 2010c, Cardenas and Wilson, 2007a, Elliott and Brooks, 1997b, Tonina and Buffington, 2011), alternate bars (Marzadri et al., 2011, Marzadri et al., 2010) and river meanders (Boano et al., 2006, Cardenas, 2009a, Stonedahl et al., 2013, Stonedahl et al., 2010). These morphology features produce hydraulic head gradients along the water-sediment interface (WSI), which drive stream water flows through the hyporheic zone. Referred to as 'hyporheic pumping', these gradients drive river water into the hyporheic zone at high-pressure regions, and the flow returns to the stream from low-pressure regions (Azizian et al., 2015, Elliott and Brooks, 1997a).

Hyporheic flow is known to produce biogeochemical gradients supporting important ecological processes, including the transformation of pollutants, river metabolism, and provision of habitats for microfauna and macrofauna (Azizian et al., 2015, Cardenas, 2009a, Tonina and Buffington, 2007). Meanders are large topographic units and could provide an excellent opportunity for efficient biogeochemical transformations. Downwelling water flux and the residence time within the hyporheic zone are critical controls on the supply and reaction rates of these biogeochemical compounds (Cardenas, 2009b). However, complex interactions occurring in the hyporheic zone due to river morphology and the hydrodynamic variation of surface and subsurface water create large spatial and temporal patterns in the hyporheic flow. Therefore, it is essential to understand these complex interactions occurring in the hyporheic zone and apply modeling methods to quantify the residence time and flux of water residing in the hyporheic zone.

Previous studies have examined hyporheic flow in meandering rivers generally with field experiments (Fossing et al., 2004, Burkholder et al., 2008, Hoven et al., 2008, Osenbrück et al., 2013) and two-dimensional numerical models which neglect any possibility of forming vertical flow (Boano et al., 2006, Cardenas, 2009a, Gomez et al., 2012). Recently, several new three-dimensional numerical models have been developed to describe hyporheic flow in meandering rivers to examine water flow fields (Fossing et al., 2004, Balbarini et al., 2017, Pescimoro et al., 2019, Stonedahl et al., 2013, Stonedahl et al., 2010). However, all these prior studies use river static head gradient (based on the river valley slope) as the primary driver of the hyporheic flow. Even though the hyporheic flow through small topographic features are typically characterized by river hydraulics (produced by dynamic head gradients) (Boano et al., 2013, Cardenas and Wilson, 2007a, Chen et al., 2015, Tonina and Buffington, 2007, Tonina and Buffington, 2011), meandering rivers have not been studied considering river flow conditions. Additionally, natural meandering rivers are comprised of point bars at the inner bank of meanders spanning from one side to the other (creating riffles and pools) and associated secondary currents within the channel due to meandering curvature. These features are likely to produce significant vertical hyporheic flow in addition to lateral flow, violating the assumptions made for two-dimensional modeling provided by some studies.

Boano et al. (2010a) has been the first to study hyporheic flow induced by the meandering channels considering surface flow and meandering morphology. This study highlights the existence of vertical flux produce by flow acceleration at meander bends. However, this theoretical understanding requires field or laboratory validation in order to confirm the true nature and extent of exchange processes happening in the hyporheic zone of meandering channels. Therefore, in this study, we develop a three-dimensional numerical model to investigate how meandering morphology and river hydraulics influence hyporheic flow and use a set of laboratory tracer experiments to validate the model. The model involves coupled surface flow modeled with Reynold averaged Navier-Stokes equation and subsurface flow modeled with Darcy’s law. The primary outputs of this model are three-dimensional hyporheic flow paths, average downwelling flux, and residence times within the hyporheic zone.

4.3 Methodology

We developed a three-dimensional numerical model with COMSOL Multiphysics, a finite element analysis software to estimate the surface and subsurface flow and associated residence time distribution with different flow and meandering topographic conditions. Our approach includes four basics steps: generating river morphology, surface flow modeling, subsurface flow modeling, and numerical particle tracing. The surface flow model provides pressure head distributions at the water-sediment interface, which are then applied to the subsurface flow model to evaluate hyporheic flow and water fluxes in the hyporheic zone. A particle tracking method provides water travel paths in the hyporheic zone and associated residence time of individual particles released at the riverbed.

We used the resulting model to conduct a sensitivity analysis of factors potentially affecting residence time and interfacial flux at river meanders. This was conducted with Taguchi orthogonal array design to capture all possible combinations but minimize the number of simulations runs. Nine factors were considered in the analysis, including meander wavelength, sinuosity, slope, mean flow velocity, channel width/depth ratio, water density, the dynamic viscosity of water, hydraulic conductivity, porosity, alluvium width, and alluvium depth.

4.3.1 Three-dimensional modeling

4.3.1.1 Generating computational geometry for meandering morphology

We used 6 flume experiments (Table 4.1) conducted with meandering channels (Chapter 2) to validate the hyporheic flow model (conditions selected for these experiments are discussed below). Bed morphology of these experiments was surveyed with a laser scanning procedure, and water depth measurements were made at transacts alone the channel center and at each meander bend and inflection point midway between meanders. Water depth measurements were taken every second day of each experiment using a point gauge, and scanning was done when the flume water is drained. Laser scans were taken from a FARO scanner, which has an accuracy of 2mm. Four scans of the sediment were taken from four sides to capture all edges of the channel morphology, which were merged and processed using Cloud Compare, a 3D point cloud processing software. Later we used Creo Parametric software to generate channel geometry for our model. As shown in Figure 4.1, we have manually drawn cross-sections at each transect and interpolated along the channel centerline between adjacent cross-sections.

Figure 4.1 Creating river geometry with the Creo Parametric software.

Table 4.1 Experimental conditions.

	Wavelength λ, (m)	Amplitude A, (m)	Sinuosity λ/L	Flow rate (l/s)	Slope	Average velocity at the outlet (m/s)
E1	2.4	0.4	1.23	0.95	0.0033	0.06
E2	2.4	0.4	1.23	1.12	0.0033	0.07
E3	2.4	0.4	1.23	1.5	0.0033	0.1
E4	1.7	0.2	1.1	0.44	0.0033	0.03
E5	1.7	0.2	1.1	0.74	0.0033	0.05
E6	1.7	0.2	1.1	1.5	0.0033	0.1

For the sensitivity analysis, we used a generalized geometry for meandering streams. For the given parameters (Table 4.1) shape of the cross-section was designed based on Stonedahl et al. (2013) using piecewise parabolas and meandering planform was estimated from Mecklenburg and Jayakaran (2012) and Mohamad et al. (2015) using an improved method of sine-generated curves. The full geometry was created from Creo Parametric software by interpolating channel cross-sections along meander thalweg. The three-dimensional channel geometry was imported into COMSOL Multiphysics interface and a homogeneous subsurface layer, of uniform depth and width, was added using the geometry toolbox.

4.3.1.2 Modeling surface water flow for estimating pressure distribution on WSI

Calculation of pressure head distribution over WSI is one of the critical steps when modeling hyporheic flow. This model considers both kinetic and potential head components at the same time in a three-dimensional domain. This is achieved by creating the model domain with a global coordinate system to include slope effect and hence, the gravitational head component of overlying water flow and streambed elevation and considering Reynold Average Navier-Stokes (RANS) equation to capture kinetic head component.

RANS equation have been used in many previous studies to model surface flow and then to derive pressure head over the WSI (Cardenas, 2008b, Cardenas and Wilson, 2007a, Cardenas and Wilson, 2007b, Chen et al., 2015) specially to simulate turbulent flow over three-dimensional dunes (Cardenas and Wilson, 2007a, Chen et al., 2015). Chen et al. (2015) has validated the equation with vertical velocity profiles of flume experiments. Therefore, we directly used the RANS equation to model surface flow and then to generate pressure profiles on the WSI. For an incompressible fluid, the steady-state RANS equation with k-ω turbulence model can be given as follow and numerically solved using COMSOL Multiphysics software.

Turbulent kinetic energy equation;

$$\rho(u.\nabla)k = \nabla \cdot \left[\left(\mu + \frac{\mu_T}{\sigma_k}\right) \nabla k\right] + P_k - \rho\varepsilon \qquad (1)$$

And the dissipation rate equation;

$$\rho(u.\nabla)\varepsilon = \nabla \cdot \left[\left(\mu + \frac{\mu_T}{\sigma_\varepsilon}\right) \nabla \varepsilon\right] + C_{\varepsilon 1}\frac{\varepsilon}{k}P_k - C_{\varepsilon 2}\rho\frac{\varepsilon^2}{k} \qquad (2)$$

Where ρ and μ are fluid density and dynamic viscosity. u is the time-averaged velocity field, and p is the time-averaged pressure. k and ε are turbulent kinetic energy and dissipation rate respectively. $C_{\varepsilon 1}$ and $C_{\varepsilon 2}$ are turbulent model constants, and σ_k and σ_ε are turbulent Prandtl numbers for k and ε respectively.

In these expressions P_k is;

$$P_k = \mu_T[\nabla \mathrm{u}: (\nabla u + (\nabla u)^T)] \qquad (3)$$

And turbulent viscosity is given by;

$$\mu_T = \rho C_\mu \frac{k^2}{\varepsilon} \qquad (4)$$

4.3.1.3 Calculating the hyporheic flow field and interfacial water flux

COMSOL is also used to model hyporheic velocity fields. We model hyporheic flow as water flowing through a porous media using Darcy's flow equation (Boano et al., 2006, Boano et al., 2010c, Cardenas and Wilson, 2007b, Cardenas et al., 2008, Marzadri et al., 2011, Salehin et al., 2004, Storey et al., 2003, Tonina and Buffington, 2007). RANS equation and Darcy's equation were coupled through the pressure distribution at the sediment-water interface.

Water flow through the hyporheic sediments is given by pore water velocity, u from Darcy's law,

$$u[u, v, w] = -\frac{K}{\theta}\nabla h \qquad (5)$$

Where θ is the sediment porosity, and K is the hydraulic conductivity. ∇h is the hydraulic head gradient at any point in the porous media. Hydraulic conductivity and porosity were considered as homogeneous properties in our simulations.

Our pore water flow field has the influence of dynamic pressure distribution along the model boundaries and from the hydrostatic pressure component. Therefore ∇h is given as,

$$\nabla h = \nabla p + \rho g \nabla D \tag{6}$$

Where ∇p is the dynamic pressure distribution calculated from the Navier Stokes equation, ρ is the density of water, g is the acceleration of gravity, and D is the elevation of the stream bed.

Then, the steady state three-dimensional groundwater flow through the hyporheic zone was simulated by COMSOL Multiphysics by the Laplace equation;

$$\frac{\partial^2 h}{\partial x^2} + \frac{\partial^2 h}{\partial y^2} + \frac{\partial^2 h}{\partial z^2} = 0 \tag{7}$$

The downwelling water flux into the sediment bed (discharge per unit area per unit time) at location (x, y, z);

$$q(x,y,z) = \begin{cases} u(x,y,z) \cdot n & if\ u(x,y,z) \cdot n < 0 \\ 0 & if\ u(x,y,z) \cdot n \geq 0 \end{cases} \tag{8}$$

n is the unit vector orthogonal to the streambed surface.

4.3.1.4 Particle tracking and estimation of residence time distribution

The particle tracing module of COMSOL Multiphysics was used to estimate hyporheic flow paths and associated residence time distribution in the hyporheic zone. Flow-through hyporheic sediment is assumed to be laminar and does not mix with neighboring water paths (Azizian et al., 2015). This implies that the solute transport through the hyporheic zone relies upon advection alone (mechanical dispersion and molecular diffusion is negligible compare to advection) (Azizian et al., 2015, Marzadri et al., 2011, Marzadri et al., 2012). However mechanical dispersion may be significant for hyporheic exchange associated with larger scale topographic features (Gelhar et al., 1992).The governing equation for particle tracing is as follows.

$$\frac{d(i)}{dt} = u(x,y,z) \tag{9}$$

Where i is the position (x, y, z) of a particle released at the streambed surface.

8000 weightless particles were released randomly distributed over the streambed surface (x_0, y_0, z_0) at locations randomly selected from a probability distribution proportional to the upwelling and downwelling flux, to calculate the individual residence time, $\tau_f(x_f, y_f, z_f)$ of each particle (Time of particles entering the bed at (x_f, y_f, z_f) have spent in the sediment bed before leaving the streambed). Hyporheic zone residence times were calculated only for the particles that returned to the stream within the model domain (Pryshlak et al., 2015).

The cumulative residence time distribution, $RTD(t)$, can be calculated using the below expression (Marzadri et al., 2010, Tonina and Buffington, 2007).

$$RTD(t) = \frac{1}{\int_A q(x,y,z)\, dA} \int_A q(x,y,z) R(t)\, dA \qquad (10)$$

Where A is the downwelling area. $R(t)$ is defined as the cumulative probability of water entering at position (x, y, z) and remain in the bed after an elapsed time t. $R(t)$ is a binary variable that assumes to vary as equation 10 below.

$$R(t) = \begin{cases} 1 & if \quad t \leq \tau_f(x,y,z) \\ 0 & if \ t > \tau_f(x,y,z) \end{cases} \qquad (11)$$

4.3.1.5 Boundary conditions and mesh design

The model has two domains for separate analysis of surface flow and subsurface flow (Figure 4.2). The surface flow domain is defined with four boundary conditions. Inlet and outlet boundaries were set using experimental boundary conditions so that our model represents actual flow conditions to compare with laboratory observations. A slip (no flux) boundary condition was applied on the top surface (Free water surface). Surface flow bottom (WSI) was defined with a wall function boundary condition which changes according to the turbulence effect from the RANS equation. The subsurface flow domain has six boundary conditions. The upstream and downstream boundaries were defined as constant hydraulic heads, which were set by the calculated pressure values from the surface layer (RANS domain) for each discharge and shape. This formulation results in a continuous pressure distribution across two domains. Two sidewalls and bottom were defined as a no-flow boundary (impervious layers). The free surface outside the channel was modeled as atmospheric pressure conditions. More details on boundary conditions and equations are shown in Figure 4.2. For all model runs, initial values for velocity field and pressure were [0, 0, 0] m/s and 0 Pa.

The RANS simulation provides the average pressure distribution at the water-sediment interface which is a no-slip boundary wall in the turbulent flow model. This pressure distribution was then applied as a Dirichlet boundary condition at the top wall of the subsurface model representing the hyporheic zone. This results in coupling two domains but embed the importance of accurate estimate of RANS pressure solutions along the WSI. The mesh design of the experiments is shown in Figure 4.3.

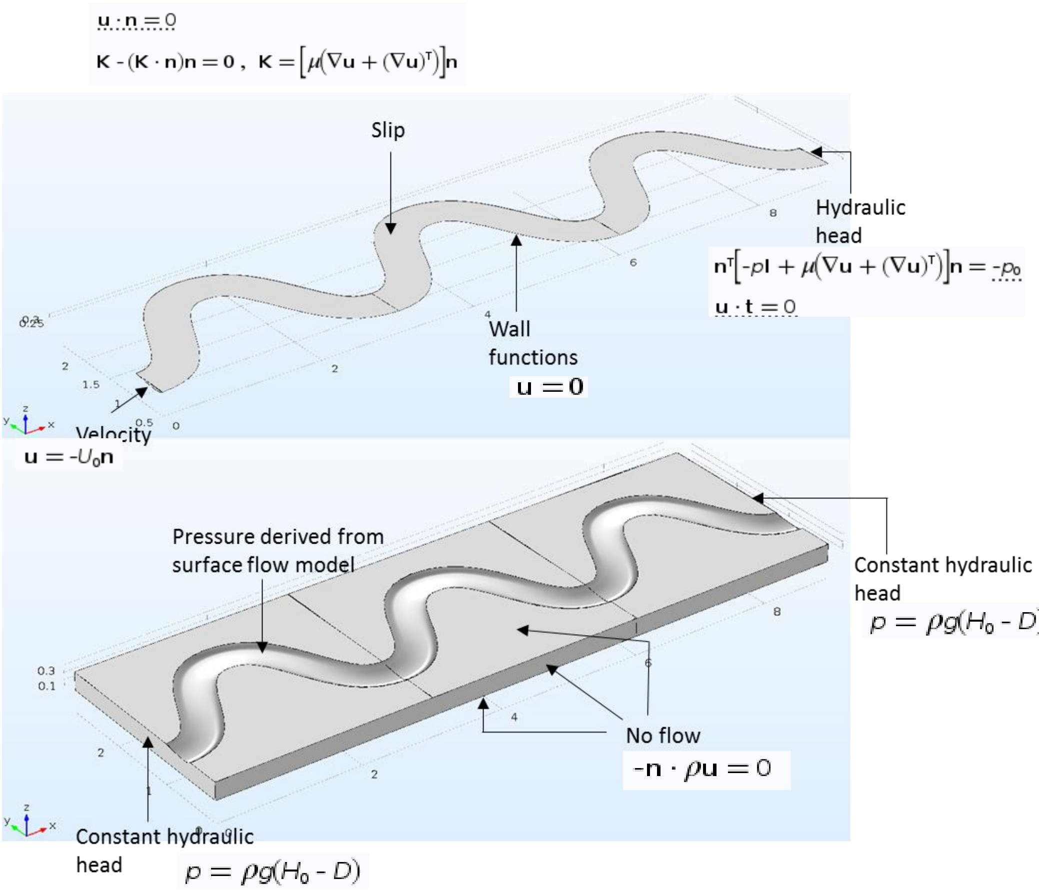

Figure 4.2 Model geometry and boundary conditions.

We created grids (Figure 4.3) for the two domains using the geometry meshing module "physics-based mesh" of COMSOL, which design the grid based on the physics and boundary conditions of the system. The mesh design was independent for each model run and composed of several tetrahedral, pyramid, prism, and triangular elements (Table 4.2). Number of mesh elements ranged from ~3000000 to ~6000000. Simulations were tested for the convergence of the grid for both domains.

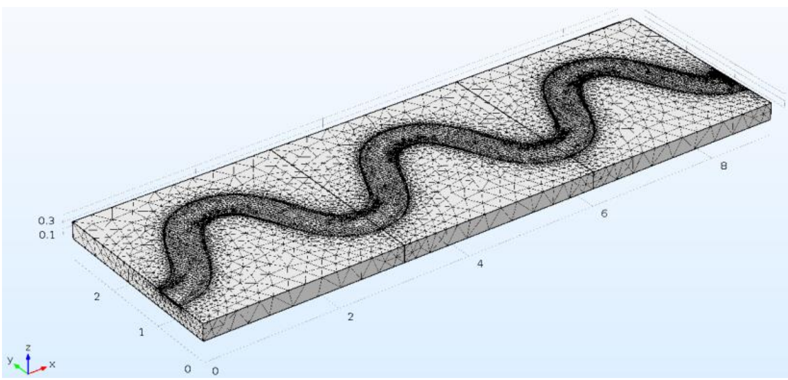

Figure 4.3 Grid design of the model geometry.

Table 4.2 Mesh statistic for experiment 1 model run

Description	**Value**
Minimum element size	0.0354m
Maximum element size	0.118m
Number of tetrahedral elements	347482
Number of pyramid elements	64
Number of prism elements	92016
Number of triangular elements	57088
Number of quadrilateral elements	100
Number of edge elements	1816
Number of vertex elements	12

4.3.2 Calculation of the residence time distribution of experiments

We observed that solute breakthrough curves $C^*(t) = C(t)/C_{start}$, (where C_{start} is the initial Rhodamine concentration in stream water) of our flume experiments follow an exponential decay distribution. Therefore, when calculating experimental RTDs, we have first fitted solute breakthrough curves with an exponential decay function (Table 4.3). The fitted curve was with two decay rates as shown in the expression below,

$$C^*(t) = (1 - C_\infty^*)[ae^{-k_1 t} + (1 - a)e^{-k_2 t}] + C_\infty^* \qquad (12)$$

Where, C_∞^* is equilibrium concentration, a is the mixing factor and k_1 and k_1 are first and second exponential decay rates, respectively.

Table 4.3 Fitted values of C_∞^*, k_1, k_2, and α for the six experimental runs.

	E1	E2	E3	E4	E5	E6
C_∞^*	0.12	0.12	0.13	0.21	0.20	0.19
k_1	0.06	0.06	0.10	0.04	0.05	0.14
k_2	1.11	1.34	1.50	1.00	1.16	1.34
a	0.34	0.27	0.13	0.48	0.35	0.26

The fitted breakthrough curves of tracer concentration measured in flume experiments were then used to determine the average cumulative residence time distribution ($\bar{R}(t)$) function using the following relationship.

$$\bar{R}\ (t) = L^{-1}\left\{\frac{L\left\{\frac{d'}{\bar{q}}\left[\frac{1}{C^{*}(t)}-1\right]\right\}}{L\{\ C^{*}(t)\}}\right\} \tag{13}$$

Where d' is the effective depth (total volume of recirculating water in the flume per unit bed surface area) and $\bar{q}$ is the average interfacial water flux (slope of the tracer time series at t = 0). This relationship was solved using Wolfram Mathematica.

4.3.3 Sensitivity Analysis

Hyporheic flux and residence time could potentially be influenced by many factors including meander wavelength, sinuosity, slope, mean flow velocity, channel width/depth ratio, water density, the dynamic viscosity of water, hydraulic conductivity, porosity, alluvium width, and alluvium depth. We use sensitivity analysis as a preliminary investigation of the relative influence of these nine characteristics for the mean residence time in the hyporheic zone. This analysis uses a Taguchi orthogonal array design (Factorial design of experiments) for the parameters considered at three levels to study if there are significant differences when the said parameters are varied. The response variables are taken as the average downwelling flux, in addition to the mean and standard deviation of the residence time of each experiment. Taguchi orthogonal array design is used to reduce the number of simulations required to carry out the said sensitivity analysis owing to the length of time taken per simulation on a personal computer. Most of the parameter values were obtained from the literature for naturally observed rivers (Table 4.4). We have kept the width of the channel constant but have varied depth according to three width/depth ratios; 10, 15, and 20 as representing the range typically recorded in the literature. Sinuosity values of 1.1, 1.5 and 2 were taken as to represent low sinuous sand-bed rivers. Slopes were within the range of Marzadri et al. (2016). Hydraulic conductivity and porosity values were selected in order to represent fine, medium and coarse sand. Table A1 in the supporting document shows numerical simulation design according to the Taguchi method used, L27(3^9).

Table 4.4 Nine parameters and values range for each parameter.

Variable		Notation	Values varied		
			1	2	3
Channel width, (m)		W	0.5		
1	Sinuosity, (m/m)	J	1.1	1.5	2
2	Wavelength, (m)	Λ	3	6	12
3	Hydraulic conductivity, (m/s)	K	2.00E-04	5.00E-04	6.00E-03
4	Inlet velocity (m/s),	V	0.01	0.08	0.4
5	Porosity	Θ	0.3	0.35	0.4
6	Slope, (m/m)	S	0.005	0.008	0.01
7	Channel width/depth	W/D	10	15	20
8	Alluvium width, (channel widths)	W_a	1.5	3	4.5
9	Alluvium depth, (channel depths)	D_a	5	10	15

4.4 Results

4.4.1 Modeled Vs. experimental residence time distributions

We compared measured cumulative residence time distributions from flume tracer experiments to that calculated from the three-dimensional numerical model presented in section 2.1 (Figure 4.4 and Figure 4.5). The three-dimensional numerical model driven by both dynamic and hydrostatic pressure gradients predict the experimental residence time distributions reasonably well with an R^2 in the range of 0.9 – 0.95 (Figure 4.5).

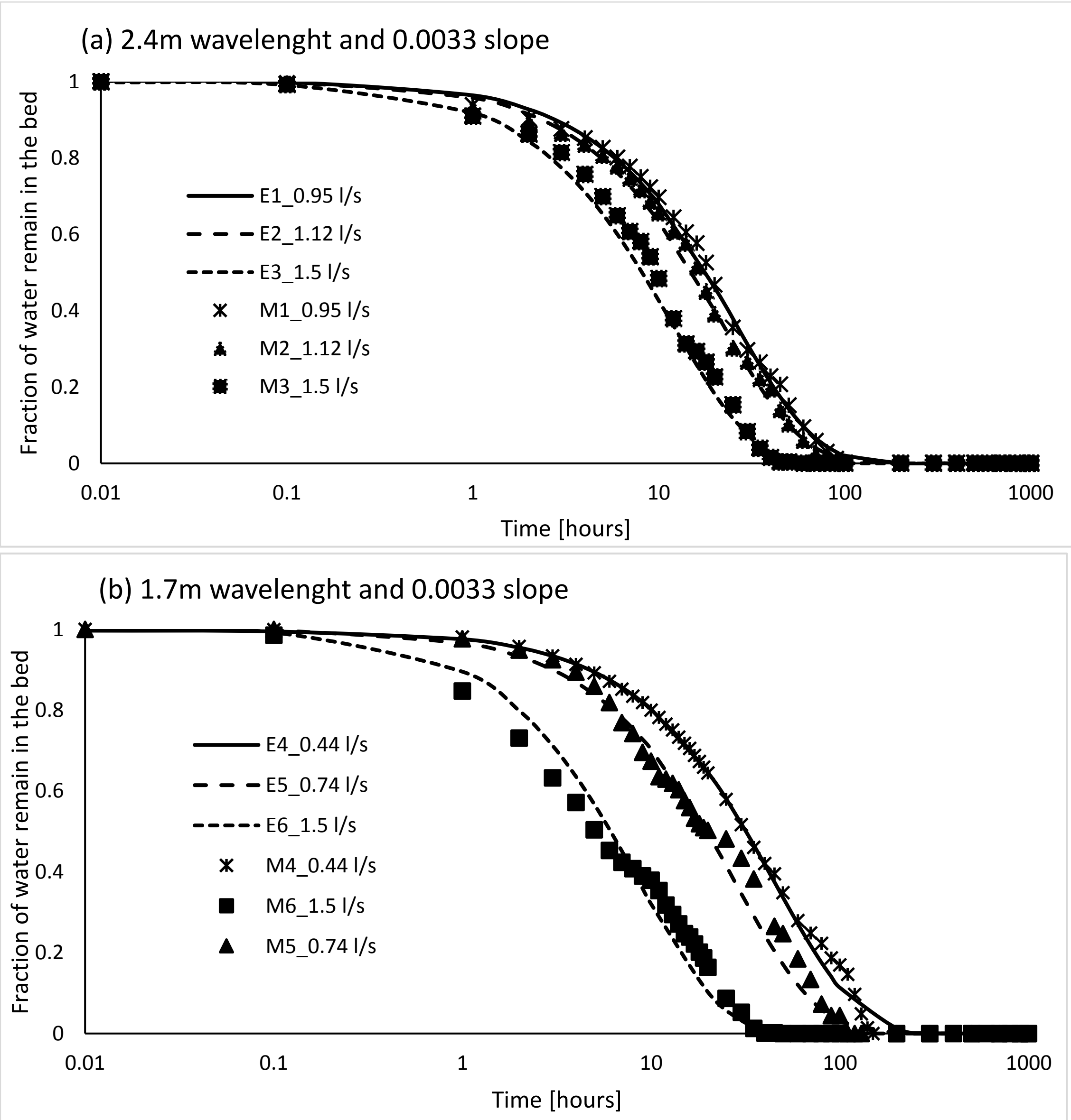

Figure 4.4 RTDs of experimental runs and corresponding numerical model for (a) 2.4m wavelength and (b) 1.7m wavelength. E1-E6 represents experimental residence times, and M1-M6 represents model predicted residence times.

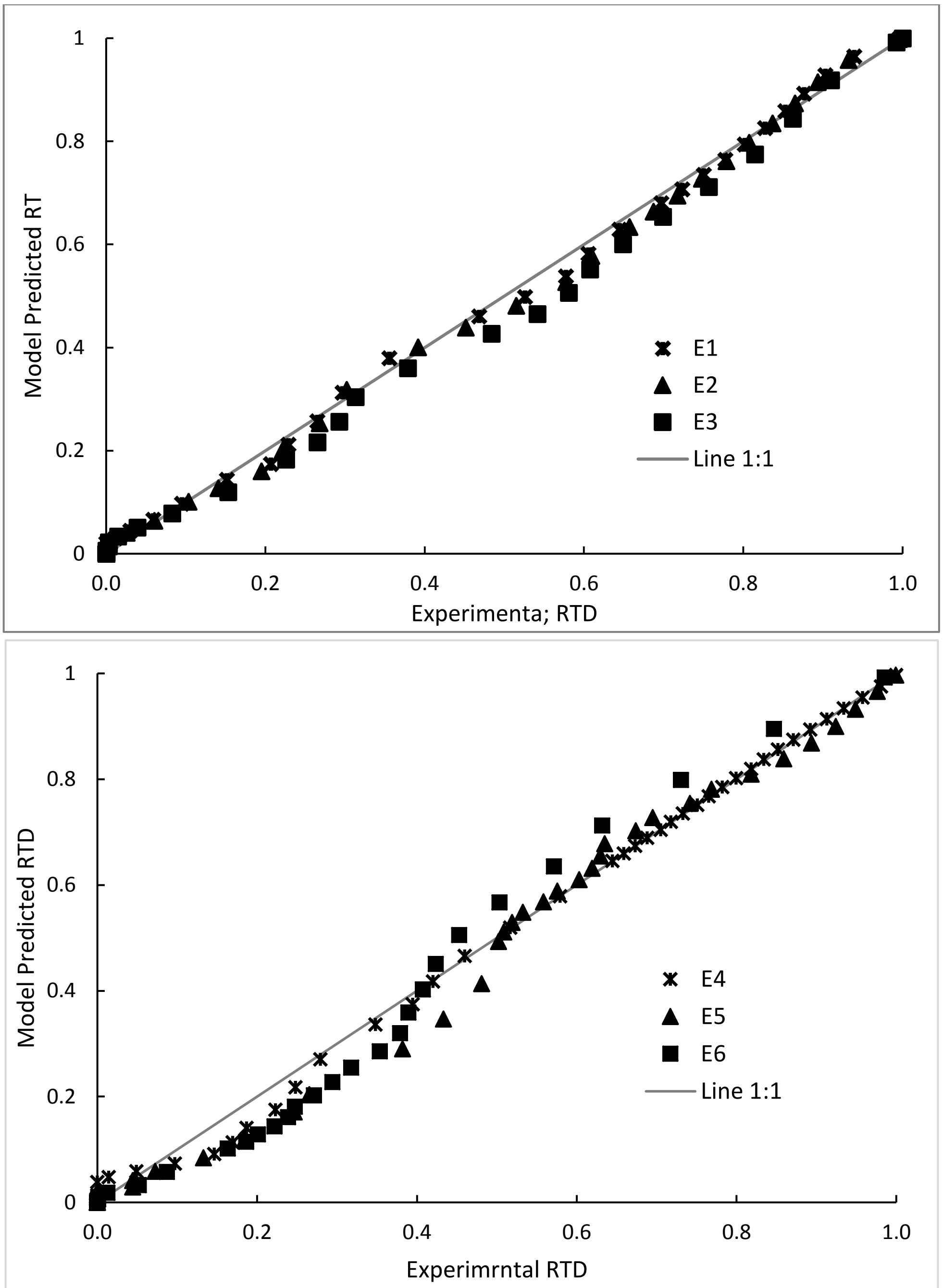

Figure 4.5 Q-Q plot of median residence time for wavelength 2.4m (top) and wavelength 1.7m (bottom) comparing the simulated cumulative residence time distributions.

We analyzed the magnitude of model error (model RTD percentiles compared to experimental percentiles); in Figure 4.6. The three-dimensional model predicts median residence times reasonably well with error <1hr. It is also observed that 90% and 75% of RTD percentiles of the experimental runs have been predicted by the model reasonably well (error <1hr) for all cases. However, the model shows errors for 10% and 25% percentiles, especially up to 8hr difference between the experimental and model-predicted residence times for 1.7m wavelength.

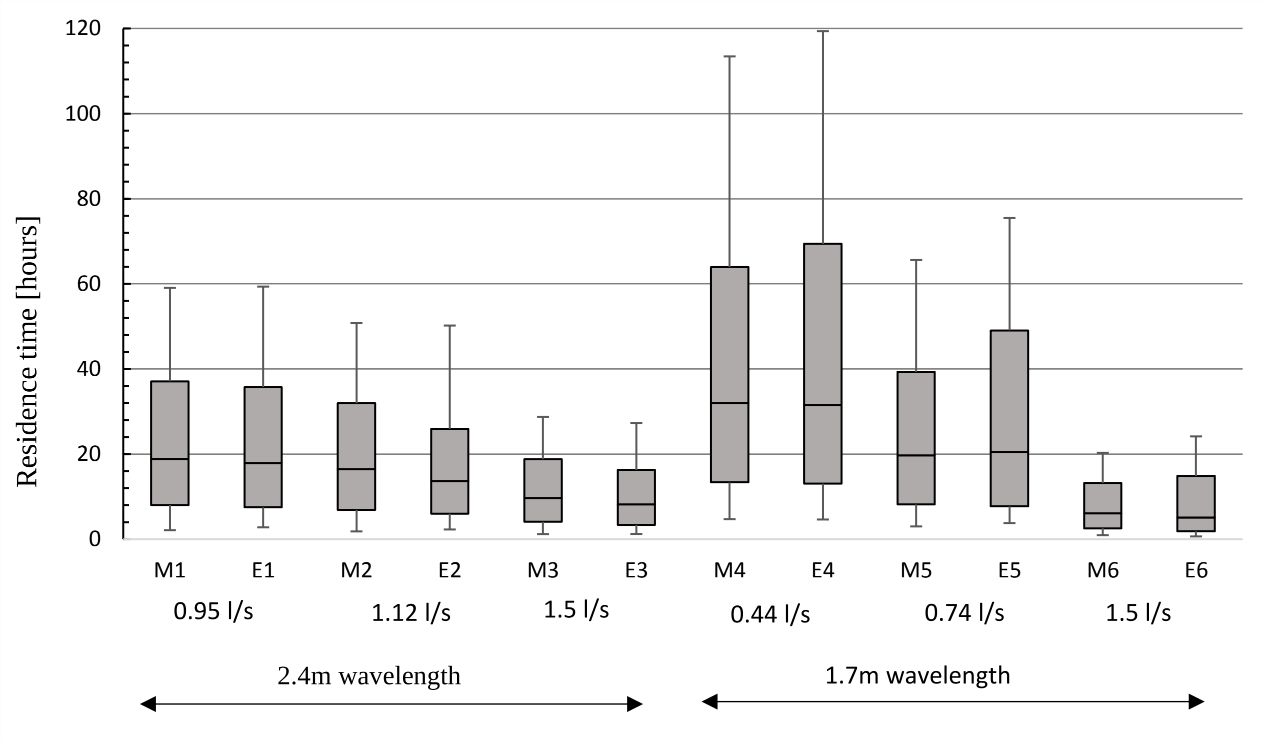

Figure 4.6 Box and whisker plot comparing model RTD percentiles to experimental percentiles relative to variations with flow and meander wavelength. Top and bottom whiskers represent the residence time when 10% and 90% of the solutes remain in the bed, respectively. Top, bottom, and middle lines of boxes show residence time when 25%, 75%, and 50% of the solutes remain in the bed, respectively.

For a given wavelength, we observe that increasing the river discharge decreases the time solutes remain in the subsurface for all the meander topographies used (Figure 3.6). An increase in wavelength increases the length of water flow paths between meanders and hence the residence times for a given discharge (experiments 3 and 6).

4.4.2 Properties of hyporheic flow through meandering morphology

The simulation results of run_S10 (J = 1.5, λ = 3m, K = 5E-4 m/s, V = 0.4 m/s, θ = 0.3, S = 0.008, W/D = 20, W_a = 1.5m and D_a = 15m) is used as a reference case to explore the hyporheic flow patterns through meanders including interfacial water flux, associated pressure distribution at the water-sediment interface and hyporheic flow pathways. Channel morphologies used in the sensitivity analysis represent typical meandering channels assumed, according to Stonedahl et al. (2013), Mecklenburg and Jayakaran (2012), and Mohamad et al. (2015).

4.4.2.1 Pressure distribution and hyporheic flux

Spatial distribution of the water flux in a meander bend is shown in Figure 4.7(a), negative, and positive values represent downwelling and upwelling water flux respectively. Downwelling and upwelling zones are previously defined for vertical hyporheic exchange occurring at river bedforms, such as dunes-ripple and pool-riffles. For consistency, we use these words although, for meanders, there is both lateral and vertical exchange. Downwelling describes any flow from surface to subsurface and upwelling for any flow from subsurface to the surface, regardless of orientation.

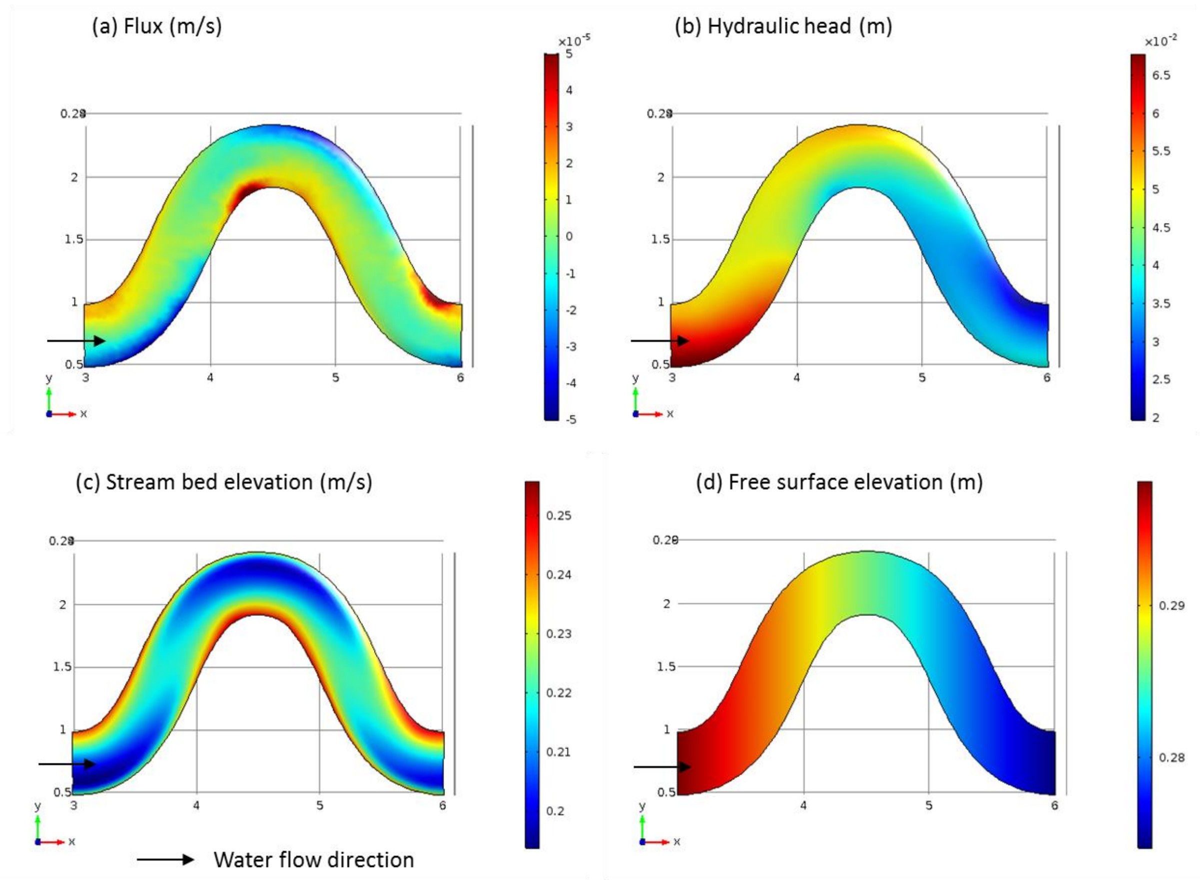

Figure 4.7 Plan view of the (a) distribution of upwelling and downwelling flux observed for the simulation S10 and (b) pressure distribution at the sediment bed. Dark blue represents high downwelling water flux and red the upwelling water flux. Spatial distribution of (c) stream bed elevation and (d) free surface elevation.

The effect of the hydraulic pressure head at the water-sediment interface is given in (Figure 4.7(b). Water enters the hyporheic zone at high-pressure zones and returns to the channel at low-pressure zones. It is noted that the hydraulic head is not directly proportional to streambed morphology nor the elevation of the streambed alone (Figure 4.7). It is the sum of both components. In a typical meandering river, point bars are developed at the inner bank of the bend (Figure 4.7(a)). The location of these point bars are sensitive to the channel curvature and the geometry of the river (Boano et al., 2010a). Variation of the streambed elevation due to point bars exert a variation in the static pressure (from the weight of the overlying water) at the streambed. Free surface elevation decreases downstream as the channel slope decreases (Figure 4.7 (d)). The variation in free surface elevation (Figure 4.7(d)) is clearly correlated to the total hydraulic head gradient in Figure 4.7(b). Therefore, the magnitude of the total hydraulic head at the stream bed surface is the sum of channel slope and the streambed morphology.

4.4.2.2 Hyporheic flow paths

Flow paths for water particles traveling in the sediment bed (Figure 4.8 for the reference case) show two exchange processes occurring in the sediment bed; horizontal cross-meander flow and lateral hyporheic pumping. Cross-meander flows occur from the outer bank of the meander bend towards the outer bank of the adjacent downstream meander bend. Typical flow path lengths are around one meander wavelength. Lateral hyporheic pumping represents water flow from the meander outer bank towards the inner bank of the meander bend (point bars) parallel to the flow direction. Flow path lengths re around one river widths. These streamlines are a hyporheic form of river secondary currents. These lateral hyporheic currents have higher velocities than horizontal fluxes (Figure 4.8). Previous studies have explicitly reported the existence of a horizontal flow between meander bends (Boano et al., 2006, Cardenas, 2008a, Cardenas, 2009a, Gomez-Velez et al., 2017, Revelli et al., 2008, Stonedahl et al., 2013, Stonedahl et al., 2010) induced due to the sinuosity and the channel slope of the river. Boano et al. (2010a) was the first to report the existence of both vertical and lateral exchange processes.

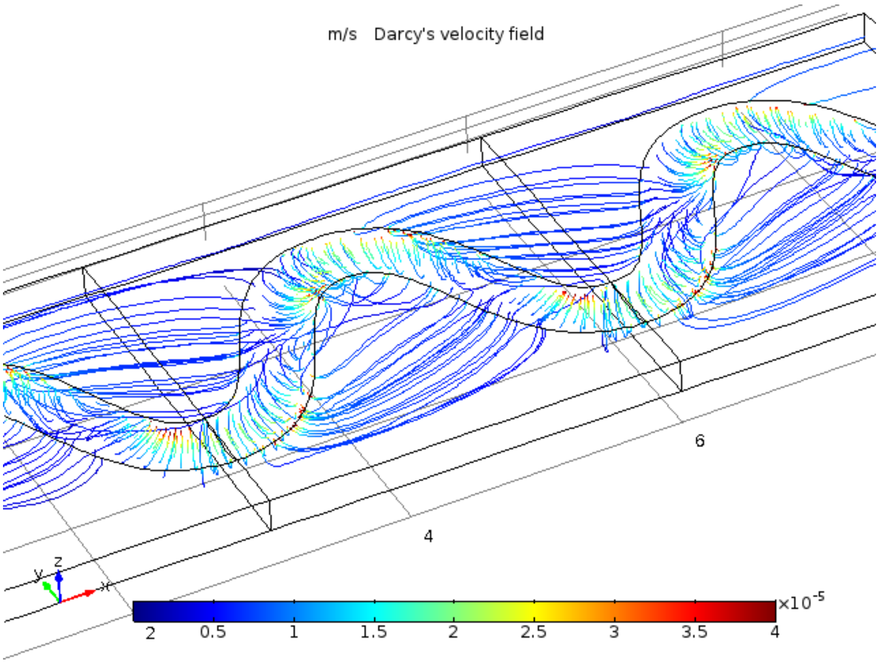

Figure 4.8 Pore water flow paths within the hyporheic zone for simulation S_10.

At t=0, particles are distributed on the bed proportional to the initial pore water velocity at the bed (Figure 4.9). We assigned the river bed to act as the outlet as well as the inlet; therefore, particles that got inward velocities will stick onto the bed at the beginning (second in Figure 4.9). When t=5h, particles move towards the adjusted meander. The rest of the graphs in Figure 4.9 shows how particles gradually move. The final graph in Figure 4.9 presents that all the particles end up at the inner bank of the meander where point bars are.

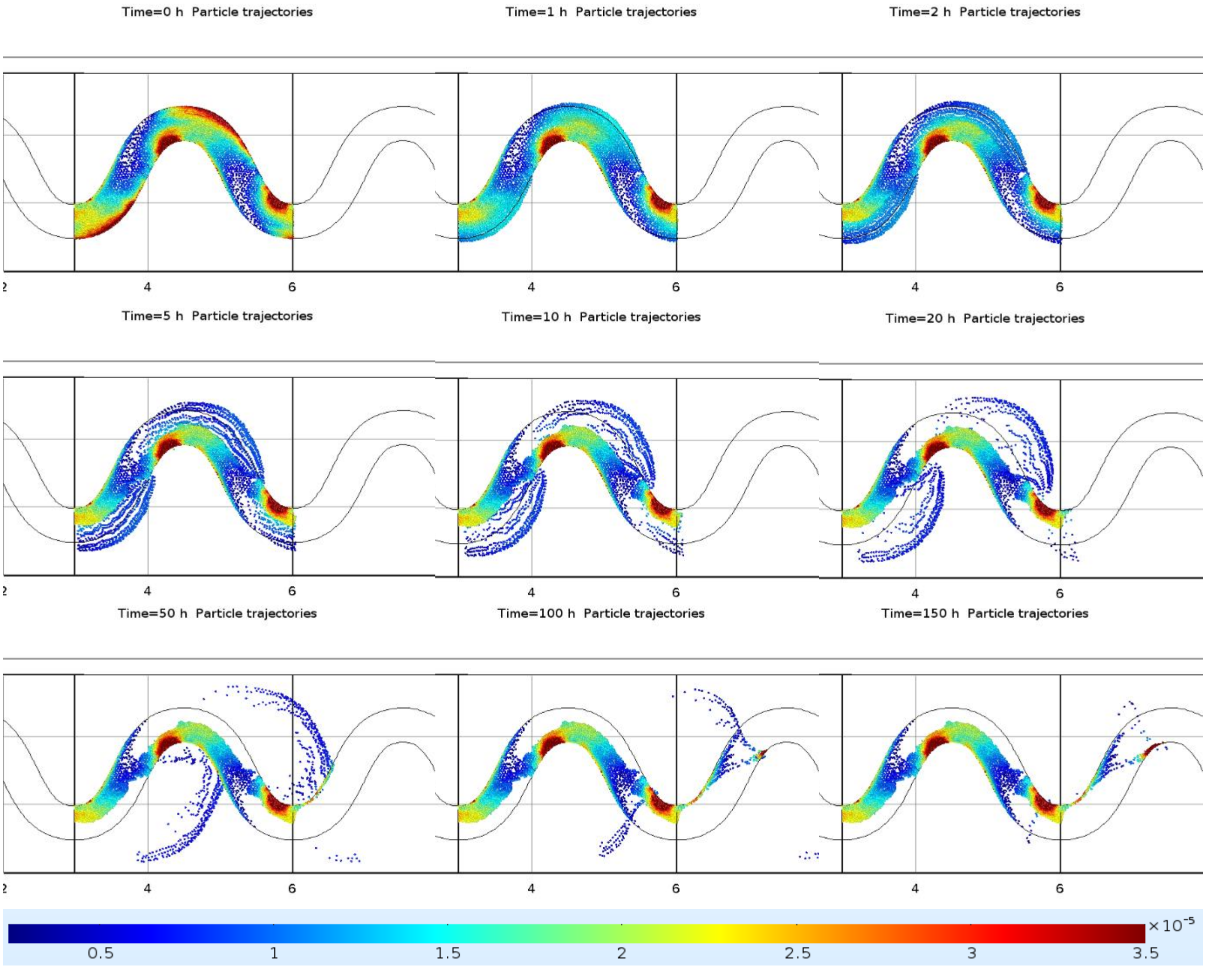

Figure 4.9 Movement of tracers in the subsurface model domain (lateral movement of particles) for simulation run S_10. Colour legend represents the velocity of particles in m/s.

Particle velocities near meander inner and outer banks are generally higher than velocities at the rest of the flow path. Particles enter the hyporheic zone at a high velocity, then start to move with a low velocity until it reaches the stream back. This behavior implies that there are two stages of mixing in the hyporheic zone by faster and slow rates of flow. Tonina and Buffington (2007) reported similar observations for the hyporheic flow in riffle-pool channels. Moreover, it is observed that the particles moving across the stream width have higher velocities than that are observed for the particles moving through intra-meanders.

Figure 4.10 presents the three-dimensional movement of particles in the subsurface domain for the reference case (side view). Both particles that move in cross-meanders and particles that move across the stream width have the same vertical penetration depths.

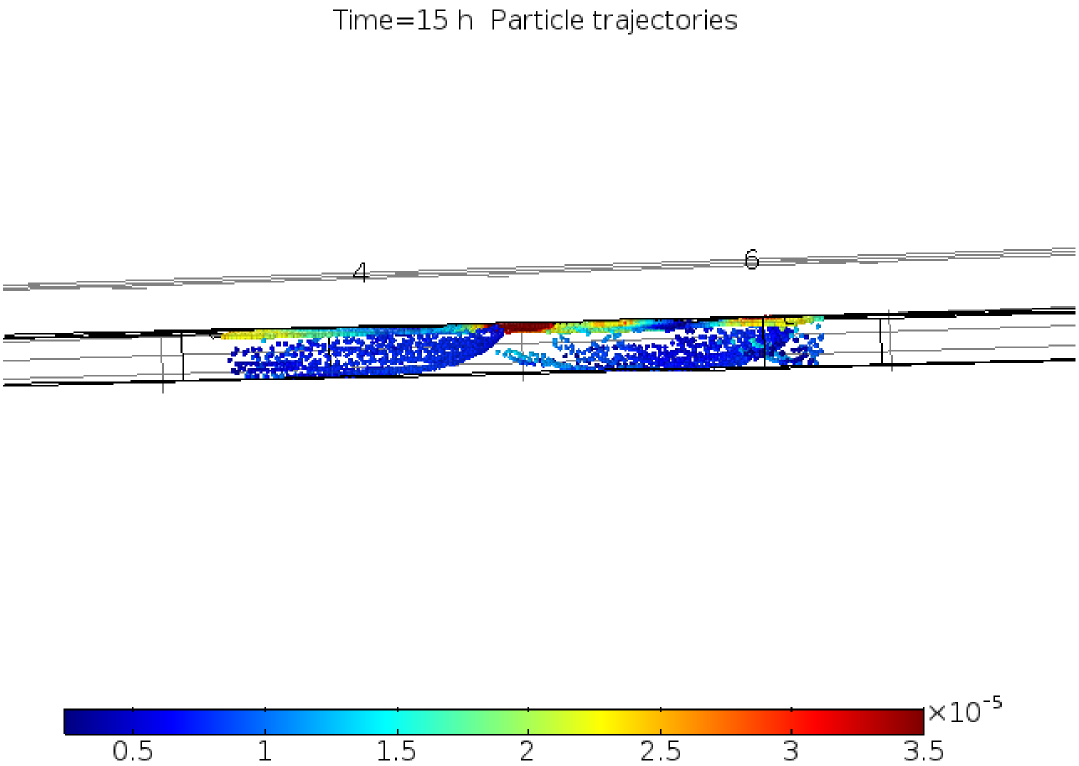

Figure 4.10 Three-dimensional representation of particle movement at t=15h.

4.4.3 Factor affecting hyporheic flow in meandering rivers

As previously discussed, residence time and downwelling interfacial flux are the two important parameters characterizing the hyporheic flow regime and biogeochemical potential. Therefore, we examined how these two factors are influenced by varying river flow conditions, river morphology, and properties of water, and the sediment bed, as discussed in section 2.2. Figure 4.11 summarises the results of the parametric analysis carried out. Delta is defined as the maximum difference of the T_{mean}, $T_{sd,}$ and flux for the three values considered for each of the factors. Therefore, a large delta implies that the T_{mean}, $T_{sd,}$ and flux are sensitive to that parameter. In order to compare all parameters together, we defined a normalized delta value as the maximum delta observed for each parameter.

Meander wavelength and channel velocity seem to be the most significant factors in solute residence times in the hyporheic zone of meandering rivers (Figure 4.11). Secondary influence comes from the hydraulic conductivity of the sediment bed. The porosity and width of the alluvium have less impact on the average residence time. All the other parameters (sinuosity, the slope of the valley, width to depth ratio, and alluvium depth) have a slight influence on the residence time. The standard deviation of the residence time defines the width of the distribution, and it seems that all the parameters have an impact on it.

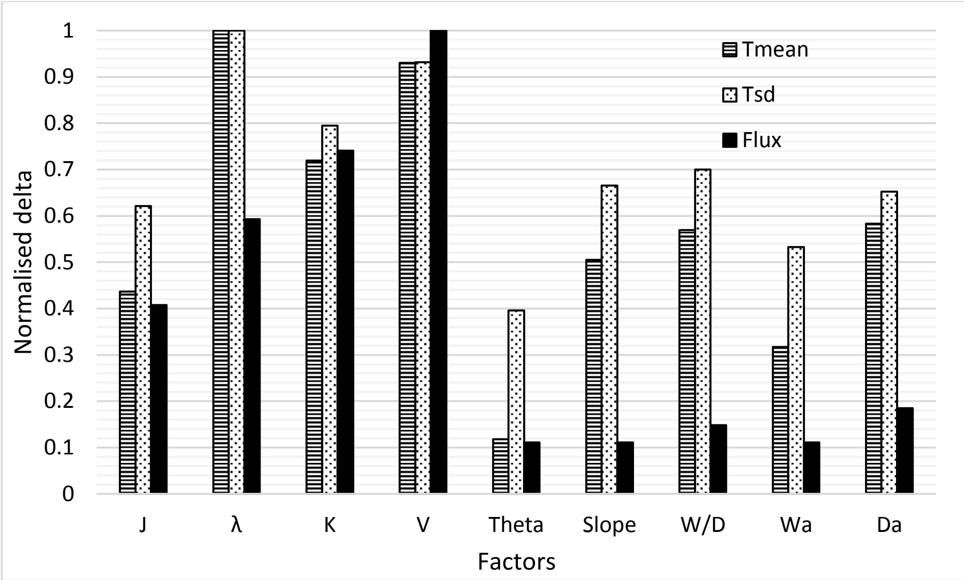

Figure 4.11 Sensitivity analysis results.

4.5 Discussion

4.5.1 Hyporheic flow

The results of my research show that there are two major mechanisms driving hyporheic flow through meanders; 1) Longitudinal flow caused by channel slope at the scale of meander wavelength and 2) lateral flow caused by surface water acceleration due to the curvature of the channel at the scale of channel width. It is observed that the two exchange mechanisms are controlled by two pressure components discussed in section 3.2. Longitudinal cross-meander flow is produced by the downstream hydraulic gradient due to the channel slope. Lateral pumping is caused by the variation of bed surface elevation (point bars) and hence, stream water depths at the meander curvature. The formation of point bar profiles in a meandering river depends on the channel curvature and the surface water flow. Moreover, superelevation of the free water surface occurs at the meander bend resulting in higher water depths at the outer bank and low water depths at the inner banks. This generates a total pressure gradient towards the inner bank and pumping of water flow through the hyporheic zone.

Downwelling flux is concentrated near the outer bank on the meander bend while upwelling flux is concentrated near the inner bank. These patterns are similar to flux profiles reported by Boano et al. (2010a), which have been simulated considering morphodynamics in meandering rivers. They have observed that hyporheic flux is concentrated near the stream banks where river curvature is high, and flux at straight river sections are much lower. However, these results contradict Stonedahl et al. (2013) that reported smooth, symmetrical patterns, where downwelling flux develops in the middle of the outer banks of the bend and extending along the straight part up to the inner bank middle of the next bend.

Water penetration depths in the hyporheic zone depends on the depth of the alluvium (Boano et al., 2010a, Tonina and Buffington, 2007). Shallow impervious layer used in this reference case does not allow water to penetrate into the subsurface. However, hyporheic depths are also a function of total hydraulic head gradient at the sediment bed and hence vary according to the channel slope and meander geometry.

4.5.2 Factors affecting hyporheic flow in meandering rivers

The result shown in Figure 4.11 indicates that velocity, hydraulic conductivity, wavelength, and sinuosity have a substantial impact on the average downwelling flux, respectively. Sediment porosity, river slope, W/D, and the width and depth of the alluvium seems to be insensitive to the downwelling flux. These results were observed to be similar to some of the hyporheic zone analysis. Velocity of the river seems to be the most influencing factor for downwelling flux. This effect has also been seen through river bedforms such as dunes (ref) and riffle-pools (Ref). However, there are not many studies that have looked for the impact of stream discharge on the hyporheic exchange through meandering streams. Previous studies have only look into variation of hyporheic flow with regard to sinuosity (Boano et al., 2006, Cardenas, 2009a) and river head gradient (Cardenas, 2009a, Stonedahl et al., 2013).

Previous studies reported that the increase in sinuosity leads to increased interfacial fluxes (Boano et al., 2006, Cardenas, 2009a, Revelli et al., 2008, Stonedahl et al., 2013). Our results also show that the sinuosity does affect downwelling flux. As reported by Storey et al. (2003), we also observed a relationship of downwelling flux with the hydraulic conductivity.

Storey et al. (2003) observed that the depth of the alluvium does not affect downwelling flux. But in contrast, Tonina and Buffington (2011) have observed a relationship of flux with the alluvium thickness for riffle-pool channels. In riffle-pool channels, more exchange occurs vertically, and the hyporheic volume available is important to develop the hyporheic flow. As we have discussed in the above sections, hyporheic flow through meandering channels observed to occur from meander chest to chest, basically in the lateral direction. Hence the hyporheic volume available for the flow is mainly depend on the sinuosity and wavelength not on the alluvium volume.

4.6 Conclusions

In this paper, we present a three-dimensional model to predict water flux and residence time distribution in the hyporheic zone of meandering streams. Surface flow was modeled using the Navier Stokes equation with given discharge and valley slope. This surface model is used to predict the pressure distribution on the WSI, and then the subsurface water flow field was modeled using Darcy's flow equation. A comparison between predicted and observed residence time showed a good agreement. Our results showed that the river discharge and meander morphology have an impact on the residence time distribution.

Results also show that hyporheic flow paths within the hyporheic zone are quite complex, and there is only one study (Stonedahl et al., 2010) available to compare our results. We observed a secondary current in the subsurface parallel to the river flow direction.

We conducted a sensitivity analysis with Taguchi design to see the effect of nine factors on the hyporheic exchange, including sinuosity, wavelength, hydraulic conductivity, river discharge, porosity, W/D, alluvium width and alluvium depth. We found that the residence time (mean and standard deviation) depends on the all factors we considered except porosity. However, average downwelling water flux mainly is only connected with river discharge, hydraulic conductivity, wavelength, and sinuosity.

Most importantly, we find that there is a significant impact from river discharge on both water flux and residence time, which has not been discovered in previous studies.

Chapter 5: Residence time of meander-driven hyporheic exchange

Chapter 5 presents the research methodology, results, and discussion for research question 3 (How does meandering morphology impact on flux and RTD in meandering streams?). This section is also presented in the journal paper format (Paper 4). Residence time distribution and flux are important parameters that determine the extent of nitrogen transformations in the hyporheic zone. However, running numerical models to determine those parameters is time-consuming and expensive. Even though many empirical relationships have been derived to estimate these parameters for small scale topographic features, there is still a significant gap in understanding these in meandering streams. Therefore, the effect of meander morphology (sinuosity and meander wavelength) on residence time and water flux in the hyporheic zone were analyzed using a series of numerical simulations using the model presented in chapter 4. I considered a low gradient river reach, which was three times the meander wavelength. Channel widths considered in the simulations ranged from 1m to1000m. There were thirty-six numerical simulations with all possible combinations of six wavelengths and six sinuosities. Results show that hyporheic residence time distribution induced by three-dimensional meanders follows a log-normal distribution. Our study showed that the meander wavelength has a significant effect on the hyporheic residence time as well as the downwelling water flux, demonstrating the importance of channel size on the hyporheic flow processes. However, the sinuosity of the river does not affect much on the time that water spends in the hyporheic zone but will alter the volume of water entering the hyporheic zone.

Paper 4: Residence time of meander-driven hyporheic exchange

5.1 Abstract

Hyporheic flow, the exchange of surface and subsurface water, is known to provide valuable ecological services in streams, including pollutant reduction and biogeochemical cycling. The volumetric flux and hydraulic residence times in the hyporheic zone are critical factors governing these processes. Meanders are extensive morphology features that drive hyporheic flow; three-dimensional morphology and the channel curvature of meanders could generate a complex spatial and temporal pattern of the hyporheic flow. In this study, we used a series of three-dimensional numerical simulations to study the effect of meander morphology on the hyporheic residence time distribution and water flux, and we propose three empirical relationships to predict downwelling water flux and characteristics of residence time distribution (mean and standard deviation). We found that the hyporheic residence time distribution induced by three-dimensional meanders follows a log-normal distribution. Our study showed that the meander wavelength has a significant effect on the hyporheic residence time as well as the downwelling water flux. River channel sinuosity has a small effect on the residence time but a substantial influence on the volume of water entering the hyporheic zone. These results imply that there is a complex interaction of channel sinuosity and wavelength in controlling the intensity and extent of hyporheic exchange in meandering rivers. Therefore, river restoration methods aiming to improve natural nitrogen attenuation in streams should incorporate these interactions to achieve improved biogeochemical rates in the hyporheic zone.

Keywords: Hyporheic flow, meandering streams, wavelength, sinuosity, residence times, water flux

5.2 Introduction

The hyporheic zone is a permeable saturated sediment layer that connects surface and subsurface water bodies in the stream ecosystem. Transport of stream water in this zone (termed hyporheic flow or hyporheic exchange) is thought to provide useful natural mechanisms in streams including cycling of organic carbons and nutrients, fish spawning and attenuation of water-born pollutants (Bardini et al., 2012, Boano et al., 2014, Cardenas, 2008a, Marzadri et al., 2013, Mulholland et al., 2008, Rivett et al., 2008, Zarnetske et al., 2011). The hyporheic zone can serve as a highly reactive biocatalytic filter characterized by; transport of water and dissolved solutes by physical and biological processes and the existence of microbial colonies and high chemical gradient compare to river water (Azizian et al., 2015). As noted in the literature, 75% of nitrogen added by agricultural activities are found to be denitrified in river sediments (Azizian et al., 2015).

Coupled aerobic-anaerobic microbial reactions play a significant role in nitrogen removal and nitrogen cycling in the hyporheic zone, including nitrification, denitrification, and ANAMMOX. (Gu et al., 2007, Jones et al., 1995, Mulholland et al., 2008, Zhou et al., 2014, Zhu et al., 2008, Zhu et al., 2013). These processes convert reactive nitrogen compounds such as Ammonia (NH_4), Nitrate (NO_3), and Nitrite (NO_2) to nitrogen gas (N_2) that is harmlessly emitted into the atmosphere. However, hydraulic residence times within the streambed can limit the extent of these processes where it is less than the biogeochemical reaction rates for nitrogen removal. Further, overall reaction rates are affected by the rate at which reactants are supplied, which depends on the downwelling water flux. Therefore, downwelling water flux and hydraulic residence time distribution within the hyporheic zone are important features of hyporheic flow influencing nitrogen fate in streams.

The concept of cumulative residence time distribution (CRTD) has become an essential tool to analyse the retention time of solutes in the hyporheic zone, proposed by Elliott and Brooks (1997) for river bedforms (Azizian et al., 2015, Cardenas, 2008b, Cardenas, 2008a, Elliott and Brooks, 1997a, Elliott and Brooks, 1997b, Gomez et al., 2012, Tonina and Buffington, 2011). CRTD can be coupled with the critical dissolved concentration of oxygen to explore the prevailing redox environment within the hyporheic zone and the extent of these biogeochemical processes. Given the CRTD and downwelling water volumes, the hyporheic zone can be modeled as a biochemical reactor to enhance our understanding of fate and transport of reactive solutes in the hyporheic zone. Therefore, most of the previous research tries to understand and model variation of CRTD over a range of stream systems, from small scale to large catchment scale. Thus, these relationships can be used to predict the fate and transport of reactive nitrogen, and other contaminants in the hyporheic zone, without numerical modeling and field investigations.

Hyporheic flow occurs across a wide range of river morphologic features, including vertical exchange over river bedforms such as pool-riffle, ripples-dunes, and bars and horizontal exchange over river side forms such as alternate bars and meanders. The exchange of stream water across these features is controlled by the variation in hydraulic head gradient at the water-sediment interface (Elliott and Brooks, 1997a, Azizian et al., 2015, Grant et al., 2014, Boano et al., 2014). Surface flow interactions with the channel morphology control spatial variation of these hydraulic heads and consequence changes in hyporheic flow. From many different geomorphic features that contribute to hyporheic exchange, our previous study suggested that hyporheic flow through meanders produces the residence times required for nitrogen biogeochemical cycling (Chapter 1).

Several studies have used numerical models to study hyporheic flow in river meanders through two-dimensional models (Boano et al., 2006, Cardenas, 2009b, Cardenas, 2008a, Gomez et al., 2012, Gomez-Velez et al., 2017) and three-dimensional models (Balbarini et al., 2017, Boano et al., 2010a, Stonedahl et al., 2013, Stonedahl et al., 2010). Cumulative hyporheic residence time distribution through river meanders have been found to be exponential when applying a two-dimensional model under homogeneous aquifer conditions (Cardenas, 2008a). However, three-dimensional morphological features have received little attention. Previous three-dimensional models have quantified hyporheic residence time and hyporheic flow fields, but the residence times haven't been characterized by the effect of morphology parameters. In most previous studies, hyporheic flow induced by river meanders is assumed to be horizontal. However, our previous study results showed that there is a relatively significant contribution from the vertical exchange component through shallow riffle-pool morphology in meandering rivers, as observed in Boano et al. (2010a). In previous literature, there is a lack of a validated three-dimensional model for characterization of the residence time in meandering rivers.

Therefore, in this paper, we analyzed residence time distribution for meandering rivers using a three-dimensional numerical model that has been validated with a set of laboratory tracer experiments. Previous three-dimensional models consider hydrostatic head (based on the river valley slope) alone to determine the hydraulic gradient at the sediment bed. However, our model extends the two-dimensional models proposed by Boano et al. (2006) and Cardenas

(2009b) to a three-dimensional domain and have include consideration of the hydrodynamic head component when estimating pressure distribution on the river bed. Numerical simulations are undertaken over a range of meander wavelengths and sinuosities.

5.3 Methodology

We conduct a series of three-dimensional numerical simulations to examine how residence time distribution and average interfacial flux in meandering rivers are influenced by channel wavelength and sinuosity. We use COMSOL Multiphysics software to predict residence time and average flux into the hyporheic zone (Chapter 4). Modeling subsurface flow include four basics steps: 1) Generating a model of the three-dimensional channel geometry; 2) applying surface flow model using Reynold Averaged Navier-Stokes equation, 3) modeling subsurface flow with Darcy's flow equation for porous media; and 4) particle tracing in the subsurface to estimate residence time distributions. This modeling procedure has been validated with experimental data previously (Chapter 4).

5.3.1 CFD modeling with COMSOL Multiphysics

A finite element model, COMSOL Multiphysics software, was to model river flow over three-dimensional meanders using Reynold Average Navier-Stokes (RANS) equation and hyporheic flow using Darcy's law (Chapter 4). This is similar to the computational fluid dynamics (CFD) approach used in many previous models for river bedforms (Cardenas and Wilson, 2007a, Chen et al., 2015, Sawyer et al., 2011). The model domain was designed to represent both the hydrostatic component that results from the slope of the river reach and gravity effect of overlying water depth and hydrodynamic component produced by flow acceleration at meander bends. This contrasts with previous studies that use hydrostatic head alone based on the river valley slope (Stonedahl et al., 2013, Stonedahl et al., 2010).

Steady-state RANS model for incompressible flow with k-ω turbulence model is expressed as;

Turbulent kinetic energy equation;

$$\rho(u.\nabla)k = \nabla \cdot \left[\left(\mu + \frac{\mu_T}{\sigma_k}\right) \nabla k\right] + P_k - \rho\varepsilon \qquad (1)$$

And the dissipation rate equation;

$$\rho(u.\nabla)\varepsilon = \nabla \cdot \left[\left(\mu + \frac{\mu_T}{\sigma_\varepsilon}\right) \nabla \varepsilon\right] + C_{\varepsilon 1}\frac{\varepsilon}{k}P_k - C_{\varepsilon 2}\rho\frac{\varepsilon^2}{k} \qquad (2)$$

Where ρ and μ are fluid density and dynamic viscosity. u is the time-averaged velocity field, and p is the time-averaged pressure. k and ε are turbulent kinetic energy and dissipation rate, respectively. $C_{\varepsilon 1}$ and $C_{\varepsilon 2}$ are turbulent model constants, and σ_k and σ_ε are turbulent Prandtl numbers for k and ε respectively.

In these expressions P_k is;

$$P_k = \mu_T[\nabla \mathrm{u}: (\nabla u + (\nabla u)^T)] \quad (3)$$

And turbulent viscosity is given by;

$$\mu_T = \rho C_\mu \frac{k^2}{\varepsilon} \quad (4)$$

The water flow field in the hyporheic zone was estimated using Darcy's flow equation for porous media and the continuity equation.

$$U = -\frac{K}{\mu}(\nabla p + \rho g \nabla D) \quad (5)$$

Where U is the three-dimensional Darcy velocity vector. D is the elevation of the stream bed. p is the pressure on the stream bed from the RANS solution. $K$and μ are permeability of the porous media and viscosity of water, respectively.

The residence time distribution, $R(t)$ is defined as the cumulative probability that a tracer entering the bed at position (x, y, z) and at t=0 remains in the bed after an elapsed time t. $R(t)$ =1 when none of the fluid particles have left the hyporheic zone and $R(t)$ =0, after all fluid particles, leave the bed. $R(t)$ is defined as (Elliott and Brooks, 1997b, Tonina and Buffington, 2011);

$$R(t) = \begin{cases} 1 \ \ when\ t \leq \tau_f \\ 0 \ \ when\ t\ > \tau_f \end{cases} \quad (6)$$

Where τ_f is the final age or the residence time of fluid particles.

Downwelling flux into the hyporheic zone varies according to the position and $R(t)$ must be weighted by local downwelling flux $q(x, y, z)$ to estimate spatially averaged residence time. Therefore, in our simulations $R(t)$ is calculated using the below expression.

$$R(t) = \frac{1}{\bar{q}} \int_A q(x, y, z)\ \tau_f(x, y, z)\ dA \quad (7)$$

Where $\bar{q}$ is the average downwelling flux over the total area of the stream bed, A.

The two parameters most commonly used to characterize the $R(t)$ are mean residence time, τ and standard deviation, σ^2. Probability distribution $E(t)$ and cumulative distribution $R(t)$ of residence times of fluid particles can be related as; $E(t) = dR(t)/dt$. Therefore, τ and σ^2 have the following forms;

$$\tau = \int_0^\infty tE(t)dt \quad (8)$$

$$\sigma^2 = \int_0^\infty (t-\tau)^2 E(t)dt \quad (9)$$

We use τ and σ^2 to characterize the hyporheic residence time for hyporheic flow through river meanders.

5.3.2 Parameters varied in simulations

All variables and values used in our simulations are presented in Table 5.1. We consider six river widths and corresponding meander wavelengths calculated using, $\lambda = 7.5\,W^{1.12}$ (Williams, 1986) and six sinuosities. Sinuosity (S) is defined as the ratio of channel length to down valley length and wavelength (λ) is defined as the distance of one meander along the down-valley axis. River widths are selected to represent a large range of natural rivers. Sinuosities are chosen to represent a large range of sinuous rivers which haven't been studied much previously. Meander wavelength of streams reported to be 6.28-10 stream widths (Leopold and Wolman, 1960, Williams, 1986). Our wavelengths also remain in this range. River slope for each simulation is 0.001, which was in the range of some reported for meandering rivers (Callander, 1978, Schumm, 1963). Mean flow velocity was decided based on Manning's n value. For natural rivers, Manning's n should be in the range 0.01-0.08, so we calculated river mean velocity taking Manning's n as 0.08. The average water depth was calculated using, $d = 0.027\,\lambda^{0.66}$ (Williams, 1986). Water density and dynamic viscosity were taken as 1000 kg/m^3 and 8.9×10^{-4}Pa s ,respectively. Hydraulic conductivity and porosity of the sediment was 0.005 m/s and 0.34, respectively for all model runs. Alluvium volume was selected in order to keep enough space to develop the hyporheic flow; alluvium width was assumed as four times meander amplitude and the alluvium depth as ten times the river depth.

Table 5.1 Variables and values used in simulations.

Variable			Values					
			1	2	3	4	5	6
Morphology	1	channel width, W (m)	1	3	10	30	100	1000
	2	meander wavelength, λ (m)	7.50	25.67	98.87	338.41	1303.35	17181.51
	3	Sinuosity, J	1	1.05	1.2	1.5	2	3.3
	4	Slope, S	0.001					
Flow	5	mean flow velocity, v (m/s)	0.08	0.13	0.14	0.5	0.9	3.7
	6	average water depth, d (m)	$0.027\ \lambda^{0.66}$					
Properties of water	7	water density, ρ (kg/m^3)	1000					
	8	dynamic viscosity of water, μ (Pas)	8.9×10^{-4}					
Sediment properties	9	Hydraulic Conductivity, K (m/s)	0.005					
	10	porosity, θ	0.34					
	11	alluvium width, W_a	4A					
	12	alluvium depth, da	10d					

5.3.3 Generating meandering planforms

In this study, we use a generalized topographic geometry for meandering channels. Meander planform was designed as sine-generated meanders according to (Mecklenburg and Jayakaran, 2012, Mohamad et al., 2015), and thalweg cross-sections were predicted using piecewise parabolas according to Stonedahl et al. (2013). Creo Parametric software was used to interpolate meander cross-sectional shapes along the meander thalweg.

5.3.3.1 Meander planform

We present our meandering planforms using an improved sine-generated curve (SGC) as an idealized version of river meanders (Mecklenburg and Jayakaran, 2012, Mohamad et al., 2015). These idealized patterns (Figure 5.1) have been proven to approximate actual planform sufficiently (Mecklenburg and Jayakaran, 2012, Mohamad et al., 2015). We used six numbers of wavelengths and sinuosities. For each combination of wavelength and sinuosity, meander amplitude was calculated using the following equation (Hagerman and Williams, 2000),

$$A = \lambda(0.9743 \ln(J) + 0.0803) \quad (10)$$

The average radius of curvature has been reported to be in the range of 1.1-4.7 stream widths (Leopold and Langbein, 1966 , Stonedahl et al., 2013, Williams, 1986). Relationship for the radius of curvature R_c, with meander wavelength and sinuosity, is as follows (Mecklenburg and Jayakaran, 2012).

$$R_c = \frac{\lambda S^{1.25}}{17(S^{0.5}-1)^{0.5}} \qquad (11)$$

Arc angle can be calculated using equation 12 for a given wavelength, sinuosity, amplitude and curvature radius (Mecklenburg and Jayakaran, 2012, Mohamad et al., 2015),

$$\frac{\theta}{2} = \cos^{-1}\left(\frac{16R^2-8AR+\lambda\sqrt{4A^2-16RA+\lambda^2}}{4A^2-16RA+\lambda^2+16R^2}\right) \qquad (12)$$

We use the above parameters to build the meandering planform in Creo parametric software. Creo Parametric has widely been used as a 3D CAD software in engineering applications. For this analysis, we created the channel with three meander bends.

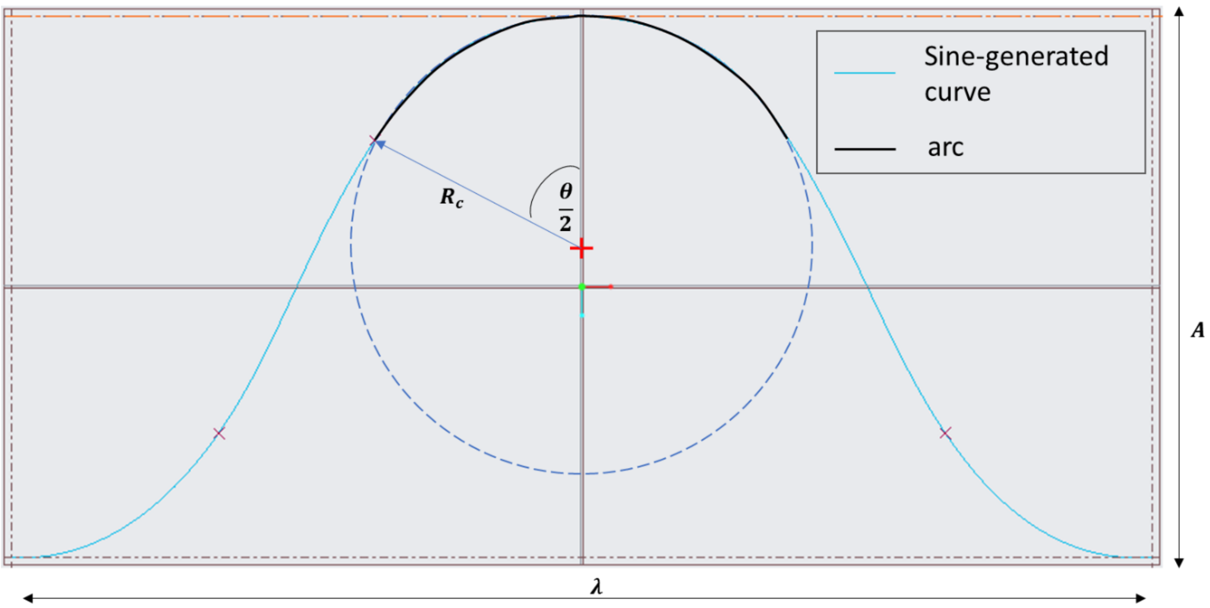

Figure 5.1 Plan view of meander illustrating the arc lines and notations.

5.3.3.2 Channel cross-sections

Channel cross-section along with the meandering channel changes, as shown in Figure 5.2. Point bars are observed at the inner bank of meandering bends. The maximum depth of the channel is observed close to the outer bank of the meander bend (thalweg). This thalweg usually shifts one side to the other. Formula for the depths of channel cross-sections (Figure 5.2) based on piecewise parabolas as given by Stonedahl et al. (2013),

$$d(\delta) = \begin{cases} \frac{d_{max}}{s^2}(\delta - s)^2 - d_{max} & \delta \leq s \\ \frac{d_{max}}{(W-s)^2}(\delta - s)^2 - d_{max} & \delta > s \end{cases} \quad (13)$$

Where δ is the transverse coordinates and $d(\delta)$ is the stream depth at the transverse coordinates. d_{max} and W are the maximum depth and width of the channel. s represents a transverse distance of the location of the maximum depth.

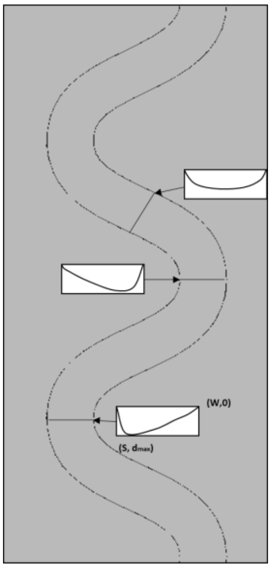

Figure 5.2 Meander cross-sectional shapes at the bend and at the meander chest (modified from Stonedahl et al. (2013)).

River topographies used in simulations for wavelength 7.5m are given in Figure 5.3. Sinuosity of one represents straight channels with alternate bars.

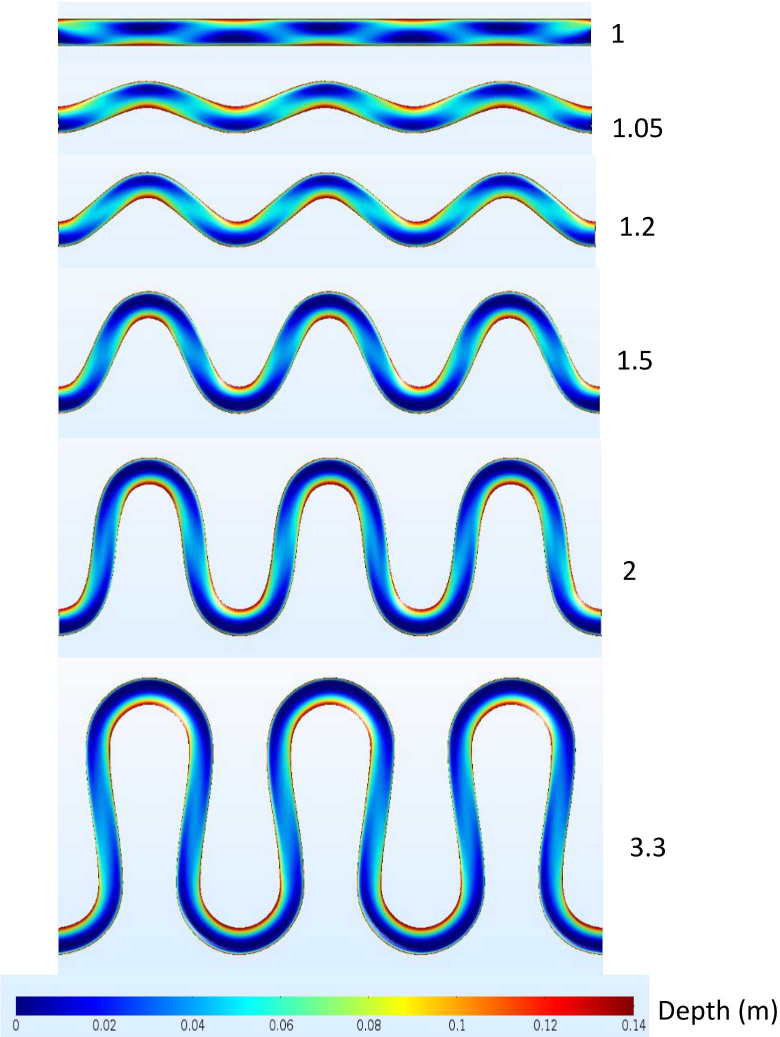

Figure 5.3 Streambed topographies used in the simulations and their sinuosities for wavelength 7.5m.

5.3.4 Taguchi orthogonal design and numerical simulations

We applied the model described in section 2.1 to analyze the hyporheic flow behavior through a range of meandering topographies. These numerical simulations were used to develop empirical equations for predicting characteristic values of the residence time distribution (mean and standard deviation) and average downwelling flux. Taguchi array design was used to reduce the number of simulations required. This is a highly fractional orthogonal design that is based on a design matrix proposed by Dr. Genichi Taguchi. Taguchi design consider a selected subset of combinations of multiple factors at multiple levels. Taguchi design of numerical simulations is given in Table 5.2.

Table 5.2 Taguchi design of the numerical simulations.

Run	W	λ	J	displacement	Rc	A	Beta_deg	Length of the channel	D	D_max	W/D	Wa	Da	A (m^2)	V_inlet
1	1	7.50	1	22.50	0.00	0.60	9.12	22.50	0.10	0.15	9.80	5	1.5	0.1	0.08
2	1	7.50	1.05	22.50	2.98	0.96	19.33	23.37	0.10	0.15	9.80	9	1.5	0.1	0.08
3	1	7.50	1.2	22.50	1.79	1.93	37.30	27.03	0.10	0.15	9.80	12	1.5	0.1	0.08
4	1	7.50	1.5	22.50	1.54	3.57	62.05	35.49	0.10	0.15	9.80	17	1.5	0.1	0.08
5	1	7.50	2	22.50	1.63	5.67	79.73	44.31	0.10	0.15	9.80	23	1.5	0.1	0.08
6	1	7.50	3.3	22.50	2.17	9.33	97.17	74.42	0.10	0.15	9.80	34	1.5	0.1	0.08
7	3	25.67	1	77.01	0.00	2.06	9.12	77.01	0.23	0.34	13.05	24	3.4	0.59	0.13
8	3	25.67	1.05	77.01	10.21	3.28	19.33	86.63	0.23	0.34	13.05	28	3.4	0.59	0.13
9	3	25.67	1.2	77.01	6.14	6.62	37.30	88.46	0.23	0.34	13.05	38	3.4	0.59	0.13
10	3	25.67	1.5	77.01	5.29	12.20	62.05	119.01	0.23	0.34	13.05	55	3.4	0.59	0.13
11	3	25.67	2	77.01	5.58	19.40	79.73	155.45	0.23	0.34	13.05	76	3.4	0.59	0.13
12	3	25.67	3.3	77.01	7.43	31.92	97.17	247.92	0.23	0.34	13.05	114	3.4	0.59	0.13
13	10	98.87	1	296.61	0.00	7.94	9.12	98.87	0.56	0.84	17.86	84	8.4	3.99	0.14
14	10	98.87	1.05	296.61	39.34	12.64	19.33	307.86	0.56	0.84	17.86	98	8.4	3.99	0.14
15	10	98.87	1.2	296.61	23.64	25.50	37.30	340.74	0.56	0.84	17.86	137	8.4	3.99	0.14
16	10	98.87	1.5	296.61	20.36	47.00	62.05	436.81	0.56	0.84	17.86	201	8.4	3.99	0.14
17	10	98.87	2	296.61	21.49	74.71	79.73	598.66	0.56	0.84	17.86	284	8.4	3.99	0.14
18	10	98.87	3.3	296.61	28.63	122.95	97.17	934.94	0.56	0.84	17.86	429	8.4	3.99	0.14
19	30	338.41	1	1015.22	0.00	27.17	9.12	338.41	1.26	1.89	23.79	262	18.9	42.00	0.5
20	30	338.41	1.05	1015.22	134.64	43.26	19.33	1053.68	1.26	1.89	23.79	310	18.9	42.00	0.5
21	30	338.41	1.2	1015.22	80.93	87.29	37.30	1169.39	1.26	1.89	23.79	442	18.9	42.00	0.5
22	30	338.41	1.5	1015.22	69.70	160.86	62.05	1495.10	1.26	1.89	23.79	663	18.9	42.00	0.5
23	30	338.41	2	1015.22	73.56	255.71	79.73	2049.08	1.26	1.89	23.79	947	18.9	42.00	0.5
24	30	338.41	3.3	1015.22	97.98	420.82	97.17	3204.11	1.26	1.89	23.79	1442	18.9	42.00	0.5
25	100	1303.35	1	3910.05	0.00	104.66	9.12	1303.35	3.07	4.61	32.56	914	46.1	354.20	0.9
26	100	1303.35	1.05	3910.05	518.55	166.62	19.33	4058.19	3.07	4.61	32.56	1100	46.1	354.20	0.9
27	100	1303.35	1.2	3910.05	311.68	336.18	37.30	4491.64	3.07	4.61	32.56	1609	46.1	354.20	0.9
28	100	1303.35	1.5	3910.05	268.46	619.54	62.05	5756.32	3.07	4.61	32.56	2459	46.1	354.20	0.9
29	100	1303.35	2	3910.05	283.33	984.86	79.73	7889.09	3.07	4.61	32.56	3555	46.1	354.20	0.9
30	100	1303.35	3.3	3910.05	52.97	1620.77	70.41	12341.00	3.07	4.61	32.56	5462	46.1	354.20	0.9
31	1000	17181.51	1	51544.52	0.00	1379.68	9.12	17181.51	24.88	37.32	40.19	10139	373.2	28490.00	3.7
32	1000	17181.51	1.05	51544.52	6835.87	2196.42	19.33	53497.20	24.88	37.32	40.19	12589	373.2	28490.00	3.7
33	1000	17181.51	1.2	51544.52	4108.77	4431.73	37.30	59210.30	24.88	37.32	40.19	19295	373.2	28490.00	3.7
34	1000	17181.51	1.5	51544.52	3539.01	8167.14	62.05	75902.40	24.88	37.32	40.19	30501	373.2	28490.00	3.7
35	1000	17181.51	2	51544.52	3734.97	12982.92	79.73	104016.00	24.88	37.32	40.19	44949	373.2	28490.00	3.7
36	1000	17181.51	3.3	51544.52	4974.54	21365.87	97.17	162699.00	24.88	37.32	40.19	70098	373.2	28490.00	3.7

5.3.5 Statistical analysis

5.3.5.1 Residence time distribution

Several probability functions have been proposed for the residence time distribution of the hyporheic zone, including exponential (Bencala and Walters, 1983, Runkel, 1998), lognormal (Marzadri et al., 2010, Tonina and Buffington, 2011, Wörman et al., 2002) and power law distribution (Cardenas, 2008b, Cardenas, 2008a, Haggerty, 2002). Specially Cardenas (2008b) has reported that hyporheic residence time through all channel features follows a power-law distribution, and meandering flow through the two-dimensional point bars has been shown to be a power-law distribution (Cardenas, 2008a). Gomez et al. (2012) has also reported the residence time through two-dimensional meanders follow a power low behavior when characterized by aquifer dispersity. Additionally, Tonina and Buffington (2011) showed that residence time distribution around partially submerged riffle-pools (hence flow meanders around these bedforms) follow a lognormal distribution. Considering these previous results, we examined residence time distribution through a meandering channel with three-dimensional meander topographies. We tested the fit of simulated residence times for the distributions (Equations 14 – 17) previously reported and Weibull distribution.

Lognormal distribution can be presented as (Marzadri et al., 2010, Tonina and Buffington, 2011);

$$Lognormal\ (t) = \frac{1}{\sqrt{2\pi\sigma^2}\ t} e^{\left(-\frac{(\ln t-\mu)^2}{2\sigma^2}\right)} \qquad (14)$$

Where μ and σ^2 are the natural log of the mean and standard deviation of the residence time (Tonina and Buffington, 2011).

We also fit the observed residence time distribution with exponential distribution (eq 15) and power law (eq 16) according to (Tonina and Buffington, 2011);

$$exponential\ (t) = \lambda_e e^{-\lambda_e t} \qquad (15)$$

Where λ_e is the rate parameter, inverse of the mean residence time (Tonina and Buffington, 2011).

$$Power\ law\ (t) = \left(\frac{t}{t_{min}}\right)^{\alpha} e^{-\lambda_p t} \qquad (16)$$

Where t_{min} is a threshold parameter which was set equal to the shortest residence time observed (Tonina and Buffington, 2011). α and λ_p were estimated using the maximum likelihood method in Excel.

Weibull probability density function can be expressed as;

$$Weibull\ (t) = \frac{\gamma}{\alpha}\left(\frac{t}{\alpha}\right)^{(\gamma-1)} e^{-\left(\frac{t}{\alpha}\right)^{\gamma}} \qquad (17)$$

Where γ is the shape parameter, and α is the scale parameter, which was estimated through the maximum likelihood method in Excel.

We applied the Kolmogorov-Smirnov test (KS test) to compare residence time distributions to the proposed probability distribution functions discussed above (Figure 5.4). KS test is based on the maximum distance between two cumulative probability distribution curves (KS statistics).

5.3.5.2 Predicting downwelling water flux and residence time

We use our simulation results to predict empirical relationships for average downwelling flux and residence times. These two parameters are important when making management decisions in practice. Empirical prediction of these parameters will make the process easier without any requirement of mathematical and numerical modeling. This study used a method similar to Tonina and Buffington (2011), where they have derived empirical formulas for residence time and mean hyporheic depths for riffle-pool channels. For river management, it is vital to understand the characteristics of residence time for all channel features which drive hyporheic flow, and there is paucity for such understanding for meanders.

In this analysis, we assumed that mean and standard deviation of the residence time are function of river width W, meander wavelength λ, sinuosity J, mean channel flow velocity v, average water depth d, valley slope S, density of water ρ, dynamic viscosity of water μ, acceleration of gravity g, hydraulic conductivity K, sediment porosity θ, width of the alluvium W_a, and the depth of the alluvium d_a. We use the Buckingham pi theorem to reduce the number of variables. Hydraulic conductivity, mean flow velocity, and water density were considered as dimensionally independent variables for the analysis. There was a total of fifteen variables including flux, the mean, and standard deviation of residence time.

$\pi_1 = \frac{W}{\sqrt{K}}$; $\pi_2 = \frac{\lambda}{\sqrt{K}}$; $\pi_3 = J$; $\pi_4 = \frac{d}{\sqrt{K}}$; $\pi_5 = \frac{\mu}{\rho v \sqrt{K}}$; $\pi_6 = s$

$\pi_7 = \frac{g\sqrt{K}}{v^2}$; $\pi_8 = \theta$; $\pi_9 = \frac{W_a}{\sqrt{K}}$; $\pi_{10} = \frac{d_a}{\sqrt{K}}$; $\pi_{11} = \frac{\tau v}{\sqrt{K}}$; $\pi_{12} = \frac{SD\tau v}{\sqrt{K}}$

$\pi_{13} = \frac{qv}{\sqrt{K}}$

Residence time distribution was approximated with regression models;

$$\frac{\tau v}{\sqrt{K}} = exp\left[\sum_{i=1}^{5} A_i \ln(\pi_i)\right] \quad (18)$$

$$\frac{SD\tau v}{\sqrt{K}} = exp\left[\sum_{i=1}^{5} B_i \ln(\pi_i)\right] \quad (19)$$

$$\frac{qv}{\sqrt{K}} = exp\left[\sum_{i=1}^{n} C_i \ln(\pi_i)\right] \quad (20)$$

We conducted a linear regression analysis similar to Tonina and Buffington (2011) to determine regression coefficients for the above-proposed equations. Relationships were considered using forward and backward Akaike Information Criteria (AIC) method in R software. During the regression analysis, it was observed that only some of the pi terms have an impact on the residence time, and other pi terms could be removed from the empirical formula. Since we have not varied valley slope in our simulations (because we were interested in exploring the influence of meandering topography on residence time and hence we kept other factors constant to reduce the number of simulation required), the slope was not used in the final equation. Sediment porosity and alluvium volume were not used in the final form. The sensitivity analysis described in chapter 4 showed that porosity have little impact on the residence time. Hoever the hydraulic conductivity plays an important role in controlling residence time. Since we used a sufficiently large alluvium volume, there is no impact from the alluvium volume as well. This is because our objective was to explore the effect of meandering topography on residence time and hence keeping other parameters constant to reduce the number of simulations.

5.4 Results

5.4.1 Residence time distribution

Kolmogorov-Smirnov test (KS test) results were compared for possible distribution functions for residence time distributions (Figure 5.4). We use a significance level of 0.01 to specify the most appropriate probability distribution for the residence time distribution. In total, there were 36 numerical simulation results for the test. For a 0.01 significant level and 36 numerical simulations, the critical statistics value was 0.27. Our hypothesis regarding the distribution form can be accepted if KS statistics are below the critical value. Results (Figure 5.4) indicate that residence time distribution is log-normal, having more than 75% of the model runs below the critical value (only run 12 and 18 show KS statistics higher than the critical value). All the other distributions had more significant deviations from our observed residence time distribution.

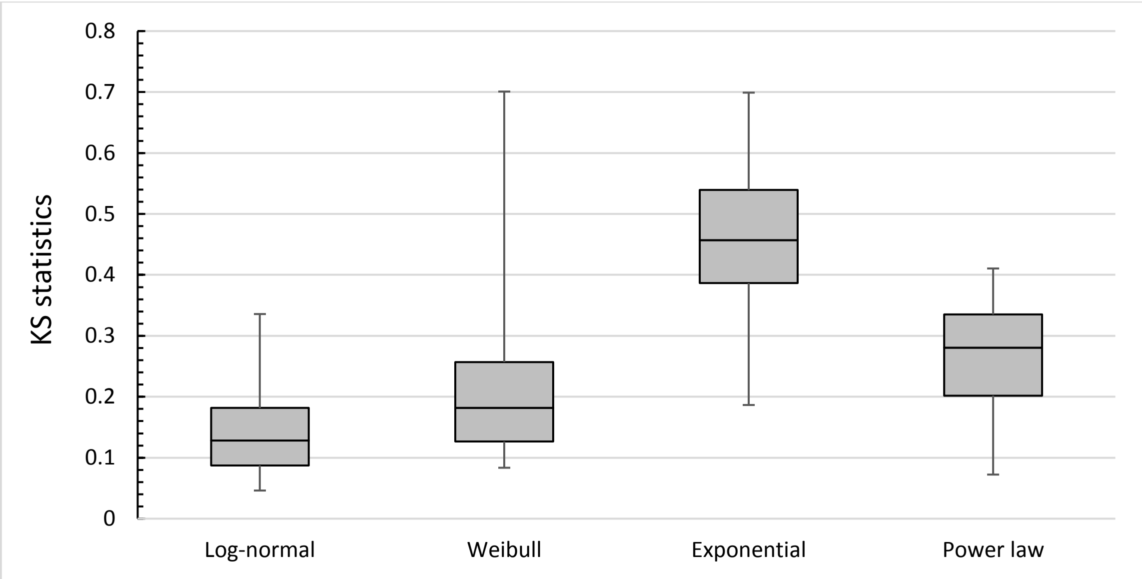

Figure 5.4 Kolmogorov Smirnov test results for the four distributions we considered.

Variation in the mean and standard deviation of residence time distribution with different meander wavelengths and sinuosities are shown in Figures 5.5 and 5.6. Both mean and standard deviation of the residence time increases with the wavelength for all the sinuosities. However, there is no pronounced relationship visible for residence times with various sinuosities. This is further examined in Figure 5.5, which compares the variation of mean and SD of residence time with respect to the sinuosity. Generally, when the wavelength increases, the distance between two meander peaks increases resulting in long hyporheic flow paths. Longer flow paths generally leads to increased residence times.

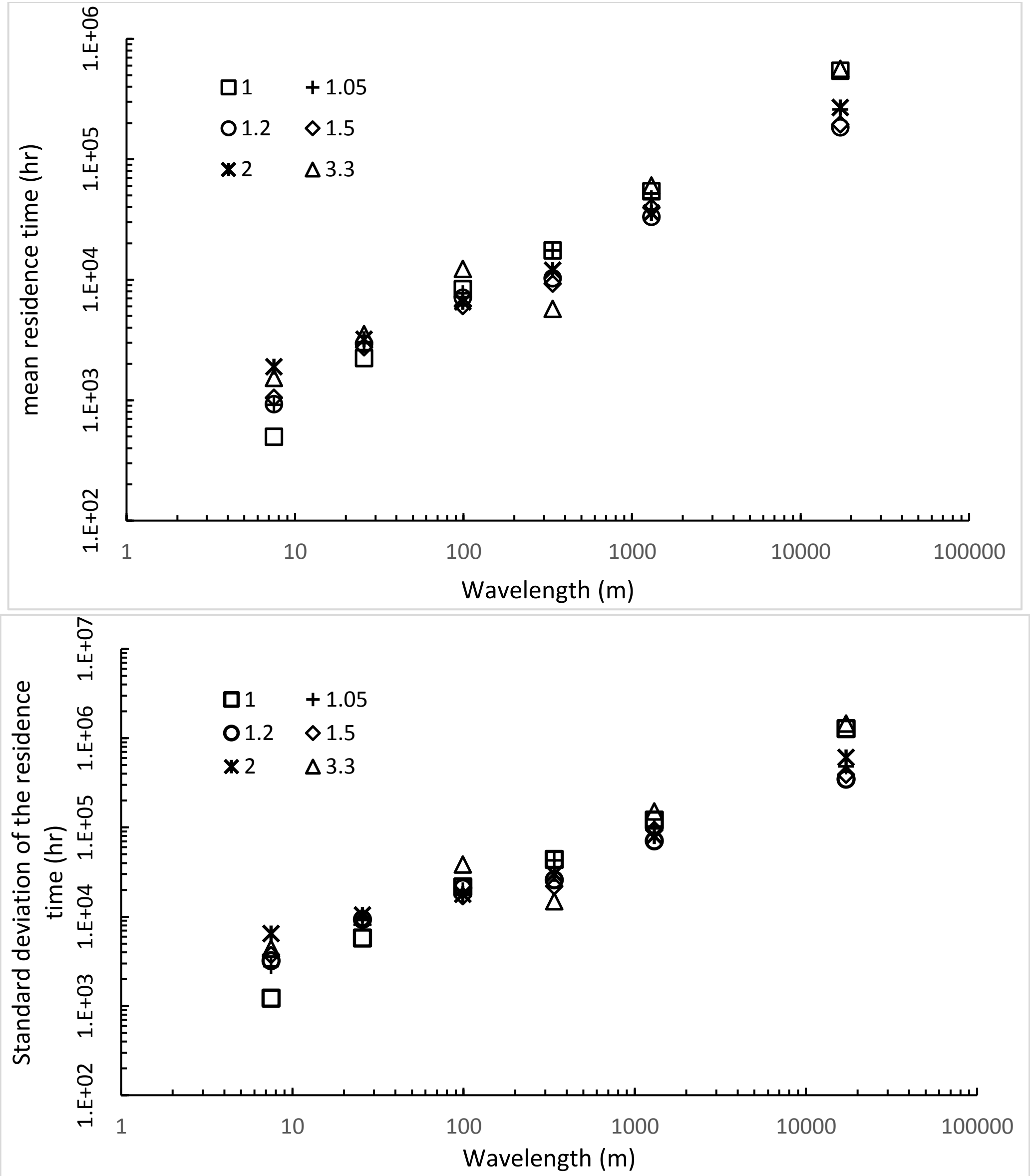

Figure 5.5 Mean (up) and standard deviation (bottom) of the residence time with respect to the meander wavelength. Different symbols show different sinuosities used for simulations.

We cannot see a clear relationship between residence time and river sinuosity (Figure 5.6). There is a slight increase in the residence time with the sinuosity for the shortest wavelengths used (7.5m and 25.7m). For all the other wavelengths, residence time shows a decreasing pattern with the sinuosity for low sinuosities and then an increase with high sinuous meanders. However, sinuosity does not represent direct influence for the hyporheic residence time.

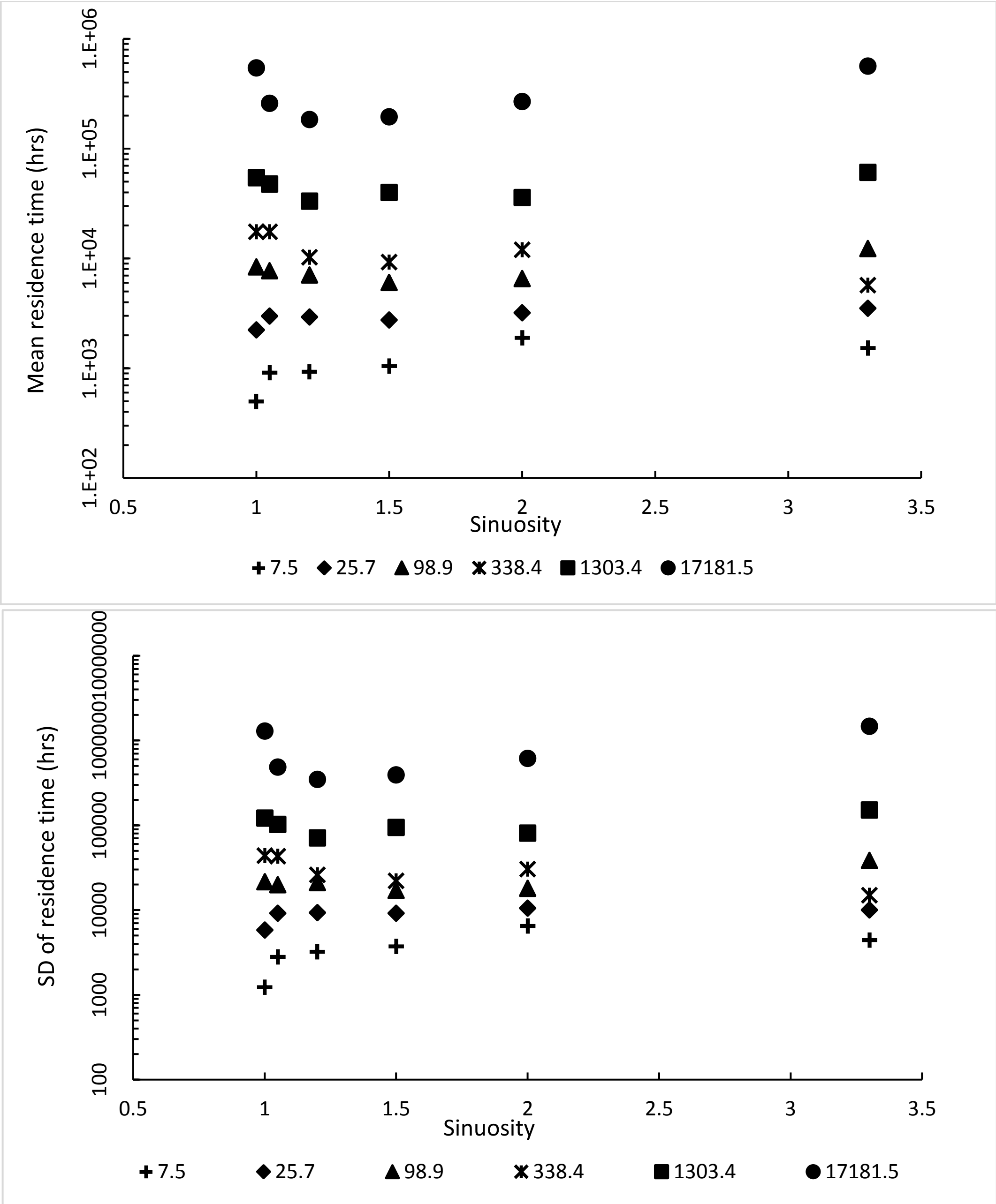

Figure 5.6 Mean (up) and standard deviation (bottom) of the residence time with respect to the meander sinuosity. Different symbols show different wavelengths used for simulations.

5.4.2 Average downwelling flow

Average downwelling water flux represents the total water volume that comes into the sediment bed per unit volume per unit time and unit area of the stream bed and has units equivalent to a velocity, m/s. The model results show that average downwelling flux shows a decreasing trend with increasing meander wavelength regardless of sinuosity (Figure 5.7). Higher interfacial flux has been observed for the shortest wavelength (7.5m) used in the simulations, and the flux gradually decreases with increasing wavelength. It is also apparent that interfacial flux generally increases with the sinuosity.

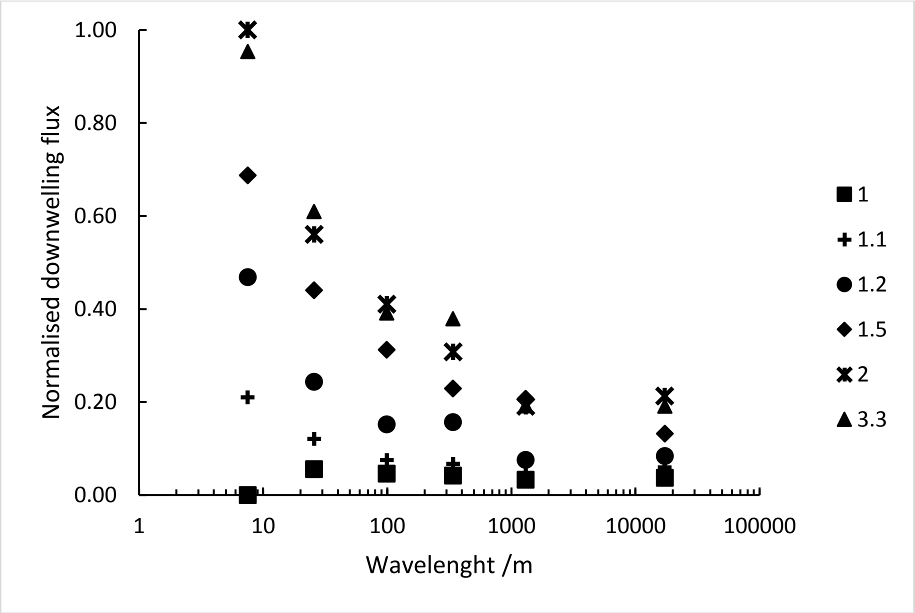

Figure 5.7 Normalised average downwelling interfacial flux (q/qmax, where qmax is the maximum predicted average downwelling flux) with respect to the meander wavelength. Different notations show different sinuosities used for simulations.

The model results show that for a given wavelength, average downwelling water flux increases as the sinuosity increases (Figure 5.8). Low downwelling flux has been observed in the straight channel.

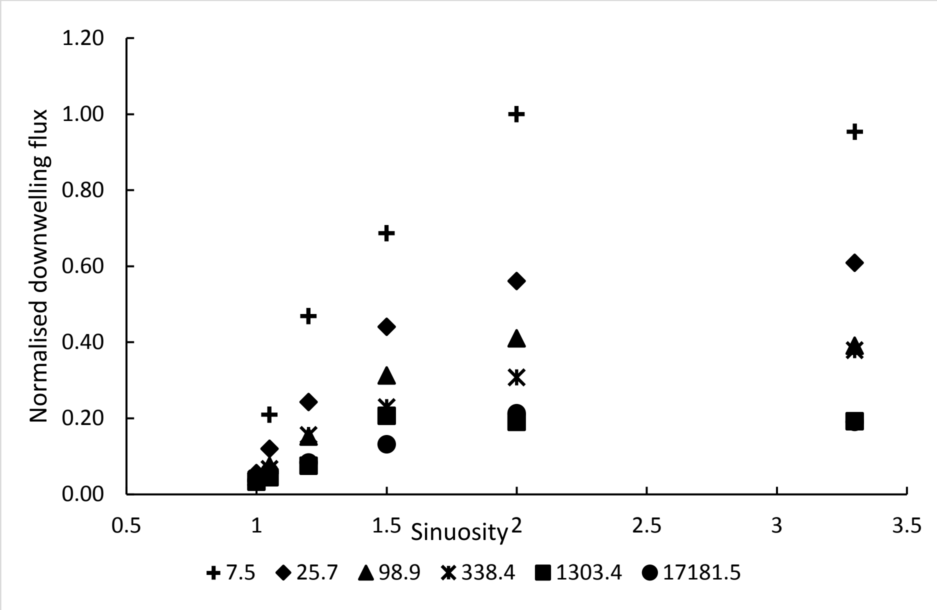

Figure 5.8 Normalised average downwelling interfacial flux (q/qmax, where qmax is the maximum predicted average downwelling flux) with respect to the meander sinuosity. Different notations show different wavelengths used for simulations.

5.4.3 Predicting downwelling water flux and residence time

We attained the following empirical relationships (equations 21, 22, and 23) for the mean and standard deviation of the residence time and downwelling water flux using a linear regression procedure described in section 5.3.5.2. Predicted values show an excellent approximation with the simulated values with an R^2 of 0.9997 and 1 (Figure 5.9).

$$\frac{\tau v}{\sqrt{K}} = \exp\left[-5.4373\ln\frac{W}{\sqrt{K}} + 5.0970\ln\frac{\lambda}{\sqrt{K}} + 0.2436\ln J + 1.0342\ln\frac{\mathrm{d}}{\sqrt{K}} - 0.5029\ln\frac{\mu}{\rho v\sqrt{K}}\right] \quad (21)$$

$$\frac{SD\tau v}{\sqrt{K}} = \exp\left[-9.5125\ln\frac{W}{\sqrt{K}} + 8.4708\ln\frac{\lambda}{\sqrt{K}} + 0.3237\ln J + 1.2956\ln\frac{\mathrm{d}}{\sqrt{K}} - 0.5595\ln\frac{\mu}{\rho v\sqrt{K}}\right] \quad (22)$$

$$\frac{qv}{\sqrt{K}} = \exp\left[-12.042\ln\frac{W}{\sqrt{K}} + 8.359\ln\frac{\lambda}{\sqrt{K}} - 1.449\ln J - 2.611\ln\frac{\mu}{\rho v\sqrt{K}} + 1.588\ln\frac{W_a}{\sqrt{K}}\right] \quad (23)$$

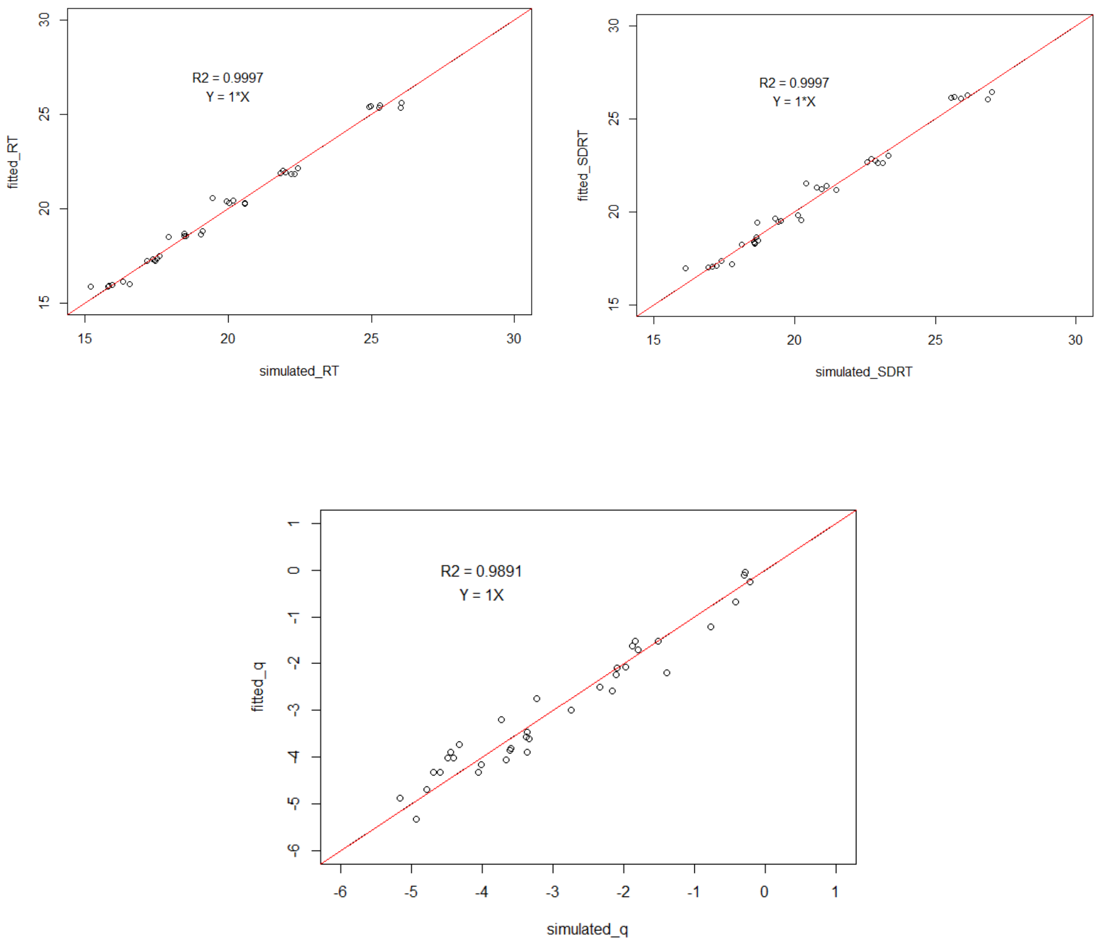

Figure 5.9 Simulated and predicted mean residence time, Standard deviation of the average residence time, and downwelling water flux (in the log domain).

5.5 Discussion

5.5.1 Effect of meander topography on residence time and downwelling water flux

The results of the model simulations showed that meander morphology affects hydraulic residence times in the hyporheic zone. For a given sinuosity, high wavelengths have high residence times. Generally, when the wavelength increases, the distance between two meander peaks increases, resulting in long hyporheic flow paths. Longer flow paths generally leads to increased residence times. This effect has also been observed by Boano et al. (2010a), indicating that large meandering rivers tent to have long residence times, but less surface water exchange with the streambed compare to small rivers. River sinuosity does not represent direct influence for the hyporheic residence time. In contrast, Gomez et al. (2012) have found that increasing river sinuosity has increased residence times in the hyporheic zone. However, similar results have been reported by Stonedahl et al. (2013), where residence time does not follow a direct relationship with sinuosity.

When wavelength increases, it is obvious to see an increase in residence time due to the increase in flow path lengths. However, the reduction in interfacial fluxes is more challenging to interpret. Tonina and Buffington (2011) reported an increase in flux with the alluvium volume of riffle-pool channels, arguing that a larger hyporheic zone volume would develop higher hyporheic flux. In contrast, we observed reduced flux with increasing alluvium volume. This is due to the flow resistance at the bend curvature. As discussed in chapter 4, there are two major transport processes occurring within the hyporheic zone of meandering rivers, lateral and longitudinal pumping. Therefore, high wavelengths have low curvature causing reduced lateral pumping compared to longitudinal pumping of water; therefore, a decrease in downwelling flux. This is due to the acceleration and declaration of flow due to the curvature. Therefore, when the meander curvature is small (small wavelengths), streamflow pump more lateral pumping of stream water into the hyporheic zone, increasing the total sum of downwelling flux. When the radius of curvature is large, the secondary current is small, resulting in reduced flux into the hyporheic zone. This shows that the large rivers tend to exchange less river water with the hyporheic zone compared to smaller rivers.

The model results show that for a given wavelength, average downwelling water flux increases as the sinuosity increases. Similar behavior of downwelling flux with meander sinuosity has been reported in previous literature (Cardenas, 2009a, Stonedahl et al., 2013). When sinuosity increases, channel length perpendicular to the channel head gradient increases. Therefore, the inter-meander distance will occupy a more significant head gradient resulting in higher flux into the subsurface. The lowest flux has been observed in the straight channel. Our straight channel geometry includes a three-dimensional alternate bars and hydraulic head gradient acting on the bed is smaller compared to a meandering channel.

5.5.2 Predicting downwelling flux and residence time

We derived three empirical relationships to predict residence time distribution and downwelling water flux in meandering rivers with isotropic and homogeneous alluvium. These relationships can provide a good approximation for flux and residence time distribution of hyporheic flow in low gradient meandering channels. Channel width, depth, sinuosity, wavelength, channel discharge, hydraulic conductivity, and alluvium width are the basic parameters required for estimations. These parameters can be estimated in the field.

Estimate for average residence time (equation 18) suggest high water retention time in the hyporheic zone and dominating biogeochemical conditions. High τ would allow for both aerobic conditions and anaerobic conditions, supporting complete biogeochemical nitrogen reactions. However, small τ could only support aerobic conditions facilitating oxidation reactions such as nitrification and ammonification.

5.6 Conclusions

We studied residence time distribution and downwelling water flux in the hyporheic zone of meandering rivers through a set of three-dimensional simulations. Distribution of the residence time was approximated by a log-normal distribution. Many factors influence the hyporheic flow, including, meander wavelength, sinuosity, river discharge, width and depth of the river, hydraulic conductivity, and alluvium volume. We investigated the importance of these factors in controlling the hyporheic flow characteristics. We have considered three-dimensional channel topographies (including point bar profiles) in our model geometry. Therefore, complex interactions, vertical flow (secondary currents), and lateral connectivity through meander bends occur.

The magnitude of downwelling water flux and downwelling locations are primarily controlled by the curvature of the meander. When meander wavelength increases (high radius of curvature), the flow turbulence at the meander bend decreases, reducing the secondary currents through the hyporheic zone. A similar phenomenon exists for low sinuous cases. Additionally, there is less hydraulic gradient acting on the low sinuosity rivers, and the water pump is low.

Even though sinuosity does not directly impact on the residence time, wavelength is one of the critical factors impacts on the residence time. Long wavelengths are associated with long hyporheic flow paths, eventually resulting in longer residence times.

We develop three empirical formulas to estimate characteristics of residence time and downwelling flux in the hyporheic zone of meandering rivers.

Chapter 6: Hyporheic flow through river meanders and implications for nitrogen processing

6.1 Background

Dissolved organic nitrogen compounds are essential nutrients in the stream ecosystem. Nitrate (NO_3^-), nitrite (NO_2^-) and ammonium (NH_4^+) are some commonly found forms of reactive nitrogen in rives (Taylor et al., 2005, Zhou et al., 2014). However, agricultural runoffs and discharges from urban areas can increase the load of nitrogen compounds in rivers beyond their carrying capacity (Marzadri et al., 2011). Severe effects include blue-green algal blooms, eutrophication with excessive phytoplankton growth leading to depletion of oxygen (Lee et al., 2006, Omnes et al., 1996) and deadly effects on quality of drinking water for terrestrial animals and human (Cook et al., 2010, Rivett et al., 2008). Depletion of oxygen in rivers severely affects aquatic species; for instance, massive fish kill took place in Murray River, Australia, in 2019 due to high nutrient loads and low oxygen levels. Massive efforts are made in Australia as well as in other countries to mitigate the impacts of excessive nitrogen loads in rivers. Catchment-scale interventions to reduce nitrogen delivery rates, such as the construction of riparian buffer, can be costly. Therefore, major research and management practices are essential to promote the processing and removal of nitrogen in streams.

Microbial processes are the primary mechanisms of reducing nitrogen loads from stream water (Marzadri et al. 2012). The hyporheic zone, where surface-subsurface water exchange happens, is rich with the microbial community (Marzadri et al. 2012) and an important location to assimilate nitrogen. Therefore, recent research focus has been on the understanding of biogeochemical processes that occur in the hyporheic zone (Hill et al. 1998). This exchange is controlled by both physical transport and biogeochemical reaction kinetics (Haggerty et al., 2002, Zarnetske et al., 2012). Hyporheic zone increases hydrologic retention time and the volume of stream water in contact with sediment biota, enhancing biologic reactions supporting pollutant reduction and biogeochemical cycling (Sheibley et al. 2003).

Most nitrogen removal reactions occur in an anaerobic environment. When river water first enters the hyporheic zone, it is high in dissolved oxygen, producing an aerobic region near downwelling areas. Under aerobic conditions, ammonification microorganisms convert organic nitrogen into ammonium, and nitrification microorganisms convert ammonium into nitrate. As the water travels through the hyporheic flow paths, these oxidation reactions use oxygen as a terminal acceptor creating an anaerobic environment. Denitrification and anammox reactions occur under an anaerobic environment. These reactions convert nitrate into dinitrogen gas, which can escape from the river system. Previous chapters determined that meandering morphology is an essential channel feature for nitrogen removal reactions. There is a complex interaction between meandering morphology and channel flow rate in controlling hydraulic residence times and downwelling water flux in the hyporheic zone.

Given these potentially significant interactions in the riverbed, there is a lack of understanding of how to control river bed morphology to achieve sufficient nitrogen attenuation (Marzadri et al., 2012). For the complete transformation of ammonia and nitrates to harmless nitrogen gas, residence time distribution and average interfacial fluxes through the hyporheic zone are important. In this chapter, I have present how meandering morphology impacts the nitrogen reactions, transforming ammonium and nitrates to nitrogen gas and removing from the streambed. To address this aim, I have considered an approach of using a dimensionless number (Da, Damköhler number), defined as the ratio between the median residence time and the critical concentration of dissolved oxygen below which nitrogen removal reactions occur (Marzadri et al., 2012). We have used the numerical simulations conducted in the previous chapter when estimating empirical relationships for the characteristics of residence time distributions induced by river meanders.

6.2 Median hyporheic residence time

The median hyporheic residence time, for which 50% of the solutes have a residence time shorter than its value (which is the time when half of the solutes has left the sediment bed), can be used as a good parameter to estimate the available time for biogeochemical reactions (Marzadri et al., 2012, Tonina and Buffington, 2011). Figure 6.1 shows the variation of median residence time with meander wavelength. Channel widths range from 1m to 1000m.

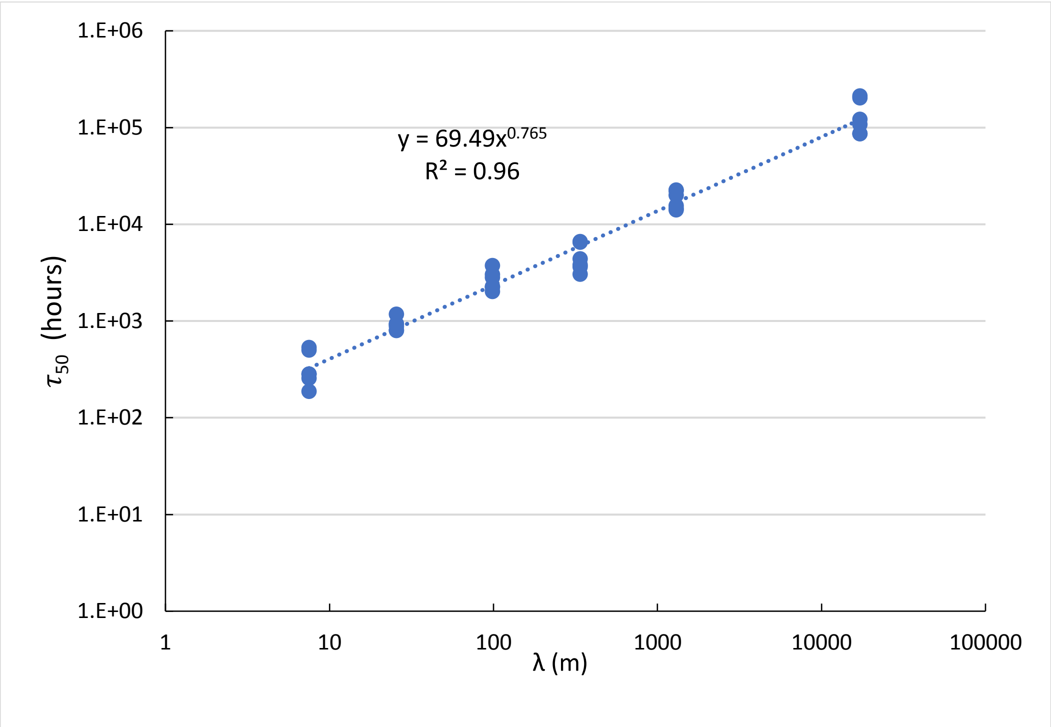

Figure 6.1 Hyporheic median residence time as a function of meander wavelength.

6.3 Damkolar number and hyporheic aerobic-anaerobic zones

Nitrogen transformation processes occurring in the hyporheic zone depend on the time required to achieve anaerobic conditions. Therefore, a limiting residence time, τ_{lim} is defined as the time needed to deplete oxygen concentration to a threshold value, $C_{O,lim}$ reaching anaerobic conditions. Previous literature identifies this limiting oxygen concentration as 4mg/l (Marzadri et al., 2012). We use Marzadri et al. (2012) biogeochemical model to define limiting residence time. This model considers nitrification, respiration, denitrification, and nitrogen consumption by living microorganisms. The limiting residence time, τ_{lim} assumes the following expression (Marzadri et al., 2011, Marzadri et al., 2012).

$$\tau_{lim} = \frac{1}{K_{RN}} . \ln\left(\frac{C_{O,0}}{C_{O,lim}}\right)$$

Where K_{RN} is the rate coefficients of nitrification and respiration reactions. $C_{O,0}$ is the in-stream dissolved oxygen concentration.

Given the importance of limiting residence time on nitrogen transformations in the hyporheic zone, we consider dimensionless Damköhler number to evaluate prevailing biogeochemical conditions in the hyporheic zone of meandering rivers. Therefore an indication of the biogeochemical conditions of the hyporheic zone can be provided by the dimensionless Damköhler number, Da (Marzadri et al., 2012).

$$Da = {}^{\tau_{50}}/_{\tau_{lim}}$$

Values of Da <1 indicate prevailing aerobic conditions, and Da >1 indicates that more than 50% of the solutes are in the anaerobic conditions. The Da allows us to analyze the redox conditions of the hyporheic zone induced by meanders as a function of meander wavelength (Figure 6.2). In simulations, hydraulic conductivity and sediment porosity were kept constant at 0.005 m/s and 0.34, respectively.

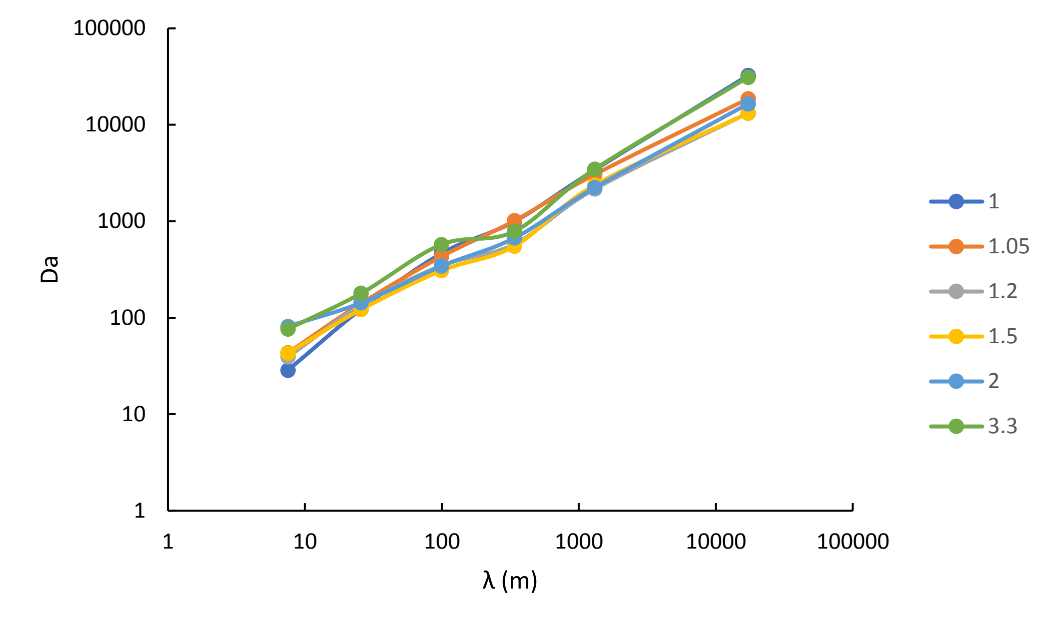

Figure 6.2 Damköhler number as a function of meander wavelengths for different sinuosities.

Results show that meander sinuosity has less impact on the Da, hence less impact for the redox conditions within the hyporheic zone. However, it is noticed that Da increases as the wavelength increases showing that the areas with anaerobic conditions increase with wavelength. For the given biogeochemical and hydraulic characteristics of the subsurface, all channel reaches showed prevailing anaerobic conditions in the hyporheic zone. This suggests that all the channels we considered in the study (widths >1m) are potential areas to drive anaerobic nitrogen reactions (denitrification and ANAMOX).

Chapter 7: Discussion

The overall aim of this research was to establish the impact of meandering morphology and river flow rates on water flux and residence time distribution in the hyporheic zone and to identify primary mechanisms that drive hyporheic flow in meandering rivers. This aim was achieved through a combination of two consecutive approaches: Laboratory-based conservative tracer experiments performed for various meander wavelengths and channel flow rates, and numerical simulations (with numerical particle tracking analysis) performed through a three-dimensional model. The experiment and model results discussed in chapters 3, 4 and 5 indicate that meander morphology affects both residence time distribution and average downwelling flux for a given stream flow rate. One of the primary findings of my study is that meander sinuosity, and channel valley slope in meandering rivers (which were considered as major controlling factors in previous studies) are not the only key factors that control hyporheic exchange, but there is also a complex interaction between meander morphology (both sinuosity and wavelength), channel valley slope and river flow rate.

There is limited progress in understanding surface water – subsurface water exchange processes through river meanders (Boano et al., 2010a). Solute breakthrough curves in the tracer experiments showed that there are two stages of mixing occurring in the hyporheic zone of meandering rivers. My model results confirmed the observed mixing behavior, demonstrating two-directional transport of particles in the hyporheic zone; the longitudinal movement of particles between meanders and the lateral movement of the particle across meander point bars at the bend apex. The presence of two exchange stages has also been discussed by Tonina and Buffington (2007) and Salehin et al. (2004) for riffle-pool channels, shallow (fast rates), and deep (slower rates) mixing areas in the streambed. Shallow mixing rates are subjected to strong influence by the surface water, and the deep mixing layer is less sensitive to the surface water. For meanders; previous studies have explicitly reported the existence of a horizontal flow between meander bends (Boano et al., 2006, Cardenas, 2008a, Cardenas, 2009a, Gomez-Velez et al., 2017, Revelli et al., 2008, Stonedahl et al., 2013, Stonedahl et al., 2010) and long timescales. These studies do not identify different hyporheic exchange rates through meandering morphology. However, Boano et al. (2010a) report similar observations as in this work (longitudinal and lateral exchange processes through meanders) highlighting possible complex spatial and temporal variations of hyporheic flow (residence time distributions and downwelling water flux), which could affect nitrogen biogeochemical processes as discussed in section 6.2.

Longitudinal cross-meander flow is produced by the downstream hydraulic head gradient due to the channel valley slope and the sinuosity of the river. Lateral pumping is caused by the acceleration of river water at the meander curvature, and it is sensitive to channel flow rate and curvature of the river. Variability in the hydraulic gradient, channel curvature, and flow path lengths are important factors in determining the transit times and downwelling flux through meanders. The results of this study show that lateral hyporheic currents have higher velocities and short flow paths compare to longitudinal fluxes. Therefore, lateral flow paths are associated with short residence times and large fluxes compare to longitudinal flow paths. This will create different surroundings (aerobic and anaerobic zones) for the microbial community; and hence affect the rates of biogeochemical reactions, which is discussed in section 6.2 of this chapter.

The results of my experiments and model simulations showed that meander morphology affects water volume and transit times in the hyporheic zone (Table 6.1). For a given sinuosity, high wavelengths have low curvature causing a reduction in lateral pumping compared to longitudinal pumping of water; therefore, a decrease in downwelling flux. Further, long wavelengths have long flow paths (due to more longitudinal pumping) and hence long residence times. This effect was also observed by Boano et al. (2010a), indicating that large meandering rivers tent to have long residence times, but less surface water exchange with the streambed compare to small rivers. For a given wavelength, sinuosity increases curvature effect on hyporheic flow resulting in higher flux into the hyporheic zone. Similarly, previous literature reports that increasing sinuosity causes an increase in downwelling flux due to the increased hydraulic head on the bed (Boano et al., 2006, Cardenas, 2009a, Gomez et al., 2012, Stonedahl et al., 2013). However, my results did not show a clear relationship between sinuosity and residence time, contrasting with previous results by Stonedahl et al. (2013) and Gomez et al. (2012). These studies report a decrease in residence time with increasing sinuosity. However, at very high sinuosities, flow paths become very short (very low wavelength) and can have short residence time. Sinuosity and wavelength, coupled with the flow path and curvature variability, result in complex residence time distribution and downwelling flux patterns in the hyporheic zone.

Table 7.1 Effect of meander morphology and channel flow rate on residence time and downwelling water flux within the hyporheic zone. Green arrows show miner increase or decrease of the parameter.

Parameter		Flow path lengths	Channel curvature	Lateral pumping	Residence time	Flux
Wavelength	↑	↑	↓	↓	↑	↓
Sinuosity	↑	↑ (green)	↑	↑	↑ (green)	↑
Flow rate	↑	-	-	↑	↓	↑

Higher discharges produce comparatively rapid lateral exchange, and hence large fraction of solutes are associated with shorter residence times. This is due to the increased acceleration of water at the meander bend pumping lateral water currents through the subsurface at meander apex. Increased advective pumping has been reported for flume and studies associated with dune-riffle morphologies (Elliott and Brooks, 1997a, Salehin et al., 2004) and riffle-pool morphologies (Tonina and Buffington, 2007, Tonina and Buffington, 2011). But, none of the previous studies have investigated the effect of channel discharge on hyporheic flow in meandering rivers, and assume valley slope and meander sinuosity as the major controlling factors. Results of the sensitivity analysis identify river discharge as the primary factor controlling downwelling water flux and a secondary influencing factor on residence time distribution. Therefore, the effect of river discharge cannot be ignored. These findings may be applied in stream ecosystems to manage biogeochemical nitrogen transformations by controlling the environmental water delivery and flow rates.

Numerical simulations show that surface water - groundwater exchange across meanders occurs across a broad timescale and follow a lognormal distribution. The timescale of this exchange is sensitive to the meander morphology of the river, particularly curvature and the length of hyporheic flow paths. This has implications for nitrogen transformation as the above-mentioned variables control both the rate at which substrates are supplied and the contact time with sediments in the hyporheic zone. This leads to competition between reactant supply and demand, resulting in nonlinear dependency of reaction rates on hyporheic flux (Chen et al., 2015). The results of this study indicate that this competition is potentially more complex for meanders because of the impact of surface flow characteristics and meandering morphology (wavelength and sinuosity) on hyporheic flux and volume. This is further discussed in detail in the next section.

7.1 Effect of Meanders on nitrogen processing

7.1.1 Use of Damköhler number

As discussed in the previous Chapter 6, Da provides an indication of prevailing redox conditions within the hyporheic zone from the downwelling area to the upwelling area. The use of median residence time for estimating Da implies that 50% of dissolved solutes are in the desired redox environment. However, this does not guarantee that the channel feature can support complete nitrogen removal reactions. Generally, stream nitrogen loads travel through the hyporheic zone without change when Da number is small and partially or entirely removed when Da number is large. I have re-introduced Figure 2.4 of chapter 2 to show the effect of channel size on nitrogen reactions (Figure 6.3). The light blue area in Figure 6.3 shows Da >1 indicating prevailing anaerobic conditions.

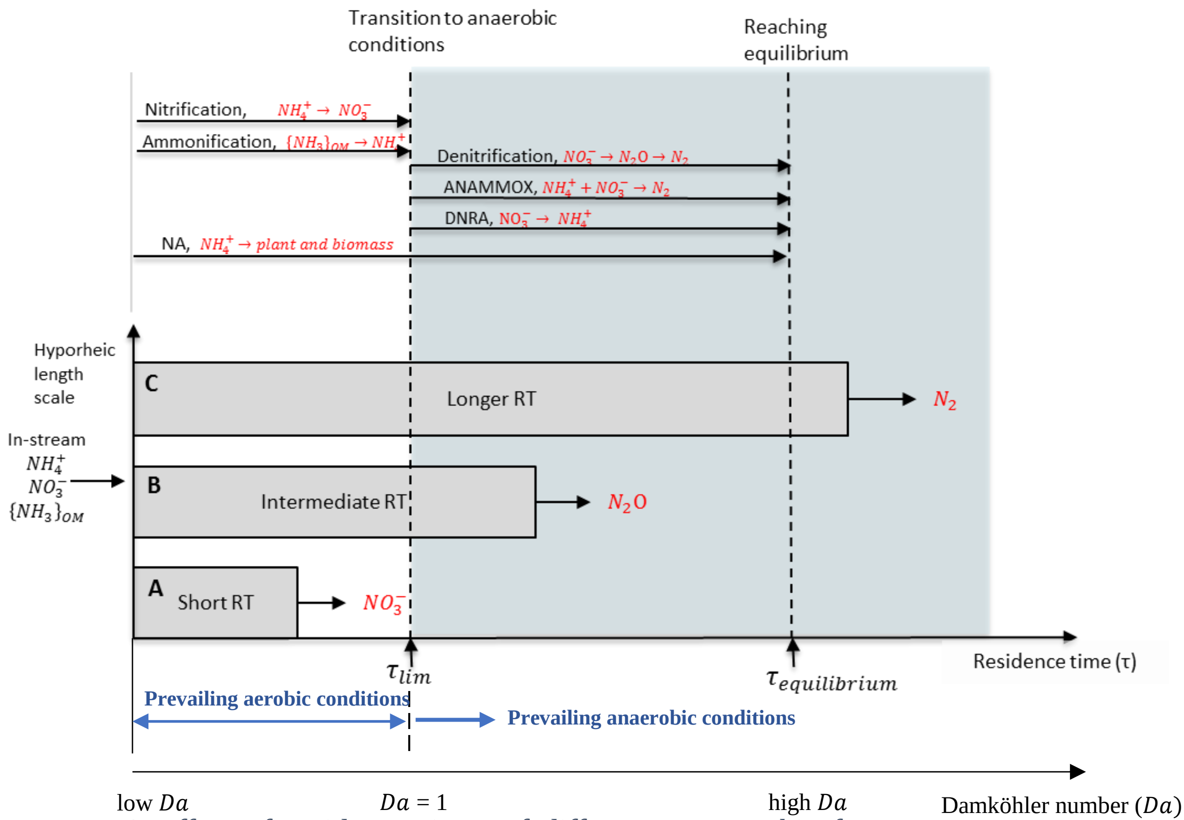

Figure 7.1 3 Effect of residence times of different geomorphic features on nitrogen evolution in the hyporheic zone. Residence time on the horizontal axis denotes the travel time of water entering the hyporheic zone, and the first vertical dashed line shows the transition of the aerobic region into anaerobic (Da =1). Light blue area represents Da >1; indicating prevailing anaerobic reactions.

At the start of the hyporheic flow path (low Da), stream water contains high oxygen concentration and will support nitrification and ammonification reactions which consume oxygen and increase nitrates in the system. This promotes denitrification reaction when oxygen concentration depletes beyond the limiting threshold for anaerobic conditions ($Da \geq 1$) and increased nitrate concentration. Water spends more time in the flow paths promoting dominant denitrification reaction (and other nitrogen removal reactions) as traveling towards the end of the flow paths (high Da) before reaching the river. However, Zarnetske et al. (2012) observed that the denitrification does not precisely occur at the assumed $Da = 1$ but at values closer to 10. This is because of the additional time required to denitrify nitrate mass generated from the nitrification reaction. If the system has low nitrification reaction rates, denitrification is possible at $Da < 1$, and on the other hand, high nitrification reactions will shift net denitrification to much longer time scales

(Zarnetske et al., 2012). The presence of high ammonium and organic nitrogen concentrations would further shift denitrification time scales to higher values.

Previous studies define Da number as a simple and effective approach of investigating systems as reaction-limited and transport-limited, enhancing the ability to identify nitrogen behavior within the hyporheic zone of streams (Marzadri et al., 2012, Zarnetske et al., 2012, Marzadri et al., 2016). Da number can be effectively calculated for any river system using simple field measurements of oxygen decay rate and quantifying residence times. This method has been used to assess biogeochemical redox potential at microzones (Briggs et al., 2015a), bedforms (Marzadri et al., 2016, Azizian et al., 2015) and alternate bar morphology (Marzadri et al., 2012) in the hyporheic zones.

The Damköhler number increases with rapid dissolved oxygen utilization rates and/ or increases in water residence times in the hyporheic zone, providing more opportunities for denitrification reaction. Based on $Da < 1$, we are confident that the hyporheic zone act as a source of nitrate to the river. However, further analysis is needed to identify critical Da numbers for complete denitrification and for identifying equilibrium conditions for nitrous oxide emission (due to incomplete denitrification reaction). Previous studies provide possible ranges for Da numbers by comparison of nitrate uptake rates and nitrous oxide emission rates applied to field and model data. Azizian et al. (2015) proposes $Da > 10^3$ for complete nitrate removal. Removal of nitrate within the hyporheic zone stabilises when $Da > 10^2$ which we can call critical Da, above which the hyporheic zone act as a sink of nitrate (Marzadri et al., 2012). According to (Marzadri et al., 2012) model predictions, nitrous oxide production rates peak at $Da \approx 5$. This implies that the hyporheic zones can act as sink of nitrate and nitrous oxide when $Da \geq 5$. However, this will depend on the availability of dissolved oxygen, nitrate, ammonium and organic nitrogen in stream water as discussed above.

I advocate that critical Damköhler numbers (for peak nitrous oxide production and complete denitrification reaction) must be established by considering the time to reach equilibrium nitrous oxide and nitrate concentration rather than the time to reach limiting oxygen concentration (τ_{lim}).

7.1.2 Effect of meandering morphology on hyporheic nitrogen removal

Results of this study show that wavelength increases the potential of denitrification reaction by enhancing the available anaerobic area within the hyporheic zone. However, sinuosity is less sensitive in determining aerobic – anaerobic redox potential within the hyporheic zone. It was observed that all river reaches ($\lambda \geq 7.5$m and $W \geq 1m$) used in the study could facilitate anaerobic nitrogen removal reactions, but this does not ensure if these can support the full transformation of nitrate and ammonia into nitrogen gas. Da numbers range from 20 to 3000, which are relatively large. I have analyzed simulated Da numbers for the critical values that were identified from literature (Figure 6.4).

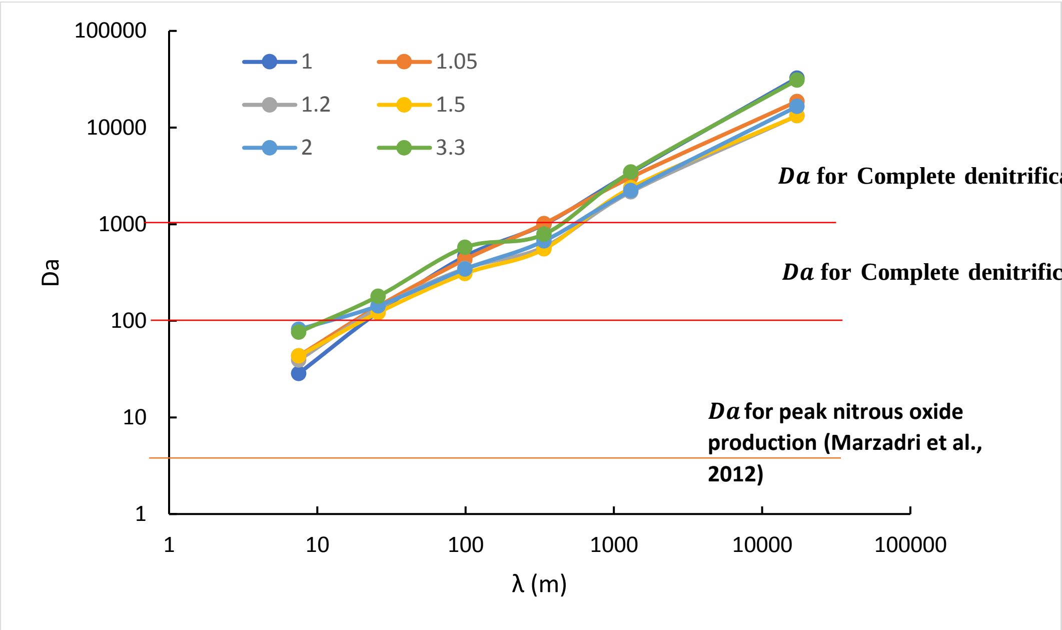

Figure 7.2 Damköhler number as a function of meander wavelengths for different sinuosities and critical Damköhler numbers for peak nitrous oxide production and complete denitrification reaction.

Figure 6.4 indicates that all meander morphologies ($\lambda \geq 7.5$m and $W \geq 1m$) are associated with high Da numbers beyond the critical value for peak nitrous oxide production, and consequently, the hyporheic zone act as a sink for nitrous oxide. Previous results show that complete nitrogen removal is possible in rivers with wavelengths above 11m, according to the observed nitrate removal rates in Marzadri et al. (2012). Similarly, the critical wavelength of 600m will be required to achieve complete nitrate removal with respect to the Da number reported in Azizian et al. (2015). However, rethe duction in nitrate loads relative to in-stream concentration reduces with steam flowrates.

As discussed in chapter 4, there are two important processes occurring within the hyporheic zones of meandering rivers, lateral pumping, and longitudinal pumping. Lateral pumping of water at the meander neck (fluvial HE) was observed to have short flow path length and higher velocities compared to longitudinal flow through intra-meanders (Floodplain HE). Therefore, it is essential to quantify residence time distributions and the magnitude of downwelling fluxes for each of the hyporheic processes to understand the combined effect that meanders could have on nitrogen fate and transport. I hypothesize that fluvial HE will produce nitrate and nitrous oxide masses, while floodplain HE generates a full transformation of nitrates and ammonia into nitrogen gas (Figure 6.5).

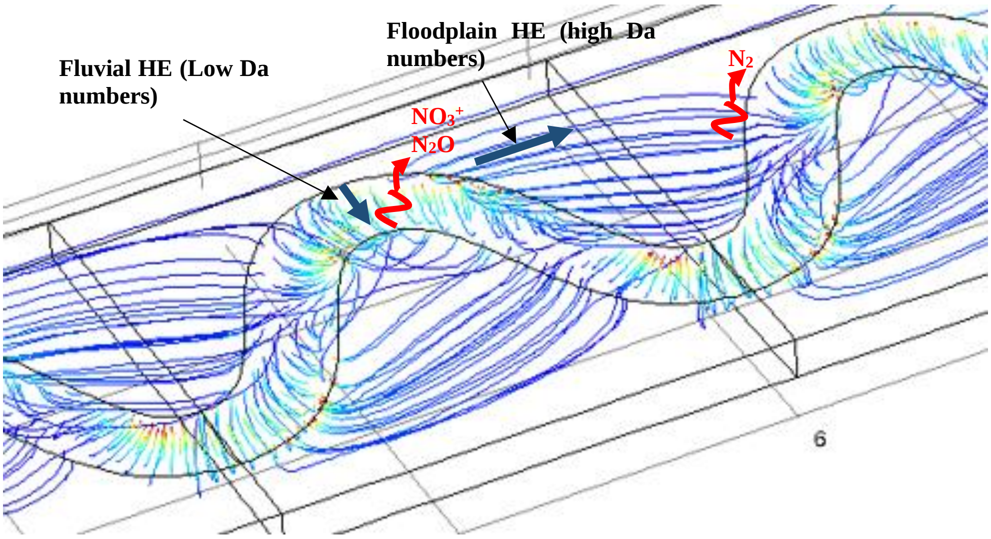

Figure 7.3 Interaction of transport processes and Damköhler number in estimating nitrogen source and sink functionality within the hyporheic zone of meandering rivers.

Overall, the results of this research suggest that meandering morphology is an important feature in the river ecosystem. Additionally, the hyporheic zone can also be a source or a sink of nitrate depending on other parameters such as demand for biological nitrogen, availability of required substrates, and abiotic factors such as pH and temperature. Therefore, more research is needed to understand the combined effect of these parameters on nitrogen fate and transport processes.

Chapter 8: Conclusions

This research aims to understand hyporheic flow behavior in meandering rivers as an important ecosystem mechanism of removing excess nitrogen loads in rivers. Mainly I looked at flux and residence time of solutes in the hyporheic zone through meandering morphology. I conducted laboratory flume experiments and numerical modeling to study the effect of flow and morphology characteristics in modifying flux and residence times of solutes in the hyporheic zone.

The results of this research show that there are two significant mechanisms driving hyporheic flow through meanders; 1). Longitudinal flow caused by channel slope at the scale of meander wavelength and 2). lateral flow caused by surface water acceleration due to the curvature of the channel at the scale of channel width. There is a complex interaction between meander wavelength and sinuosity in controlling these two processes, as discussed in chapters two and three. The experimental results suggest that residence time is sensitive to the length of the hyporheic flow path; increasing wavelength increases length scale and hence increase in residence time; sinuosity does not effectively increase or decrease length scales or vary the residence times. However, flux is sensitive to the curvature of the meandering stream; high sinuosity increases the curvature resulting in higher water flux into the hyporheic zone; increasing wavelength decreases curvature effect and also decrease in flux. This study also demonstrates that flux and residence times of solutes are dependent on river flow rates. We advocate that future research must be directed to conduct more intensive field experiments to advance our understanding of the role of meandering morphology in controlling flux and hydraulic residence times in the hyporheic zone.

8.1 Research Outcome and recommendations

My research explores a critical knowledge gap in understanding a large-scale channel feature (meandering morphology) and its flux and residence distribution, which were less understood in hyporheic literature but are very important for nitrogen biogeochemical cycling in rivers. This study presents the first-ever laboratory examination of solute transport through meandering streams. Another novel feature of my research methodology is the development of an experimentally validated three-dimensional model to examine hyporheic flow in the hyporheic zone. My thesis proposes three empirical relationships to predict downwelling water flux and characteristics of residence time distribution (mean and standard deviation) for low gradient meandering streams with widths ranging from 1m to 1000m. Thus, these empirical relationships can approximate the retention of solutes in the hyporheic zone without the need for a numerical model.

Even though the focus of this study is on nitrogen removal, these findings can be potentially applied in investigating the fate and transport of other waterborne contaminants. The outcome of this research could be used to inform river and catchment management authorities to improve the ecosystem services provided by rivers, thereby providing improved natural mechanisms of the environment as well as extending current knowledge to include more biogeochemical processes happening in the hyporheic zone. This study extends the existing knowledge in the science supporting improved river management solutions by exploring if we can use the hyporheic exchange as a future ecosystem engineering tool to protect our rivers from excess nitrogen.

8.2 Recommendation for future research

Laboratory flume and numerical experiments carried out in this study were for ideal meandering morphology, which does not accurately represent the real-world river systems. Therefore, the developed numerical model should be tested against the field observed morphology for its application in catchment management practices. Therefore, this approach could potentially be expanded, using field-specific parameters such as morphology, streamflow conditions, and sediment characteristics.

In this study, we did not vary sediment properties and alluvium volume, which are also major influencing factors, as identified in previous literature (Tonina and Buffington, 2007). Using different sand material with varied grain size distribution would enhance further understanding of water transport in the subsurface.

We used a smaller number of tracer experiments without replication due to time and resource constraints, which might have potentially led to some uncertainties in tracer breakthrough curves. Therefore, I believe that future research must be done with more intensive laboratory and field experiments to increase our understanding of hyporheic flow processes through river meanders.

References

ACUÑA, V. & TOCKNER, K. 2009. Surface-subsurface water exchange rates along alluvial river reaches control the thermal patterns in an Alpine river network. *Freshwater Biology,* 54**,** 306-320.

ANZECC & ARMCANZ 2000. National water quality management strategy: Australian and New Zealand guidelines for fresh and marine water quality. *Agriculture and Resource Management Council of Australia and New Zealand and Australian and New Zealand Environment and Conservation Council, Canberra, ACT*.

AUBENEAU, A. F., MARTIN, R. L., BOLSTER, D., SCHUMER, R., JEROLMACK, D. & PACKMAN, A. 2015. Fractal patterns in riverbed morphology produce fractal scaling of water storage times. *Geophysical Research Letters,* 42**,** 5309-5315.

AZIZIAN, M., BOANO, F., COOK, P. L. M., DETWILER, R. L., RIPPY, M. A. & GRANT, S. B. 2017. Ambient groundwater flow diminishes nitrate processing in the hyporheic zone of streams. *Water Resources Research,* 53**,** 3941-3967.

AZIZIAN, M., GRANT, S. B., KESSLER, A. J., COOK, P. L., RIPPY, M. A. & STEWARDSON, M. J. 2015. Bedforms as biocatalytic filters: A pumping and streamline segregation model for nitrate removal in permeable sediments. *Environmental science & technology,* 49**,** 10993-11002.

BALBARINI, N., BOON, W. M., NICOLAJSEN, E., NORDBOTTEN, J. M., BJERG, P. L. & BINNING, P. J. 2017. A 3-D numerical model of the influence of meanders on groundwater discharge to a gaining stream in an unconfined sandy aquifer. *Journal of Hydrology,* 552**,** 168-181.

BARDINI, L., BOANO, F., CARDENAS, M. B., REVELLI, R. & RIDOLFI, L. 2012. Nutrient cycling in bedform induced hyporheic zones. *Geochimica et Cosmochimica Acta,* 84**,** 47-61.

BARDINI, L., BOANO, F., CARDENAS, M. B., SAWYER, A. H., REVELLI, R. & RIDOLFI, L. 2013. Small-scale permeability heterogeneity has negligible effects on nutrient cycling in streambeds. *Geophysical Research Letters,* 40**,** 1118-1122.

BENCALA, K. E. & WALTERS, R. A. 1983. Simulation of solute transport in a mountain pool-and-riffle stream: A transient storage model. *Water Resour. Res.,* 19(3)**,** 718–724.

BHASKAR, A. S., HARVEY, J. W. & HENRY, E. J. 2012. Resolving hyporheic and groundwater components of streambed water flux using heat as a tracer. *Water Resources Research,* 48.

BOANO, F., CAMPOREALE, C. & REVELLI, R. 2010a. A linear model for the coupled surface-subsurface flow in a meandering stream. *Water Resources Research,* 46.

BOANO, F., CAMPOREALE, C., REVELLI, R. & RIDOLFI, L. 2006. Sinuosity-driven hyporheic exchange in meandering rivers. *Geophysical Research Letters,* 33.

BOANO, F., DEMARIA, A., REVELLI, R. & RIDOLFI, L. 2010b. Biogeochemical zonation due to intrameander hyporheic flow. *Water Resources Research,* 46.

BOANO, F., HARVEY, J. W., MARION, A., PACKMAN, A. I., REVELLI, R., RIDOLFI, L. & WÖRMAN, A. 2014. Hyporheic flow and transport processes:Mechanisms,models, and biogeochemical implications. *Rev. Geophys.,* 52**,** 603–679.

BOANO, F., REVELLI, R. & RIDOLFI, L. 2010c. Effect of streamflow stochasticity on bedform-driven hyporheic exchange. *Advances in Water Resources,* 33**,** 1367-1374.

BOANO, F., REVELLI, R. & RIDOLFI, L. 2013. Modeling hyporheic exchange with unsteady stream discharge and bedform dynamics. *Water Resources Research,* 49**,** 4089-4099.

BONIN, P., OMNES, P. & CHALAMET, A. 1998. Simultaneous occurrence of denitrification and nitrate ammonification in sediments of the French Mediterranean Coast. *Hydrobiologia,* 389**,** 169–182.

BOULTON, A. J., DATRY, T., KASAHARA, T., MUTZ, M. & STANFORD, J. A. 2010. Ecology and management of the hyporheic zone: stream–groundwater interactions of running waters and their floodplains. *Journal of the North American Benthological Society,* 29**,** 26-40.

BOULTON, A. J., FINDLAY, S., MARMONIER, P., STANLEY, E.H.,VALETT, H.M. 1998. The functional significance of the hyporheic zone in streams and rivers. *Annu. Rev. Ecol. Syst.,* 29**,** 59-81.

BRIGGS, M. A., DAY-LEWIS, F. D., ZARNETSKE, J. P. & HARVEY, J. W. 2015a. A physical explanation for the development of redox microzones in hyporheic flow. *Geophysical Research Letters,* 42**,** 4402-4410.

BRIGGS, M. A., DAY-LEWIS, F. D., ZARNETSKE, J. P. & HARVEY, J. W. J. G. R. L. 2015b. A physical explanation for the development of redox microzones in hyporheic flow. 42**,** 4402-4410.

BUFFINGTON, J. M. & TONINA, D. 2009. Hyporheic Exchange in Mountain Rivers II: Effects of Channel Morphology on Mechanics, Scales, and Rates of Exchange. *Geography Compass,* 3**,** 1038–1062.

BURKHOLDER, B. K., GRANT, G. E., HAGGERTY, R., KHANGAONKAR, T. & WAMPLER, P. J. 2008. Influence of hyporheic flow and geomorphology on temperature of a large, gravel-bed river, Clackamas River, Oregon, USA. *Hydrological Processes,* 22**,** 941-953.

BUSS, S., CAI, Z., CARDENAS, B., FLECKENSTEIN, J., HANNAH, D., HEPPELL, K., HULME, P., IBRAHIM, T., KAESER, D., KRAUSE, S., LERNER, D., MANT, J., MALCOLM, I., OLD, G., PARKIN, G., PICKUP, R., PINAY, G., PORTER, J., RHODES, G., RICHIE, A., RILEY, J., ROBERTSON, A., SEAR, D., SHIELDS, B., SMITH, J., TELLAM, J. & WOOD, P. 2009. *The Hyporheic Handbook: a handbook on the groundwater-surface water interface and hyporheic zone for environment managers,* Joanne Briddock, Yorkshire and North East Region, Environment Agency.

CALLANDER, R. A. 1978. River meandering. *Ann. Rev. Fluid Mech.,* 10**,** 129-158.

CARDENAS, M. B. 2008a. The effect of river bend morphology on flow and timescales of surface water–groundwater exchange across pointbars. *Journal of Hydrology,* 362**,** 134-141.

CARDENAS, M. B. 2008b. Surface water-groundwater interface geomorphology leads to scaling of residence times. *Geophysical Research Letters,* 35.

CARDENAS, M. B. 2009a. A model for lateral hyporheic flow based on valley slope and channel sinuosity. *Water Resources Research,* 45.

CARDENAS, M. B. 2009b. Stream-aquifer interactions and hyporheic exchange in gaining and losing sinuous streams. *Water Resources Research,* 45.

CARDENAS, M. B. & WILSON, J. L. 2007a. Dunes, turbulent eddies, and interfacial exchange with permeable sediments. *Water Resources Research,* 43.

CARDENAS, M. B. & WILSON, J. L. 2007b. Hydrodynamics of coupled flow above and below a sediment–water interface with triangular bedforms. *Advances in Water Resources,* 30**,** 301-313.

CARDENAS, M. B., WILSON, J. L. & HAGGERTY, R. 2008. Residence time of bedform-driven hyporheic exchange. *Advances in Water Resources,* 31**,** 1382-1386.

CARRERA, J., BAEZA, J. A., VICENT, T. & LAFUENTE, J. 2003. Biological nitrogen removal of high-strength ammonium industrial wastewater with two-sludge system. *Water Research,* 37**,** 4211-4221.

CHEN, X., CARDENAS, M. B. & CHEN, L. 2015. Three-dimensional versus twodimensional bed form-induced hyporheic exchange. *Water Resour. Res.,* 51**,** 2923–2936.

CIRMO, C. P. & MCDONNELL, J. J. 1997. Linking the hydrologic and biogeochemical controls of nitrogen transport in near-stream zones of temperate-forested catchments: a review. *Journal of Hydrology,* 199**,** 88-120.

CONLEY, D. J., PAERL, H. W., HOWARTH, R. W., BOESCH, D. F., SEITZINGER, S. P., HAVENS, K. E., LANCELOT, C. & LIKENS, G. E. 2009. Controlling Eutrophication: Nitrogen and Phosphorus. *Science,* 323**,** 1014-1015.

COOK, P. L., HOLLAND, D. P. & LONGMORE, A. R. 2010. Effect of a flood event on the dynamics of phytoplankton and biogeochemistry in a large temperate Australian lagoon. *Limnology and Oceanography,* 55**,** 1123-1133.

DAHM, C. N., GRIMM, N. B., MARMONIER, P., VALETT, H. M. & VERVIER, P. 1998. Nutrient dynamics at the interface between surface waters and groundwaters. *Freshwater Biology,* 40**,** 427-451.

DALSGAARD, T., CANFIELD, D. E., PETERSEN, J., THAMDRUP, B. & ACUNA-GONZALEZ, J. 2003. N2 production by the anammox reaction in the anoxic water column of Golfo Dulce, Costa Rica. *Nature,* 422**,** 606-8.

DALSGAARD, T., THAMDRUP, B. & CANFIELD, D. E. 2005. Anaerobic ammonium oxidation (anammox) in the marine environment. *Res Microbiol,* 156**,** 457-64.

DENT, C. L., GRIMM, N. B. & FISHER, S. G. 2001. Multiscale effects of surface–subsurface exchange on stream water nutrient concentrations. *J. N. Am. Benthol. Soc.,* 20**,** 162–181.

EBERSOLE, J. L., LISS, W. J. & FRISSELL, C. A. 2003. Thermal heterogeneity, stream channel morphology, and salmonid abundance in northeastern Oregon streams. *Canadian Journal of Fisheries and Aquatic Sciences,* 60**,** 1266-1280.

ELLIOTT, A. H. & BROOKS, N. H. 1997a. Transfer of nonsorbing solutes to a streambed with bed forms: Laboratory experiments. *Water Resources Research,* 33**,** 137-151.

ELLIOTT, A. H. & BROOKS, N. H. 1997b. Transfer of nonsorbing solutes to a streambed with bed forms: Theory. *Water Resources Research,* 33**,** 123-136.

EVRARD, V., GLUD, R. N. & COOK, P. L. M. 2012. The kinetics of denitrification in permeable sediments. *Biogeochemistry,* 113**,** 563-572.

FERNEX, F., BERNAT, M., BALLESTRA, S., FERNANDEZ, L. V. & MARQUES JR., A. N. 1992. Ammonification rates and Pb in sediments from a lagoon under a wet tropical climate: Marica, Rio de Janeiro state, Brazi. *Hydrobiologia,* 242**,** 69 - 76.

FIELDS, S. 2004. Global nitrogen: cycling out of control. *Environmental Health Perspectives.* National Institue of Environmental Health Sciences.

FINDLAY, S. 1995. Importance of surface-subsurface exchange in stream ecosystems: The hyporheic zone. *Limnol. Oceanogr.,* 40**,** 159-164.

FISHER, S. G., GRIMM, N. B., MARTI, E. & GOMEZ, R. 1998. Hierarchy, spatial configuration, and nutrient cycling in a desert stream. *Australian Journal of Ecology* 23**,** 4 1 - 5 2.

FOLLETT, R. F. & HATFIELD, J. L. 2001. Nitrogen in the environment: sources, problems, and management. *The Scientific World Journal,* 1**,** 920-926.

FOSSING, H., BERG, P., THAMDRUP, B., RYSGAARD, S., SORENSEN, H. M. & NIELSEN, K. 2004. A model set-up for an oxygen and nutrient flux model for Aarhus Bay (Denmark). *NERI technical report,* 483.

FRISSELL, C. A., LISS, W. J., WARREN, C. E. & HURLEY, M. D. 1986. A Hierarchical Framework for Stream Habitat Classification: Viewing Streams in a Watershed Context. *Environmental Management,* 10**,** 199-214.

GALLOWAY, J. N., TOWNSEND, A. R., ERISMAN, J. W., BEKUNDA, M., CAI, Z., FRENEY, J. R., MARTINELLI, L. A., SEITZINGER, S. P. & SUTTON, M. A. 2008. Transformation of the nitrogen cycle: recent trends, questions, and potential solutions. *Science,* 320**,** 889-892.

GARBAN, B., OLLIVON, D., POULIN, M., GAULTIER, V. & CHESTERIKOF, A. 1995. Exchanges at the sediment-water interface in the river seine, downstream from Paris. *Wat. Res.,* 29**,** 473-481.

GELHAR, L. W., WELTY, C. & REHFELDT, K. R. J. W. R. R. 1992. A critical review of data on field-scale dispersion in aquifers. 28**,** 1955-1974.

GOLDMAN, A. E., GRAHAM, E. B., CRUMP, A. R., KENNEDY, D. W., ROMERO, E. B., ANDERSON, C. G., DANA, K. L., RESCH, C. T., FREDRICKSON, J. K. & STEGEN, J. C. 2017. Biogeochemical cycling at the aquatic–terrestrial interface is linked to parafluvial hyporheic zone inundation history. *Biogeosciences,* 14**,** 4229-4241.

GOMEZ-VELEZ, J. D. & HARVEY, J. W. 2014. A hydrogeomorphic river network model predicts where and why hyporheic exchange is important in large basins. *Geophysical Research Letters,* 41**,** 6403-6412.

GOMEZ-VELEZ, J. D., WILSON, J. L., CARDENAS, M. B. & HARVEY, J. W. 2017. Flow and Residence Times of Dynamic River Bank Storage and Sinuosity-Driven Hyporheic Exchange. *Water Resources Research,* 53**,** 8572-8595.

GOMEZ, J. D., WILSON, J. L. & CARDENAS, M. B. 2012. Residence time distributions in sinuosity-driven hyporheic zones and their biogeochemical effects. *Water Resources Research,* 48.

GOOSEFF, M. N., WONDZELL, S. M., HAGGERTY, R. & ANDERSON, J. 2003. Comparing transient storage modeling and residence time distribution (RTD) analysis in geomorphically varied reaches in the Lookout Creek basin, Oregon, USA. *Advances in Water Resources,* 26**,** 925-937.

GRANT, S. B., STOLZENBACH, K., AZIZIAN, M., STEWARDSON, M. J., BOANO, F. & BARDINI, L. 2014. First-order contaminant removal in the hyporheic zone of streams: physical insights from a simple analytical model. *Environ Sci Technol,* 48**,** 11369-78.

GU, C., ANDERSON, W. & MAGGI, F. 2012. Riparian biogeochemical hot moments induced by stream fluctuations. *Water Resources Research,* 48.

GU, C., HORNBERGER, G. M., MILLS, A. L., HERMAN, J. S. & FLEWELLING, S. A. 2007. Nitrate reduction in streambed sediments: Effects of flow and biogeochemical kinetics. *Water Resources Research,* 43**,** n/a-n/a.

HAGERMAN, J. R. & WILLIAMS, J. D. 2000. Meander shape and the design of stable meanders. *Proceedings aMERICAN wATER rESOURCES Association, Specialty Conference, Anchorage, Alaska, April 20-May,* 4.

HAGGERTY, R. 2002. Power-law residence time distribution in the hyporheic zone of a 2nd-order mountain stream. *Geophysical Research Letters,* 29.

HAGGERTY, R., WONDZELL, S. M., BAKER, M. & GOOSEFF, M. N. 2002. Controls on hyporheic nitrate retention – Discriminating among transport, reaction-rate, and substrate limitation.

HESTER, E. T. & DOYLE, M. W. 2008. In-stream geomorphic structures as drivers of hyporheic exchange. *Water Resources Research,* 44.

HESTER, E. T. & GOOSEFF, M. N. 2010. Moving beyond the banks: Hyporheic restoration is fundamental to restoring ecological services and functions of streams. ACS Publications.

HESTER, E. T. & GOOSEFF, M. N. 2011. Hyporheic Restoration in Streams and Rivers. *In:* SIMON, A., BENNETT, S. J. & CASTRO, J. M. (eds.) *Stream Restoration in Dynamic Fluvial Systems: Scientific Approaches, Analyses, and Tools.*

HESTER, E. T., YOUNG, K. I. & WIDDOWSON, M. A. 2014. Controls on mixing-dependent denitrification in hyporheic zones induced by riverbed dunes: A steady state modeling study. *Water Resources Research,* 50**,** 9048-9066.

HILL, A. R., LABADIA, C. F. & SANMUGADAS, K. 1998. Hyporheic zone hydrology and nitrogen dynamics in relation to the streambed topography of a N-rich stream. *Biogeochemistr,* 42**,** 285-310.

HOLMES, R. M., FISHER, S. G. & GRIM, N. B. 1994. Parafluvial nitrogen dynamics in a desert stream ecosystem. *J. N. Am. Benthol. Soc.,* 13**,** :468-478.

HOVEN, S. J. V., FROMM, N. J. & PETERSON, E. W. 2008. Quantifying nitrogen cycling beneath a meander of a low gradient, N-impacted, agricultural stream using tracers and numerical modelling. *Hydrological Processes,* 22**,** 1206-1215.

HU, H., BINLEY, A., HEPPELL, C. M., LANSDOWN, K. & MAO, X. 2014. Impact of microforms on nitrate transport at the groundwater–surface water interface in gaining streams. *Advances in Water Resources,* 73**,** 185-197.

JONES, J. B., JR., FISHER, S. G. & GRIMM, N. B. 1995. Nitrification in the hyporheic zone of a desert stream ecosystem. *J. N. Am. Benthol. Soc.,,* 14**,** 249-258.

KÄSER, D., BINLEY, A. & HEATHWAITE, A. L. 2013. On the importance of considering channel microforms in groundwater models of hyporheic exchange. *River Research and Applications,* 29**,** 528-535.

KASVI, E., LAAMANEN, L., LOTSARI, E. & ALHO, P. 2017. Flow Patterns and Morphological Changes in a Sandy Meander Bend during a Flood—Spatially and Temporally Intensive ADCP Measurement Approach. *Water,* 9**,** 106.

KESLO, B. H. L., SMITH, R. V., LAUGHLIN, R. J. & LENNOX, S. D. 1997. Dissimilatory Nitrate Reduction in Anaerobic Sediments Leading to River Nitrite Accumulation. *Applied and Environmental Microbiology,* 63 (12)**,** 4679 - 4685.

KESSLER, A. J., GLUD, R. N., CARDENAS, M. B. & COOK, P. L. 2013. Transport zonation limits coupled nitrification-denitrification in permeable sediments. *Environmental science & technology,* 47**,** 13404-13411.

KESSLER, A. J., GLUD, R. N., CARDENAS, M. B., LARSEN, M., BOURKE, M. F. & COOK, P. L. 2012. Quantifying denitrification in rippled permeable sands through combined flume experiments and modeling. *Limnology and Oceanography,* 57**,** 1217-1232.

KHIN, T. & ANNACHHATRE, A. P. 2004. Novel microbial nitrogen removal processes. *Biotechnol Adv,* 22**,** 519-32.

KIEL, B. A. & BAYANI CARDENAS, M. 2014. Lateral hyporheic exchange throughout the Mississippi River network. *Nature Geoscience,* 7**,** 413-417.

KULIKOWSKA, D. & KLIMIUK, E. 2004. Removal of Organics and Nitrogen from Municipal Landfill Leachate in Two-Stage SBR Reactors. *Polish Journal of Environmental Studies* 13**,** 389-396.

LANSDOWN, K., HEPPELL, C. M., TRIMMER, M., BINLEY, A., HEATHWAITE, A. L., BYRNE, P. & ZHANG, H. 2015. The interplay between transport and reaction rates as controls on nitrate attenuation in permeable, streambed sediments. *J. Geophys. Res. Biogeosci.,* 120**,** 1093–1109.

LANSDOWN, K., TRIMMER, M., HEPPELL, C. M., SGOURIDIS, F., ULLAH, S., HEATHWAITE, A. L., BINLEY, A. & ZHANG, H. 2012. Characterization of the key pathways of dissimilatory nitrate reduction and their response to complex organic substrates in hyporheic sediments. *Limnology and Oceanography,* 57**,** 387-400.

LAWRENCE, J. E., SKOLD, M. E., HUSSAIN, F. A., SILVERMAN, D. R., RESH, V. H., SEDLAK, D. L., LUTHY, R. G. & MCCRAY, J. E. 2013. Hyporheic Zone in Urban Streams: A Review and Opportunities for Enhancing Water Quality and Improving Aquatic Habitat by Active Management. *Environmental Engineering Science,* 30**,** 480-501.

LEE, S. Y., DUNN, R. J. K., YOUNG, R. A., CONNOLLY, R. M., DALE, P. E. R., DEHAYR, R., LEMCKERT, C. J., MCKINNON, S., POWELL, B., TEASDALE, P. R. & WELSH, D. T. 2006. Impact of urbanization on coastal wetland structure and function. *Austral Ecology,* 31**,** 149-163.

LEOPOLD, L. B. & LANGBEIN, W. B. 1966 River meanders. *SCIENTIFIC AMERICAN, INC***,** 60-70.

LEOPOLD, L. B. & WOLMAN, M. G. 1960. River Meanders. *Geological Society of America Bulletin,* 71**,** 769.

MARZADRI, A., TONINA, D. & BELLIN, A. 2011. A semianalytical three-dimensional process-based model for hyporheic nitrogen dynamics in gravel bed rivers. *Water Resources Research,* 47.

MARZADRI, A., TONINA, D. & BELLIN, A. 2012. Morphodynamic controls on redox conditions and on nitrogen dynamics within the hyporheic zone: Application to gravel bed rivers with alternate-bar morphology. *Journal of Geophysical Research: Biogeosciences,* 117.

MARZADRI, A., TONINA, D. & BELLIN, A. 2013. Quantifying the importance of daily stream water temperature fluctuations on the hyporheic thermal regime: Implication for dissolved oxygen dynamics. *Journal of Hydrology,* 507**,** 241-248.

MARZADRI, A., TONINA, D., BELLIN, A. & TANK, J. L. 2014. A hydrologic model demonstrates nitrous oxide emissions depend on streambed morphology. *Geophysical Research Letters,* 41**,** 5484-5491.

MARZADRI, A., TONINA, D., BELLIN, A. & VALLI, A. 2016. Mixing interfaces, fluxes, residence times and redox conditions of the hyporheic zones induced by dune-like bedforms and ambient groundwater flow. *Advances in Water Resources,* 88**,** 139-151.

MARZADRI, A., TONINA, D., BELLIN, A., VIGNOLI, G. & TUBINO, M. 2010. Semianalytical analysis of hyporheic flow induced by alternate bars. *Water Resources Research,* 46**,** n/a-n/a.

MAZZA, R., WONDZELL, S. & ZARNETSKE, J. 2014. The stream subsurface: nitrogen cycling and the cleansing function of hyporheic zones. *Science Findings 166. Portland, OR: US Department of Agriculture, Forest Service, Pacific Northwest Research Station. 6 p.,* 166.

MECKLENBURG, D. E. & JAYAKARAN, A. D. 2012. Dimensioning the sine-generated curve meander geometry. *Journal_of_the_American_Water_Resources_Association,* 48**,** 635-642.

METCALF & EDDY, I. 1991. *Waste Water Engineering, Treatment, Disposal and Reuse*.

MEYER, R. L., RISGAARD-PETERSEN, N. & ALLEN, D. E. 2005. Correlation between anammox activity and microscale distribution of nitrite in a subtropical mangrove sediment. *Appl. Environ. Microbiol.,* 71**,** 6142-6149.

MOHAMAD, I. N., WEI-KOON, L. & RAKSMEY, M. 2015. Idealized River Meander using Improved Sine-Generated Curve Method.

MULHOLLAND, P. J., HELTON, A. M., POOLE, G. C., HALL, R. O., HAMILTON, S. K., PETERSON, B. J., TANK, J. L., ASHKENAS, L. R., COOPER, L. W., DAHM, C. N., DODDS, W. K., FINDLAY, S. E., GREGORY, S. V., GRIMM, N. B., JOHNSON, S. L., MCDOWELL, W. H., MEYER, J. L., VALETT, H. M., WEBSTER, J. R., ARANGO, C. P., BEAULIEU, J. J., BERNOT, M. J., BURGIN, A. J., CRENSHAW, C. L., JOHNSON, L. T., NIEDERLEHNER, B. R., O'BRIEN, J. M., POTTER, J. D., SHEIBLEY, R. W., SOBOTA, D. J. & THOMAS, S. M. 2008. Stream denitrification across biomes and its response to anthropogenic nitrate loading. *Nature,* 452**,** 202-5.

NARANJO, R. C., NISWONGER, R. G. & DAVIS, C. J. 2015. Mixing effects on nitrogen and oxygen concentrations and the relationship to mean residence time in a hyporheic zone of a riffle-pool sequence. *Water Resour. Res,* 51**,** 7202–7217.

OMNES, P., SLAWYK, G., GARCIA, N. & BONIN, P. 1996. Evidence of denitrification and nitrate ammonification in the River Rhone plume (northwestern Mediterranean Sea). *lMar Ecol Prog Se,* 141**,** 275-281.

OSENBRÜCK, K., WÖHLING, T., LEMKE, D., ROHRBACH, N., SCHWIENTEK, M., LEVEN, C., CASTILLO ALVAREZ, C., TAUBALD, H. & CIRPKA, O. A. 2013. Assessing hyporheic exchange and associated travel times by hydraulic, chemical, and isotopic monitoring at the Steinlach Test Site, Germany. *Environmental Earth Sciences,* 69**,** 359-372.

PAINTER, S. L. 2018. Multiscale framework for modeling multicomponent reactive transport in stream corridors. *Water Resources Research,* 54**,** 7216-7230.

PARKER, S. P., BOWDEN, W. B., FLINN, M. B., GILES, C. D., ARNDT, K. A., BENEŠ, J. P. & JENT, D. G. J. E. 2018. Effect of particle size and heterogeneity on sediment biofilm metabolism and nutrient uptake scaled using two approaches. 9**,** e02137.

PESCIMORO, E., BOANO, F., SAWYER, A. H. & SOLTANIAN, M. R. 2019. Modeling Influence of Sediment Heterogeneity on Nutrient Cycling in Streambeds. *Water Resources Research*.

PINAY, G., O'KEEFE, T. C., EDWARDS, R. T. & NAIMAN, R. J. 2009. Nitrate removal in the hyporheic zone of a salmon river in Alaska. *River Research and Applications,* 25**,** 367-375.

PRYSHLAK, T. T., SAWYER, A. H., STONEDAHL, S. H. & SOLTANIAN, M. R. 2015. Multiscale hyporheic exchange through strongly heterogeneous sediments. *Water Resour. Res.,* 51**,** 9127–9140.

QUICK, A. M., REEDER, W. J., FARRELL, T. B., TONINA, D., FERIS, K. P. & BENNER, S. G. 2016. Controls on Nitrous Oxide Emissions from the Hyporheic Zones of Streams. *Environ Sci Technol,* 50**,** 11491-11500.

REVELLI, R., BOANO, F., CAMPOREALE, C. & RIDOLFI, L. 2008. Intra-meander hyporheic flow in alluvial rivers. *Water Resources Research,* 44**,** n/a-n/a.

RIVETT, M. O., BUSS, S. R., MORGAN, P., SMITH, J. W. & BEMMENT, C. D. 2008. Nitrate attenuation in groundwater: a review of biogeochemical controlling processes. *Water Res,* 42**,** 4215-32.

RUNKEL, R. L. 1998. One dimensional transport with inflow and storage (OTIS): A solute transport model for streams and rivers. *U.S. Geol. Surv. Water Resour. Invest. Rep.,* 73**,** 98-4018.

SALEHIN, M., PACKMAN, A. I. & PARADIS, M. 2004. Hyporheic exchange with heterogeneous streambeds: Laboratory experiments and modeling. *Water Resources Research,* 40.

SAUNDERS, D. L. & KALFF, J. 2001. Nitrogen retention in wetlands, lakes and rivers. *Hydrobiologia,* 443**,** 205–212.

SAWYER, A. H., BAYANI CARDENAS, M. & BUTTLES, J. 2011. Hyporheic exchange due to channel-spanning logs. *Water Resources Research,* 47.

SCHMIDT, I., SLIEKERS, O., SCHMID, M., BOCK, E., FUERST, J., KUENEN, J. G., JETTEN, M. S. M. & STROUS, M. 2003. New concepts of microbial treatment processes for the nitrogen removal in wastewater. *FEMS Microbiology Reviews,* 27**,** 481-492.

SCHUMM, S. A. 1963. Sinuosity of Alluvial Rivers on the Great Plains. *Geological Society of America Bulletin,* 74**,** 1089-1100.

SHEIBLEY, R. W., JACKMAN, A. P., DUFF, J. H. & TRISKA, F. J. 2003. Numerical modeling of coupled nitrification–denitrification in sediment perfusion cores from the hyporheic zone of the Shingobee River, MN. *Advances in Water Resources,* 26**,** 977-987.

SILVENNOINEN, H., LIIKANEN, A., TORSSONEN, J., STANGE, C. F. & MARTIKAINEN, P. J. 2008. Denitrification and N2O effluxes in the Bothnian Bay (northern Baltic Sea) river sediments as affected by temperature under different oxygen concentrations. *Biogeochemistry,* 88**,** 63-72.

SMIL, V. 1999. Nitrogen in crop production: An account of global flows. *Global Biogeochemical Cycles,* 13**,** 647-662.

STEWARDSON, M. J., DATRY, T., LAMOUROUX, N., PELLA, H., THOMMERET, N., VALETTE, L. & GRANT, S. B. 2016. Variation in reach-scale hydraulic conductivity of streambeds. *Geomorphology,* 259**,** 70-80.

STONEDAHL, S. H., HARVEY, J. W. & PACKMAN, A. I. 2013. Interactions between hyporheic flow produced by stream meanders, bars, and dunes. *Water Resources Research,* 49**,** 5450-5461.

STONEDAHL, S. H., HARVEY, J. W., WÖRMAN, A., SALEHIN, M. & PACKMAN, A. I. 2010. A multiscale model for integrating hyporheic exchange from ripples to meanders. *Water Resources Research,* 46.

STOREY, R. G., HOWARD, K. W. F. & WILLIAMS, D. D. 2003. Factors controlling riffle-scale hyporheic exchange flows and their seasonal changes in a gaining stream: A three-dimensional groundwater flow model. *Water Resources Research,* 39.

STOREY, R. G., WILLIAMS, D. D. & FULTHORPE, R. R. 2004. Nitrogen processing in the hyporheic zone of a pastoral stream. *Biogeochemistry,* 69**,** 285-313.

SWQMS 2000. State water quality management strategy: Implementation Framework for Western Australia for the Australian and New Zealand Guidelines for Fresh and Marine Water Quality and Water Quality Monitoring and Reporting (Guidelines Nos. 4 & 7: National Water Quality Management Strategy). *EPA, Perth, WA*.

TAKEUCHI, J. 2006. Habitat Segregation of a Functional Gene Encoding Nitrate Ammonification in Estuarine Sediments. *Geomicrobiology Journal,* 23**,** 75-87.

TAYLOR, G. D., FLETCHER, T. D., WONG, T. H., BREEN, P. F. & DUNCAN, H. P. 2005. Nitrogen composition in urban runoff--implications for stormwater management. *Water Res,* 39**,** 1982-9.

TONINA, D. & BUFFINGTON, J. M. 2007. Hyporheic exchange in gravel bed rivers with pool-riffle morphology: Laboratory experiments and three-dimensional modeling. *Water Resources Research,* 43**,** n/a-n/a.

TONINA, D. & BUFFINGTON, J. M. 2009. Hyporheic Exchange in Mountain Rivers I: Mechanics and Environmental Effects. *Geography Compass,* 3/3**,** 1063–1086.

TONINA, D. & BUFFINGTON, J. M. 2011. Effects of stream discharge, alluvial depth and bar amplitude on hyporheic flow in pool-riffle channels. *Water Resources Research,* 47**,** n/a-n/a.

TRAUTH, N., SCHMIDT, C., MAIER, U., VIEWEG, M. & FLECKENSTEIN, J. H. 2013. Coupled 3-D stream flow and hyporheic flow model under varying stream and ambient groundwater flow conditions in a pool-riffle system. *Water Resources Research,* 49**,** 5834-5850.

TRAUTH, N., SCHMIDT, C., VIEWEG, M., MAIER, U. & FLECKENSTEIN, J. H. 2014. Hyporheic transport and biogeochemical reactions in pool-riffle systems under varying ambient groundwater flow conditions. *J. Geophys. Res. Biogeosci.,* 119**,** 910–928.

TRAUTH, N., SCHMIDT, C., VIEWEG, M., OSWALD, S. E. & FLECKENSTEIN, J. H. 2015. Hydraulic controls of in-stream gravel bar hyporheic exchange and reactions. *Water Resources Research,* 51**,** 2243-2263.

VAN DEN BERG, E. M., VAN DONGEN, U., ABBAS, B. & VAN LOOSDRECHT, M. C. 2015. Enrichment of DNRA bacteria in a continuous culture. *ISME J,* 9**,** 2153-61.

VANZOMEREN, C. M., WHITE, J. R. & DELAUNE, R. D. 2013. Ammonification and denitrification rates in coastal Louisiana bayou sediment and marsh soil: Implications for Mississippi river diversion management. *Ecological Engineering,* 54**,** 77-81.

WANG, Z., QI, Y., WANG, J. & PEI, Y. 2012. Characteristics of aerobic and anaerobic ammonium-oxidizing bacteria in the hyporheic zone of a contaminated river. *World J Microbiol Biotechnol,* 28**,** 2801-11.

WILLIAMS, G. P. 1986. River meanders and channel size. *Journal of Hydrology,* 88**,** 147-164.

WÖRMAN, A., PACKMAN, A. I., JOHANSSON, H. & JONSSON, K. 2002. Effect of flow-induced exchange in hyporheic zones on longitudinal transport of solutes in streams and rivers. *Water Resources Research,* 38**,** 2-1-2-15.

WÖRMAN, A., PACKMAN, A. I., MARKLUND, L., HARVEY, J. W. & STONE, S. H. 2007. Fractal topography and subsurface water flows from fluvial bedforms to the continental shield. *Geophysical Research Letters,* 34.

ZARNETSKE, J. P., HAGGERTY, R. & WONDZELL, S. M. 2015. Coupling multiscale observations to evaluate hyporheic nitrate removal at the reach scale. *Freshwater Science,* 34**,** 172-186.

ZARNETSKE, J. P., HAGGERTY, R., WONDZELL, S. M. & BAKER, M. A. 2011. Dynamics of nitrate production and removal as a function of residence time in the hyporheic zone. *Journal of Geophysical Research,* 116.

ZARNETSKE, J. P., HAGGERTY, R., WONDZELL, S. M., BOKIL, V. A. & GONZÁLEZ-PINZÓN, R. 2012. Coupled transport and reaction kinetics control the nitrate source-sink function of hyporheic zones. *Water Resources Research,* 48.

ZHOU, N., ZHAO, S. & SHEN, X. 2014. Nitrogen cycle in the hyporheic zone of natural wetlands. *Chinese Science Bulletin,* 59**,** 2945-2956.

ZHU, G., PENG, Y., LI, B., GUO, J., YANG, Q. & WANG, S. 2008. Biological Removal of Nitrogen from Wastewater. *Rev Environ Contam Toxicol* 192**,** 159–195.

ZHU, G., WANG, S., WANG, W., WANG, Y., ZHOU, L., JIANG, B., OP DEN CAMP, H. J. M., RISGAARD-PETERSEN, N., SCHWARK, L., PENG, Y., HEFTING, M. M., JETTEN, M. S. M. & YIN, C. 2013. Hotspots of anaerobic ammonium oxidation at land–freshwater interfaces. *Nature Geoscience,* 6**,** 103-107.

ZIMMER, M. A. & LAUTZ, L. K. J. F. S. 2015. Pre-and postrestoration assessment of stream water–groundwater interactions: effects on hydrological and chemical heterogeneity in the hyporheic zone. 34**,** 287-300.

Appendix

Supplementary materials for Chapter 4

Table A1: Taguchi design of numerical simulations for sensitivity analysis

	1	2	3	4	5	6	7	8	9
	J	λ	K	V	Theta	Slope	W/D	Wa	Da
1	1.1	3	2.00E-04	0.01	0.3	0.005	10	1.5	5
2	1.1	3	2.00E-04	0.01	0.35	0.008	15	3	10
3	1.1	3	2.00E-04	0.01	0.4	0.01	20	4.5	15
4	1.1	6	5.00E-04	0.08	0.3	0.005	10	3	10
5	1.1	6	5.00E-04	0.08	0.35	0.008	15	4.5	15
6	1.1	6	5.00E-04	0.08	0.4	0.01	20	1.5	5
7	1.1	12	6.00E-03	0.4	0.3	0.005	10	4.5	15
8	1.1	12	6.00E-03	0.4	0.35	0.008	15	1.5	5
9	1.1	12	6.00E-03	0.4	0.4	0.01	20	3	10
10	1.5	3	5.00E-04	0.4	0.3	0.008	20	1.5	10
11	1.5	3	5.00E-04	0.4	0.35	0.01	10	3	15
12	1.5	3	5.00E-04	0.4	0.4	0.005	15	4.5	5
13	1.5	6	6.00E-03	0.01	0.3	0.008	20	3	15
14	1.5	6	6.00E-03	0.01	0.35	0.01	10	4.5	5
15	1.5	6	6.00E-03	0.01	0.4	0.005	15	1.5	10
16	1.5	12	2.00E-04	0.08	0.3	0.008	20	4.5	5
17	1.5	12	2.00E-04	0.08	0.35	0.01	10	1.5	10
18	1.5	12	2.00E-04	0.08	0.4	0.005	15	3	15
19	2.0	3	6.00E-03	0.08	0.3	0.01	15	1.5	15
20	2.0	3	6.00E-03	0.08	0.35	0.005	20	3	5
21	2.0	3	6.00E-03	0.08	0.4	0.008	10	4.5	10
22	2.0	6	2.00E-04	0.4	0.3	0.01	15	3	5
23	2.0	6	2.00E-04	0.4	0.35	0.005	20	4.5	10
24	2.0	6	2.00E-04	0.4	0.4	0.008	10	1.5	15
25	2.0	12	5.00E-04	0.01	0.3	0.01	15	4.5	10
26	2.0	12	5.00E-04	0.01	0.35	0.005	20	1.5	15
27	2.0	12	5.00E-04	0.01	0.4	0.008	10	3	5